Evolving Models of Ovarian Cancer: Defining the Role of PAX8 in Fallopian Tube Tumorigenesis

Evolving Models of Ovarian Cancer: Defining the Role of PAX8 in Fallopian Tube Tumorigenesis

A dissertation presented by

Megan Marie Emori

to

The Division of Medical Sciences

In partial fulfillment of the requirements

For the degree of

Doctor of Philosophy

In the subject of

Human Biology and Translational Medicine

Harvard University

Cambridge, Massachusetts

July, 2015

Dissertation Advisor: Dr. Ronny Drapkin Megan Marie Emori

Evolving Models of Ovarian Cancer: Defining the Role of PAX8 in Fallopian Tube Tumorigenesis

Abstract

Ovarian cancer is the most deadly gynecological malignancy in the US. Once thought to be a single disease arising from the ovarian surface epithelium, we now understand that it is in fact a heterogenous disease with origins across the female reproductive tract. Ovarian cancers can be broken down into type I and type II tumors. While type I tumors are typically slow growing and arise from the ovary, type II tumors are highly aggressive, particularly the most common and deadliest subtype, High Grade Serous Ovarian Cancer (HGSOC), which arises from the fallopian tube epithelium.

While our understanding of the complexity of ovarian cancer has evolved significantly over the last few decades, ovarian cancer is still primarily modeled by a few historical and robust cell lines which poorly recapitulate the genetics of HGSOC patient tumors. Here we characterize less studied cell lines with high genomic fidelity to HGSOC, KURAMOCHI and OVSAHO. Through in vivo xenograft experiments, we determined that these two cell lines form more diffuse tumors which better represent the HGSOC phenotype. In vitro, these lines are tractable to a variety of standard molecular biology techniques, but only express a subset of common markers of HGSOC, including PAX8 and stabilized TP53, while others were absent. These results indicate that it is important to take both molecular and genetic relevance into consideration when selecting cell lines for laboratory studies.

PAX8 is a nuclear transcription factor critical to the development of the female reproductive tract, including the fallopian tube, and is conserved in both the adult fallopian tube and HGSOC. Recent studies have identified PAX8 as a differentially expressed, essential gene to ovarian cancer, making it a promising drug target for HGSOC. Here, we identify a subset of ovarian cancers that exhibit decreased proliferation when PAX8 expression is decreased, and determine that in KURAMOCHI cells this defect

appears to be driven by cell cycle arrest. We also characterized the similarities and differences of PAX8 DNA binding and gene regulation through ChIPseq and RNAseq, respectively, in the context of the fallopian tube and HGSOC. We determined that while a small subset of PAX8 binding sites are conserved across the fallopian tube and ovarian cancer, there is a significant gain of novel binding sites in ovarian cancer that is unique to each cancer cell line. In contrast, different fallopian tube-derived lines have very similar PAX8 binding sites and many of these are uniformly lost in the context of cancer. Understanding how the role of PAX8 changes from the fallopian tube to cancer is an important step to drug development targeting PAX8.

Ultimately, this body of research seeks to improve ovarian cancer modeling techniques and to better understand fallopian tube pathogenesis, leading to more effective translation of ovarian cancer research from bench to bedside.

Table of Contents

Acknowledgements

This thesis would not have been possible without the help of so many people.

I would like to thank Dr. David Frank, who has been with me every step of the way from my first days in the LHB program to the last day of my thesis defense. I have been privileged beyond words to have you as both a mentor and role model. Next, I would like to thank Dr. Ronny Drapkin for accepting me into his lab. I have learned so much in the past six years. To the lab mates I have had the pleasure of working with over the years, especially Dr. Kevin Elias and Emily MacDuffie: this project was a team effort and your support and assistance was invaluable. I would also like to thank the members of my thesis defense committee, Dr. David Frank, Dr. Karl Munger, Dr. Myles Brown, and Dr. Susan Dymecki for their insight and guidance.

No PhD in the BBS program is possible without the support of Kate, Maria, and Danny, who solve so many problems, large and small, that the list would be impossible to include here. Thank you for everything you do.

Grad school is one of the longest, hardest roads to travel, and I am deeply indebted to my friends and fellow colleagues Jessica, Julie, Katie, Carolyn, Karen, and Mary for keeping me company. When I needed a shoulder to cry on, a mojito, someone to work skype on their smart phone so my Mum could come wedding dress shopping with me from across the continent- you were there for me. As you have told me so many times, you are brave, and strong, and you can accomplish anything.

I would like to thank all of my family for believing in me every step of the journey. For Dad, who armed me with a hammer and nails and let me "build" things alongside him when I was barely old enough to talk, and who has had unwavering faith in me and everything I have tried to take on ever since, even when I didn't quite believe in myself. For Mum, who is my lighthouse: I admired you when you were the Sunshine of my childhood, but watching you shine through the storms of life has made me truly

appreciate the unquenchable source of your strength, courage, and joy. If I have inherited even a small portion of your legacies, I am rich indeed.

I would also like to thank my adopted Grandparents- Don, Sally, Grandma Dowdel, the Windsong players, and so many others, for reminding me that life is too short to squander on anything but the wildest adventures. I still want to be like you when I grow up.

Most of all, I would like to thank my husband, Satoru. Your patience, wisdom, sense of humor, and quiet willingness to take on far more than half the chores have carried me over some of the roughest patches of grad school. You inspire me daily to be a better scientist, person, and partner. Here is to new beginnings, and many, many thesis-free years to come. I love you.

Dedication

This thesis is dedicated to the women behind every fallopian tube

Both in this study, and in the great experiment of life,

In recognition of your struggles and in honor of your strength

CHAPTER 1

Introduction

Ovarian Cancer

Ovarian Cancer Subtypes

Ovarian cancer is the most lethal gynecological malignancy in the western world[1]. Once thought to be a single cancer derived from the ovarian surface epithelium, it is now recognized to be a heterogenous disease[2,3]. Although ovarian tumors can arise from three different cell types: epithelial cells, germ cells, and sex cord stromal cells, the vast majority of ovarian cancers are epithelial in nature. Even within epithelial ovarian cancers there exist various histologic subtypes and molecular subgroups (Figure 1.1)[2–4]. This has prompted the classification of epithelial ovarian cancers into two groups. Type I tumors,

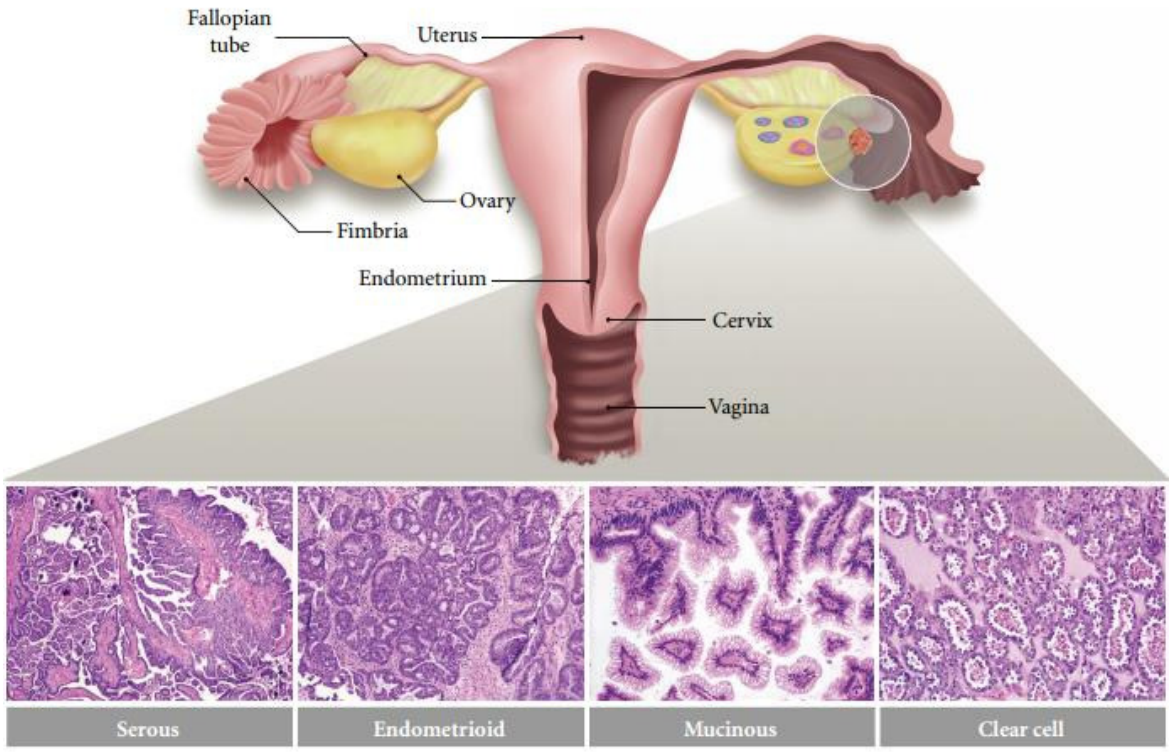

Figure 1.1: The Major Subtypes of Ovarian Cancer.
(From Karst and Drapkin 2010 Ovarian Cancer Pathogenesis: A Model in Evolution)
Once thought to arise from the single layer of ovarian surface epithelium, new models suggest ovarian cancer is a heterogeneous disease with subtypes related to different tissue within the female reproductive tract. Shaded region indicates the area where most ovarian tumors arise.

clearly linked to ovarian precursor lesions, encompass all histologic subtypes including low grade serous, endometriod, mucinous, and clear cell carcinomas. They are defined by their slow growth and multiple genetic mutations. In contrast, Type II tumors are highly aggressive, confer a much poorer prognosis, and many have been linked to precursors arising from the fallopian tube epithelium. Type I and Type II tumors are also genomically distinct. Type I tumors are frequently associated with specific mutations in oncogenes such as k-RAS and ARID1A[4]. In Type II tumors, TP53 is mutated in the vast majority of tumors (96-100%) with significant genomic instability resulting in multiple amplifications and deletions[5–7]. BRCA1 and BRCA2 mutation carriers are particularly susceptible to Type II tumors[3,4].

Fallopian Tube Epithelium

The fallopian tubes are hollow ductal structures developmentally derived from the Müllerian duct that extend outwards from the uterus to brush the surface of the ovary. The distal end of the fallopian tube closest to the ovary consists of multiple finger-like projections of epithelium called the fimbria. Immediately after ovulation the ova is caught by the cilia of the fimbria and transported through the fallopian tube for fertilization and eventual implantation in the uterus. At the cellular level, the fallopian tube is composed of a polarized layer of secretory and ciliated epithelial cells anchored by underlying stromal tissue. Throughout the menstrual cycle the balance of secretory and ciliated populations fluctuates in response to hormonal changes[8]. While ciliated cells are terminally differentiated, it is unclear whether secretory cells may differentiate into ciliated cells or if they are also a terminally differentiated population[9]. Recent research shows that a third population of low proliferating cells can be found at the base of the fimbria projections, which may suggest the presence of a stem cell population[10]. However, our understanding of the basic molecular biology of this tissue is far from complete.

High Grade Serous Ovarian Cancer

High Grade Serous Ovarian Cancer (HGSOC) accounts for nearly 70% of ovarian cancers and is the most lethal subtype, largely due to its late diagnosis and high recurrence rates[11]. Because it is rarely diagnosed before it has spread past the peritoneum, for many years HGSOC was considered to arise de

novo[12]. Epithelial cancers nearly all follow Jackman and Mayo's adenoma-carcinoma sequence, progressing from normal epithelium to tumor cell through a series of well-defined premalignant lesions[13]. Therefore, the lack of HGSOC precursors on the ovarian surface was considered an anomaly[14]. With the identification of the BRCA genes as a cause of hereditary breast and ovarian cancers, fallopian tubes were prophylactically removed and carefully examined histologically[14]. Since these women were likely to develop HGSOC, a small percentage of these specimens already contained cancer[14–18]. Surprisingly, anywhere from 42-100% of these early cancers included lesions in the distal fallopian tube, leading pathologists to propose the fallopian tube epithelium (FTE) as the cell of origin for HGSOC[19–21].

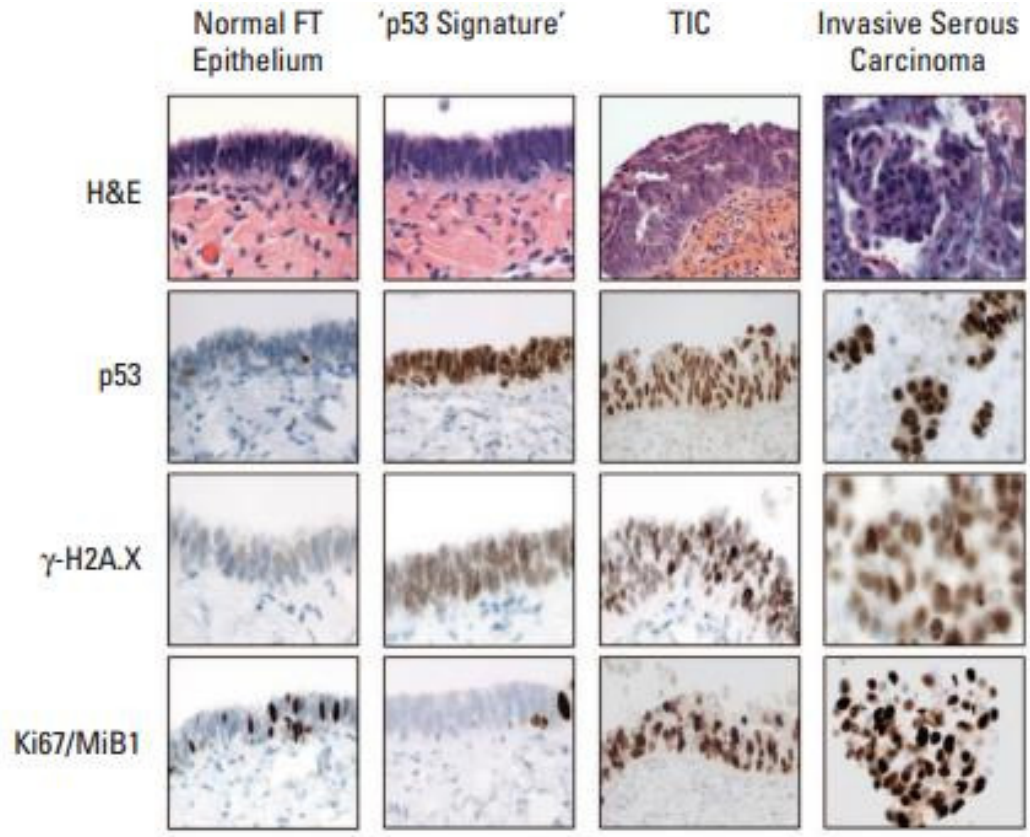

Figure 1.2: The Progression of Fallopian Tube Carcinogenesis from Normal Fallopian Tube Epithelium to High Grade Serous Carcinoma.
(from Levanon et al 2008 New Insights Into the Pathogenesis of Serous Ovarian Cancer and Its Clinical Impact.) The earliest precursor of HGSOC, a p53 signature, is characterized by p53 mutation and the onset of DNA damage as measured by ɣH2AX foci. This progresses to a Tubal intraepithelial carcinoma (TIC) with loss of single-layer architecture and increased proliferation rates as measured by Ki67/ MiB1. In invasive serous carcinomas, the basal membrane has been breached and proliferation rates continue to rise. Sloughing of tumor cells may occur very early on, before the TIC has progressed to invasive serous carcinoma.

Molecular observations have since corroborated this theory, with HGSOC sharing similar gene expression profiling with FTE but not ovarian surface epithelium[22,23]. The earliest characterized precursor lesions are called P53 Signatures (SIGs), as they consist of long stretches of FTE secretory cells which contain stabilizing mutations in the tumor suppressor P53 and exhibit increased DNA damage, but show no signs of increased proliferation[3]. Over time, SIGs progress to Tubal Intraepithelial Carcinomas (TICs), which proliferate heavily and display multilayered architecture[2] (Figure 1.2). HGSOC develops when the tumors grow and slough off, typically onto the ovarian surface epithelium or omentum, leading to a large

and often widespread tumor burden[24]. Thus the current fallopian tube cell of origin theory for HGSOC follows the adenoma-carcinoma pathway, beginning with FTE secretory cells, progressing into clonal expansion with the development of SIGs, then gaining a proliferative advantage as TICs, sloughing off onto the ovary and beyond as HGSOC[2,3]. Given the proximity of the fallopian tube fimbria to the ovary, the adhesive mesothelial surface of the OSE, and the late diagnosis of HGSOC, this theory is still consistent with the findings of end stage tumors which engulf both ovary and fallopian tube[25].

The Role of P53 in HGSOC

While P53 mutations appear necessary for HGSOC, occurring in the earliest identifiable precursors and maintained throughout the process of pathogenesis in nearly 100% of cases, they are by no means sufficient for transformation[5,6]. This is particularly evident in Li Fraumeni's syndrome, an inherited P53 germ line mutation, which is not associated with ovarian cancer even though the fallopian tubes of women with this disease are enriched for SIGs[26]. Not every BRCA carrier develops HGSOC, and germline or sporadic BRCA mutations still only account for approximately 20% of HGSOC, thus supporting the role of environmental factors[6,27,28].

Environmental Risk Factors

Our current understanding of the risk factors of HGSOC derives primarily from epidemiological data. Lifetime ovulation is positively correlated with HGSOC, and factors such as parity and birth control, which decrease lifetime ovulation, have a protective effect against HGSOC[29,30]. Alteration of hormone levels is also thought to affect a woman's risk for ovarian cancer, as oral contraceptives decrease hormone levels and have a protective effect on HGSOC[30,31]. IVF has also been correlated with increased risk, but it is unclear whether this is due to hormonal manipulation or the underlying infertility which is also a risk factor[32].

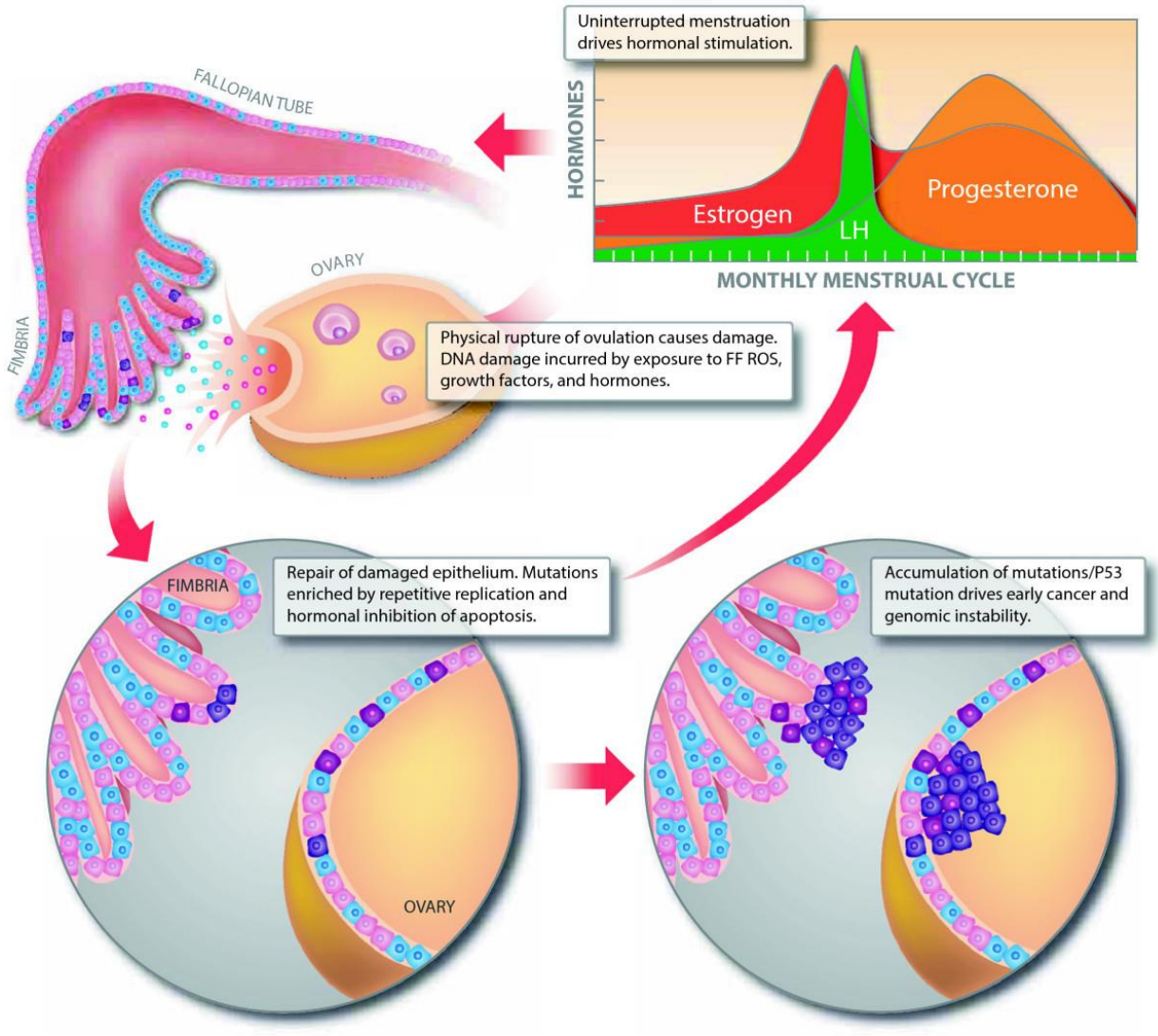

Figure 1.3: Proposed Mechanisms of HGSOC Pathogenesis.
(From Emori & Drapkin 2014 The Hormonal Composition of Follicular Fluid and Its Implications for Ovarian Cancer Pathogenesis.) Incessant Ovulation Hypothesis: monthly physical damage from ovulation necessitates increased cell proliferation during repair, eventually leading to genomic instability. Gonadotropin hypothesis: Exposure to hormones released during ovulation inhibits natural apoptosis, uninterrupted hormonal fluctuations stimulate differentiation, proliferation, and ultimately malignant transformation.

Current Hypotheses

Several hypotheses have been posited to explain how environmental factors such as menstruation and ovulation may lead to ovarian cancer (Figure 1.3). A long standing hypothesis, often called the Incessant Ovulation Hypothesis, suggests that the repetitive wounding and healing of the ovarian surface

epithelium and adjacent tubal epithelium that is induced by monthly ovulation increases cell proliferation and thus the likelihood of genomic instability which could lead to oncogenesis[29]. Another hypothesis, known as the Gonadotropin Hypothesis, implicates excessive direct and indirect stimulation of the ovarian surface epithelium by gonadotropins, leading to differentiation, proliferation, and ultimately malignant transformation[30]. More recently, the Incessant Menstruation hypothesis suggests that repeated exposure to retrograde menstruation exposes the ovary and fallopian tube to reactive oxygen species and oxidative iron from the blood[33]. Lastly, several recent papers have focused on damage induced by inflammation-mediated factors found in the follicular fluid[34,35]. The recurring theme is incessant ovulatory damage.

Models of Ovarian Cancer Progression from Fallopian Tube to Tumor

Ex Vivo Models of Fallopian Tube Epithelium

With rising interest in the fallopian tube as a likely origin of HGSOC, new experimental models of fallopian tube epithelium have evolved to study the molecular mechanisms behind early pathogenesis. One of the first models developed was an ex vivo culture system using primary human fallopian tubes from women undergoing salpingectomy for non-cancerous conditions[36,37]. This system preserves both the ciliated and secretory cell populations, as well as markers specific to the fallopian tube such as PAX8, Bcl-2, and TNFαIP2. Secretome analysis and microscopy further confirmed the ability of this system to recapitulate fallopian tube epithelium[36]. This system is limited by the need for a constant supply of fresh fallopian tubes as cultured cells, while capable of proliferation, will only survive for a few weeks[36,37].

A 3D model of primary fallopian tube epithelium has also been developed, which allows the cells to grow in spheroids[38]. These cells exhibit lower proliferation than their 2D counterparts, and are thought to more accurately represent the luteal phase of menstrual cycle. Similar 3D ex vivo culture models derived from mouse oviducts and adult baboon fallopian tubes have been reported[39].

Immortalized and Transformed Models of Fallopian Tube Epithelium

Human fallopian tube epithelium has also been successfully immortalized by a variety of different methods, which greatly extends the time cells can be cultured, but preserves only the secretory cells. Transfection with hTERT and SV40 T antigen is sufficient for immortalization, but these cells will not form xenografts without the addition of other factors such as H-Ras or c-Myc[40,41]. Baboon fallopian tubes have also been successfully immortalized with SV40 large and small T antigens[39].

To improve biological relevance, fallopian tube epithelium can be immortalized without the aid of viral oncogenes by using shRNA against p53 and mutant CDK4 to simulate viral induced pRb loss of function[40]. To transform these cells and produce xenografts in NOD.Cg-Prkdc^{scid}/Il2rg^{tm1Wjl}/SzJ (NSG) mice, c-Myc and shRNA against PP2A-B56γ can be added[40].

A genetically engineered mouse model capable of spontaneously generating ovarian cancer has also been developed which, via Cre-mediated recombination, targets fallopian tube Tp53, Pten, and either BRCA1 or BRCA2[42]. This model faithfully recapitulates the precursor lesions, histology, and metastatic potential of HGSOC.

Changing Models of Ovarian Cancer

While our deeper understanding of the origins of HGSOC has lead to recent advances in models of early ovarian cancer, most studies involving late stage ovarian cancer still focus on two widely used cell lines, SKOV3 and A2780[7]. These lines have a long history of robust performance both in vivo and in vitro, but little evidence is available about the details of their origins except that they were derived from the ascites of women with ovarian adenocarcinoma. Cell lines that faithfully recapitulate the disease they model are imperative if relevant results are to be obtained that can have a real impact on the clinic.

With the advent of comprehensive genome-wide analysis made possible through The Cancer Genome Atlas (TCGA), it is now possible for detailed comparison between the larger population of patient tumors and the much smaller set of cell lines used to study them[7,43,44]. In particular, research by

Domcke et al, published in 2013, analyzed 47 ovarian cancer lines and found that the most commonly published lines, including SKOV3 and A2780, were largely poor representatives of the genetic features of HGSOC. Specifically, these lines contained an overabundance of mutations in genes traditionally mutated in lower-grade ovarian cancers [7]. In contrast, the lines that most accurately represented HGSOC with characteristic mutations in P53, BRCA1/2 and virtually nowhere else, KURAMOCHI and OVSAHO, were virtually unexplored in published research[7].

While genetics is one important characteristic of cancer cell lines, many other factors are equally important in the larger picture of what makes a good cell line model of HGSOC. These include tractability both in vitro and in vivo, expression of clinically relevant proteins, and anatomical growth in cell culture and xenografts. Thus before these novel ovarian cancer lines can be put to efficient use in the research setting, a thorough analysis is called for to assess the utility of these lines.

Novel Ovarian Cancer Cell Lines

Two of the novel cell lines identified by Domcke et al as most genetically representative of ovarian cancer are OVSAHO and KURAMOCHI. OVSAHO was derived from an abdominal metastasis taken from a 56 year old Japanese woman diagnosed with stage IIIc serous ovarian adenocarcinoma and has been in culture since 1991[45]. It contains a mutation in TP53 and homozygous deletions in BRCA2 and RB1[7]. KURAMOCHI was derived from the ascites of a Japanese woman of unknown age diagnosed with undifferentiated ovarian carcinoma and has been in culture since 1982[46]. It contains mutations in both TP53 and BRCA2, and amplifications in both MYC and KRAS[7].

Paired Box Gene 8

PAX Family of Genes

Understanding fallopian tube development and regulation is the first step in understanding fallopian tube tumorigenesis. One particular gene of interest is PAX8, which plays an important role in both fallopian tube development and ovarian cancer. PAX8 is a member of the Paired Box (PAX) genes

which form a family of nuclear transcription factors that play a critical role in gene expression regulation during embryogenesis. First cloned from Drosophila in 1986, PAX genes are highly conserved across C. elegans, Drosophila, Xenopus, mice, and humans, as well as various fish and birds, and all help regulate segmentation and organ development[47,48]. The 9 PAX genes differ in their extra-paired box DNA binding regions, as well as their temporal and spatial expression, and can be divided into four evolutionarily distinct sub-groups (I- PAX1&9, II-PAX2, 5, & 8, III-PAX3&7, and IV- PAX4&6)[48].

PAX8 Structure

PAX8 is 450 amino acids long and contains the characteristic 128 amino acid PAX family paired domain responsible for DNA binding; PAX8 is also characterized by its octopeptide repeat and truncated homeodomain thought to regulate DNA binding[49]. The paired domain, octopeptide, and truncated homeodomain are all clustered in the N-terminal region while the C-terminus contains a transactivation domain which promotes the transcription of PAX8 target genes[50].

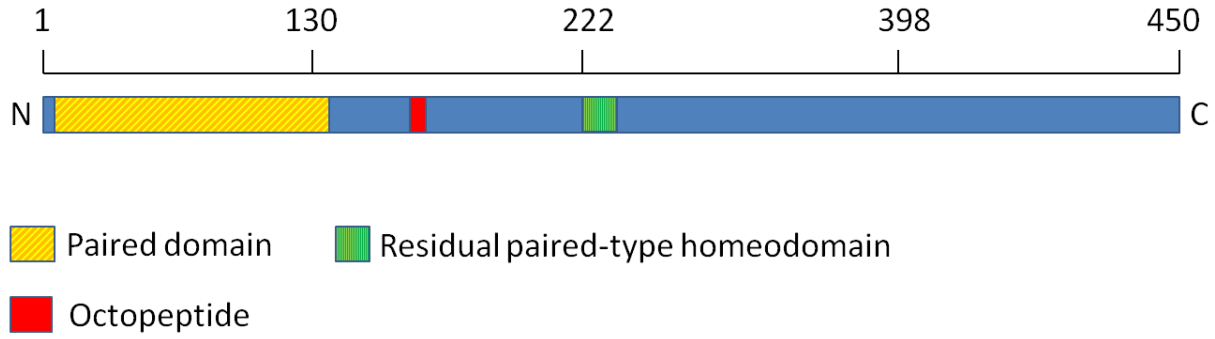

Figure 1.4: PAX8 Structure.
Diagram of PAX8 with amino acids 1 at the N-terminus (N) to 450 at the C-terminus (C). Paired domain, Residual paired-type homeodomain, and octopeptide marked in yellow, green, and red, respectively.

PAX8 contains 10 exons and the majority of PAX8 is expressed as full length isoform A with a MW of approximately 48kDA. Alternative splicing in the carboxy-terminus region generates an additional 5 isoforms whose expression is specific to developmental stages and locations within the embryo, but these shorter versions of PAX8 are rarely seen in adults[51,52]. All isoforms which retain the

paired box DNA binding domain appear to maintain their gene regulating functions, although their scarcity means much less is known about their function than their full length counterparts.

PAX8 Post-Translational Modifications

PAX8 is known to be post-transcriptionally modified. In vitro studies in rat thyroid cells have shown that PAX8 contains one sumoylation motif at lysine 309, and that the binding of small ubiquitin-like modifier (SUMO) stabilizes PAX8, leading to increased PAX8 levels within the cell[53]. Sumoylation of PAX8 does not affect either its DNA binding or transcriptional activating functions.

In rat cells, the oxidation of either cysteine 45 or 57 within the conserved paired box region resulted in a drop in both DNA binding and PAX8 transactivation[54]. Mutants lacking these cysteines have a much higher basal level of PAX8 function. Further research has indicated that regulation of this mechanism is controlled by glutathionylation[55]. It is likely that further post-translational modifications of PAX8 help to regulate DNA binding or transactivation, but more research is required on this topic.

PAX8 Expression during Development and Adulthood

In the mouse brain, PAX8 expression in the neural tube is first observed at embryonic day 10, and as the brain develops it localizes to the midbrain-hindbrain boundary[56]. By the time the mouse reaches 4 weeks of age, PAX8 expression is no longer present in the brain. In the mouse thyroid, PAX8 is first expressed beginning at embryonic day 10.5 and continues to maintain the epithelial phenotype of thyroid cells through adulthood[57,58]. In the mouse kidney, PAX8 expression begins early in development in the metanephros, and remains consistently expressed into adulthood[59,60]. PAX8 also plays a significant role in the paramesonepheric duct, also known as the Müllerian duct, which develops into the fallopian tubes, uterus, and parts of the cervix[61]. However, in the adult fallopian tube, PAX8 expression is confined to the secretory cells[62]. Importantly, PAX8 is not expressed in the ovary or ovarian surface epithelium at any time during development or adulthood[62].

In summary, PAX8 is expressed during development in the brain, kidney, thyroid, and Müllerian tract, but maintains expression only in the adult fallopian tube, kidney, and thyroid. It is not expressed in the ovary.

PAX8 Knockout Models

PAX8 -/- mice lack follicular thyroid cells and as a result will exhibit extreme growth defects and die from lack of thyroid hormone before weaning[63]. However, mouse growth and lifespan can be rescued when supplemented with thyroxine or similar thyroid hormone replacement therapy, making this model both tractable and informative. Consistent with PAX8 regulation of the developing Müllerian tract, PAX8-/- mice are infertile. Female PAX8 -/- mice lack a vaginal opening and retain only traces of smooth muscle and ligaments where the uterine horns should develop (Figure 1.5)[61]. Improperly functioning fallopian tube tissue fills with fluid to form large hydrosalpinges. Interestingly, the pituitary hormone levels, serum hormone levels, and ovarian structure and function were unaffected in thyroid hormone rescued PAX8 -/- mice[61]. Indeed, corpus lutea formation was indicative of successful ovulation. This suggests that the cause of infertility is located in the uterus and fallopian tube rather than the ovary, and is structurally and not hormonally based. Similarly, male thyroid hormone rescued PAX8-/- mice are also infertile, lacking proper ductal formation in the epididymis which leads to fluid buildup and lack of spermatozoa formation[64]. As with infertile female PAX8-/- mice, male hormone levels are within normal range, suggesting infertility due to structural and not hormonal defects.

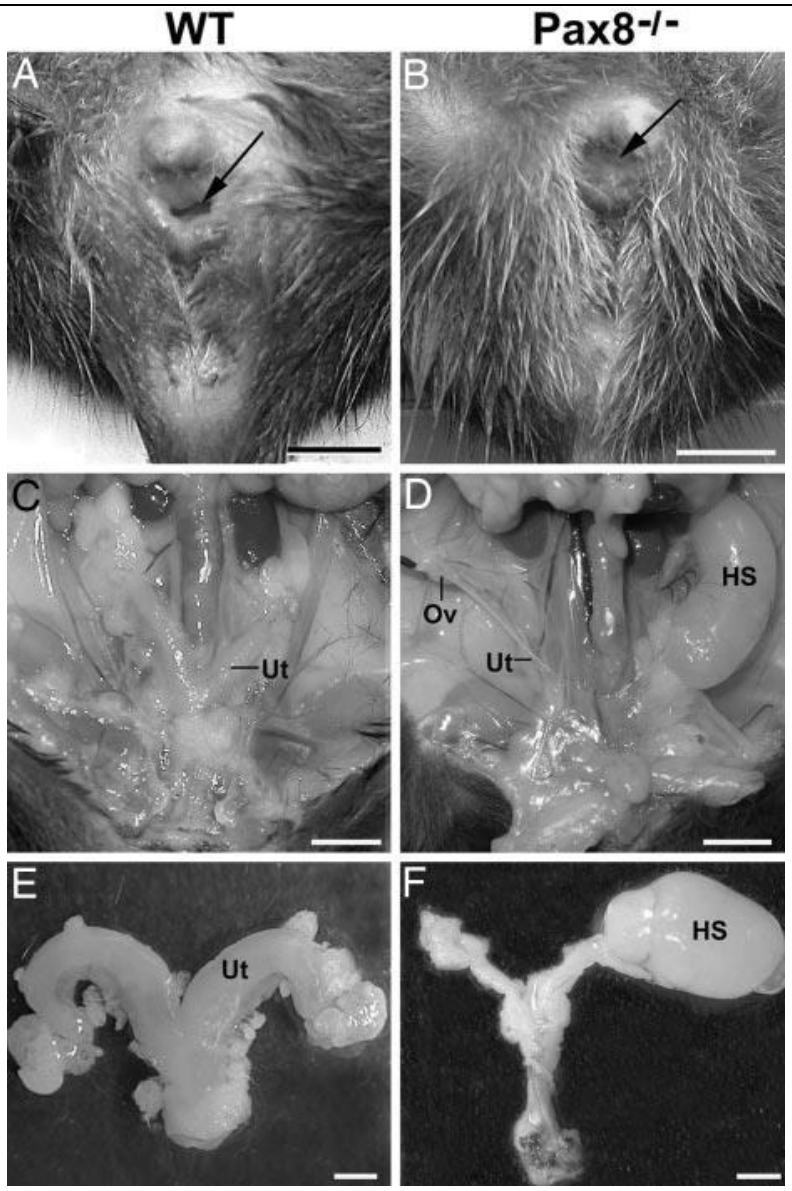

Figure 1.5: Anatomy of 6 month old female WT or PAX8-/- mice. (From Mittag et al 2007 Congenital Hypothyroid Female Pax8-Deficient Mice are Infertile Despite Thyroid Hormone Replacement Therapy) PAX8 -/- mice exhibit a lack of vaginal opening (black arrow) (B) present in WT mice (A). Where the uterine horns (UT) normally develop in WT mice (C,E), only fragments of connective tissue can be identified in PAX8-/- mice (D, F). Lastly, fluid engorged fallopian tubes, or hydrosalpinges (HS) can be found in PAX8-/- mice (D, F). Ov- Ovary.

PAX8 Mutations in Humans

PAX8 can also be found mutated in humans and accounts for a small percent of familial and sporadic congenital hypothyroidism cases. Unlike in mice, the vast majority of PAX8 mutations in

humans are heterozygous, and this is sufficient to induce a severe lack or loss of thyroid hormone production[65]. Individuals affected by PAX8 loss of function mutations generally present with a severe growth deficit, and if left untreated, intellectual disabilities may result[63,66]. However, recent genetic studies suggest a high rate of variability in phenotype among individuals with PAX8 mutations. Family members sharing the same PAX8 mutation had varying levels of serum thyroid stimulating hormone and even varying ages at which the growth deficit developed[65]. Fortunately, prenatal screening and early supplementation with thyroid hormone mean this condition is readily treatable. Modern genetic sequencing confirms that both males and females with PAX8 mutations who have been treated with thyroid hormones are fertile and capable of reproduction[65]. Whether reproduction is feasible for untreated individuals is difficult to discern, as before the advent of hormone replacement therapy the severity of growth and mental defects would have likely prohibited reproduction. It is currently unknown if a subset of infertility cases can be attributed to undiagnosed PAX8 mutations.

PAX8 in Cancer

While PAX8 expression is suppressed in most adult tissues, PAX8 expression has been shown to be upregulated in several cancers. Notably, the cancers in which PAX8 is expressed are largely those in which PAX8 plays a role in development. PAX8 is expressed in 91% of thyroid tumors, and in follicular thyroid cancer, PAX8 undergoes a fusion with PPARɣ in as many as 50% of cases[67–69]. This fuses the promotor and DNA binding regions of PAX8 to the cellular differentiation and proliferation regulating regions of PPARɣ, which is not normally found in the thyroid. The result is a highly expressed, oncogenic fusion protein. In the kidney, PAX8 is prominently expressed in both nephrogenic adenomas and clear cell adenomas, and may be useful as a biomarker to differentiate between these and other adenocarcinomas of the kidney and bladder[70]. In Wilms tumor, a rare form of kidney cancer affecting children, relatively high levels of alternate PAX8 isoforms have been shown to be expressed similar to what would be shown in the developing kidney, but mutations in PAX8 are negligible in these tumors[52,71]. Recent studies have suggested that PAX8 may also play a role in brain cancer, with PAX8 expression

highly enriched in glioblastomas as compared to lower-grade gliomas or PAX8 negative normal brain cells[72]. PAX8 expression in glioblastomas correlated with telomerase-negative tumors, and in vitro experiments showed PAX8 silencing by siRNA resulted in decreased proliferation and the downregulation of other proteins associated with poor prognosis[72]. PAX8 is expressed in many genitourinary cancers, consistent with its role in Müllerian development[67]. During a comprehensive screen, a small percent of pancreatic, lung, and esophageal cancers were also found to express PAX8, but this has yet to be followed up with further research[67].

PAX8 and Ovarian Cancer

PAX8 is strikingly expressed in 99% of high grade serous ovarian cancers (HGSOC)[67]. This fact was crucial to establishing the link between fallopian tubes and ovarian cancer as both express PAX8. In contrast, the ovarian surface epithelium which was once considered the origin for HGSOC does not express PAX8 during development or adulthood[62,67]. PAX8 is also expressed in a large number of ovarian clear cell carcinomas, mucinous and endometrioid adenocarcinomas, and other ovarian tumors of potential Müllerian origin[67]. Although PAX8 appears to function primarily as a lineage marker and is not currently thought to have any oncogenic function in ovarian cancer, it is generally expressed at higher levels in ovarian cancer as compared to fallopian tube epithelium[73]. PAX8 has also proven to be a very useful diagnostic tool. Studies have shown that PAX8 is a successful biomarker for identifying malignancies of Müllerian origin[74,75]. This is particularly helpful in ruling out metastatic intestinal or breast cancer, which commonly present similarly to late stage ovarian cancer. It is important to note that while PAX8 is both sensitive and specific to cells of Müllerian origin, this may include endometriosis, renal cell carcinoma, and endosalpingiosis ; thus, in diagnostic pelvic washes or ascites, the tandem use of other biomarkers such as Calretinin and PAX2 can help further classify tissue as benign or cancerous[75].

Project Achilles, a systematic screen of genetic weaknesses across cancer lines, identified PAX8 as differentially expressed in ovarian cancer as well as amplified in 16% of HGSOC[73]. ShRNA screens further identified PAX8 as an essential gene, with PAX8 silencing leading to decreased proliferation

across a variety of ovarian cancer cell lines[73]. Mild PARP cleavage in two cell lines treated with shRNA against PAX8 suggests an apoptotic mechanism[73]. The fact that PAX8 expression is unique to, yet pervasive within HGSOC, makes it of interest as therapeutic target. However, transcription factors are notoriously difficult to target in vivo, meaning a deeper understanding of PAX8's function and binding partners is required for it to be a viable candidate.

PAX8 Cofactors

Our understanding of PAX8 function comes almost exclusively from thyroid cells, and the most common cell lines in which PAX8 is studied are derived from rat. It is unknown how much PAX8 function is dependent upon tissue type and species, and indeed there is very little overlap in findings identified in different tissue types. Therefore the interactions and targets identified should be taken out of their experimental context with caution until they have been re-validated in the system of interest.

In the rat thyroid, retinoblastoma protein (pRb), thyroid transcription factor 1 (TTF-1), tafazzin (TAZ), and p300 have been identified as co-factors of PAX8 which help to induce the target gene expression and regulation[76–78]. Two other co-factors of PAX8, Mothers against decapentaplegic homolog 3 (Smad3) and Poly(ADP-ribose) Polymerase1 (PARP1) bind to PAX8 and subsequently decrease PAX8's ability to bind DNA[79,80]. In mouse embryonic fibroblasts and monkey kidney cells, two PAX8 co-factors, ID2 and ID3 bind to the PAX8 protein's DNA binding region and decrease PAX8's ability to complex with DNA[81].

PAX8 Regulation of Target Genes

As a transcription factor, PAX8's primary role is to bind to DNA and regulate gene expression. While most of PAX8's putative target genes have been identified outside the context of the fallopian tube, non-biased ChIP based assays and gene expression profiling gives us insight into the broader pathways in which PAX8 plays a role.

In the rat thyroid, PAX8 inhibits apoptosis through a tumor protein 53 induced nuclear protein 1 (tp53inp1) mediated pathway, but direct binding to the gene has not been established[82]. In mouse thyroid, it has been suggested that PAX8 is capable of autoregulation and can bind to its own promoter region[83]. A genome wide analysis of rat thyroid cells revealed that PAX8 binds to the promoter regions of sodium iodide symporter (NIS) and thyroperoxidase (TPO)[84]. Validation by qRT-PCR also indicated PAX8 was able to regulate BRCA1, CDH16, MYOVB, RAB17, DAB2IP, DIO1, TMOD1, Rab17, Trib1, Wnt4, Tg, Kcnj16, Cdh16, Foxe1, Runx2, Cited2, TAZ, and Sparc[84,85].

In the kidney, PAX8 has been suggested to directly bind to and regulate Gata binding protein 3 (GATA3), the apoptotic regulator BCL-2, and Wilms' tumor 1 (WT1) during development[86,87,88]. In human gliomas, PAX8 has been shown to bind directly to the promotor regions of both telomerase reverse transcriptase (hTERT) and telomerase RNA component (hTR), and to increases telomerase expression and function[89].

In general, PAX8 has been shown to bind preferentially to intronic regions (82%), specifically CPG islands and CG repeats, binding in only 6% of cases to coding regions and 2% of cases to 5' untranslated regions[84]. Gene Ontology (GO) analysis of the most extensive gene expression profiling analysis of PAX8 function to date, performed in rat thyroid cells, indicates that PAX8 is involved in such expected areas as organ development, pathways in cancer, the Wnt pathway, cell migration, and cell division, as well as less expected areas including the cell cycle, DNA replication, apoptosis, several mitochondrial functions, and the metabolism of several amino acids[85]. Despite the importance of PAX8 to fallopian tube development and ovarian cancer, the role of PAX8 in these tissues is largely underrepresented in current literature.

CHAPTER 2

Evaluating the Utility of Novel Cell Lines as Ovarian Cancer Models

Acknowledgements

This work was performed by Meg Emori, Kevin Elias, and Emily MacDuffie. Meg Emori maintained cells in culture, and performed western blotting and CA-125 analysis. Emily MacDuffie performed cisplatin sensitivity assays. Kevin Elias was responsible for luciferizing the cell lines. DFCI ARF staff injected xenografts into mice and performed luminol imaging, while Meg Emori performed subsequent imaging analysis and quantification. Meg Emori and Emily MacDuffie carried out weekly tumor and weight measurements, and tumor removal and dissection was performed primarily by Kevin Elias with assistance from Meg Emori. Tumor embedding, sectioning, and staining were outsourced to Mei Zheng. Novel tumor cell lines were graciously supplied by Gottfried Konecny at UCLA and Victor Velculescu at from Johns Hopkins generated all the genomics data. Text in this chapter relies heavily on the manuscript "Beyond genomics: critical evaluation of cell line utility for ovarian cancer research" on which Kevin Elias and Meg Emori are co-first authors with shared writing responsibilities.

Introduction

Once thought to be a single disease arising from the ovary, in the last decade ovarian cancer has been shown to be a heterogeneous disease with origins across the female reproductive tract[24]. The revelation that ovarian cancer is not one disease but many different cancers sharing the same end location has drastically changed the way we study pathogenesis and treatment. Slowly, it has also begun to change the way we think about modeling ovarian cancer at the lab bench[40].

The ability to successfully translate a discovery at the lab bench to the patient's bedside depends largely on the quality of the disease model. Established cell lines provide a solid foundation for cancer research given their potential to proliferate indefinitely, their ease of access to investigators around the world, and our well established understanding of their genetics and behavior. With the advent of The Cancer Genome Atlas (TCGA), it has recently become possible to compare the genetics of these well-established cell lines with the genetics of actual patient samples whose disease the cell lines represent[43,90].

Strikingly, reports by Domcke, et al and Anglesio, et al suggest that the most highly utilized ovarian cancer cell lines poorly represented the majority of ovarian cancers[7,44]. These lines, specifically SKOV3 and A2780, are the preferred models for researchers in vitro and in vivo because they are easy to transfect and form discrete, fast growing tumors[91–95]. While Domcke, et al clearly show that from a purely genetic level, other lines such as KURAMOCHI and OVSAHO are more closely representative of patient tumors, little is known about the tractability of these lines from the research perspective[7].

In an effort to better characterize these high fidelity genomic lines, we sought to conduct a series of in vivo and in vitro experiments that characterize these lines in terms of their transfectability, their sensitivity to traditional HGSOC chemotherapy, and their expression of various proteins associated with HGSOC, as well as their ability to form tumors in various immunocompromised mouse models. Ultimately, we hope to establish a set of standards that compare and characterize novel ovarian cancer cell lines prior to their widespread use.

Results

KURAMOCHI and OVSAHO cells were selected for characterization as they are the two models of HGSOC with the highest genomic fidelity to patient samples yet have only 10 publications between them[7]. SKOV3 cells were chosen as a control line for comparison as historically it has been one of the most commonly used, with over 2,000 publications, and is therefore one of the most well characterized ovarian cancer models available, even though it has relatively low genomic fidelity to HGSOC[7].

Genomic Properties of KURAMOCHI, OVSAHO, and SKOV3 Cells

First, detailed genetic analysis was performed by collaborators at Johns Hopkins identifying mutations, amplifications, and deletions in the traditional ovarian cancer cell line SKOV3 as well as two novel ovarian cancer cell lines, KURAMOCHI and OVSAHO (Table 2.1). SKOV3 was found to have twenty-five mutations in genes known to be relevant to human cancer, whereas OVSAHO and KURAMOCHI had significantly lower mutation rates, with five and six mutations, respectively.

Consistent with ovarian cancer genomics, all three cell lines contained mutations in tp53. NF1 was mutated in both SKOV3 and OVSAHO, and ATM was mutated in both SKOV3 and KURAMOCHI. Copy number variation identified a deletion in CDKN24 and an amplification of ERBB2 in SKOV3 cells. OVSAHO had only one amplification in FGFR4 and KURAMOCHI had amplifications in both KRAS and MYC (Table 2.1). While few mutations are typical of HGSOC, targeted genomic analysis fails to capture the significant copy number variation that is the signature of this disease. Whole genome analysis has previously estimated that KURAMOCHI and OVSAHO have 54% and 43% of their genome altered by copy number variation, respectively, while copy number changes are much lower in SKOV3 with only 14% of the genome impacted by copy number variation[7].

Table 2.1: Genetic Properties of Ovarian Cancer Cell Lines
Mutations, amplifications, and deletions in SKOV3, OVSAHO, and KURAMOCHI cells. Amino acid alteration, mutation type, and phenotypic consequence displayed for each altered gene.

Cell Line	Gene ID	Amino Acid	Mutation Type	Consequence
SKOV3	ABL1	964A>V	Substitution	Nonsynonymous coding
	AKT1	293F>L	Substitution	Nonsynonymous coding
	APC	2735G>R	Substitution	Nonsynonymous coding
	ARID1A	658S>G	Substitution	Nonsynonymous coding
	ARID1A	1873P>H	Substitution	Nonsynonymous coding
	ARID1A	586Q>X	Substitution	Nonsense
	ARID1B	2177M>V	Substitution	Nonsynonymous coding
	ATM	NA	Substitution	Splice site acceptor
	ERBB4	534E>G	Substitution	Nonsynonymous coding
	FGFR2	560P>H	Substitution	Nonsynonymous coding
	FLT3	450A>V	Substitution	Nonsynonymous coding
	FLT3	59S>A	Substitution	Nonsynonymous coding
	HNF1A	447P>S	Substitution	Nonsynonymous coding
	IGF1R	218T>M	Substitution	Nonsynonymous coding
	MLH1	NA	Large Indel	Large Indel
	NF1	1171K>M	Substitution	Nonsynonymous coding
	NF1	1702G>C	Substitution	Nonsynonymous coding
	NOTCH2	NA	Deletion	Frameshift
	PAX5	111A>D	Substitution	Nonsynonymous coding
	PIK3CA	1047H>R	Substitution	Nonsynonymous coding
	RB1	NA	Deletion	Frameshift
	ROS1	139L>V	Substitution	Nonsynonymous coding
	SMARCB1	9T>I	Substitution	Nonsynonymous coding
	STAG2	1124T>N	Substitution	Nonsynonymous coding
	TP53	NA	Deletion	Frameshift
OVSAHO	NF1	1720E>D	Substitution	Nonsynonymous coding
	PMS2	671T>M	Substitution	Nonsynonymous coding
	PMS2	485T>K	Substitution	Nonsynonymous coding
	TET2	457A>S	Substitution	Nonsynonymous coding
	TP53	342R>X	Substitution	Nonsense
KURAMOCHI	ATM	1644M>T	Substitution	Nonsynonymous coding
	BRCA2	2318R>X	Substitution	Nonsense
	TP53	281D>Y	Substitution	Nonsynonymous coding
	SMAD4	363C>S	Substitution	Nonsynonymous coding
	GNAS	160R>C	Substitution	Nonsynonymous coding

Cell Line	Gene ID	Mutation Type	Fold Amplification
SKOV3	CDKN2A	Deletion	NA
	ERBB2	Amplification	4.6
OVSAHO	FGFR4	Amplification	3.6
KURAMOCHI	KRAS	Amplification	10.6
	MYC	Amplification	3

In Vitro Properties of KURAMOCHI and OVSAHO Cells

While genetic characterization of novel ovarian cancer cell lines is the first step to better understanding their utility as a model of ovarian cancer, it fails to describe the important phenotypes that also differentiate cell lines and impact the choice of what cell line to use. Here we describe the physical and functional attributes of two novel ovarian cancer cell lines, KURAMOCHI and OVSAHO, and compare them to one of the most published and studied traditional ovarian cancer lines, SKOV3.

First, KURAMOCHI, OVSAHO, and SKOV3 cells were cultured in two-dimensional polystyrene tissue culture plates and imaged via phase contrast microscopy. KURAMOCHI cells grow in the classical cobblestone shape characteristic of carcinomas with prominent nucleoli and marked cytologic atypia, while OVSAHO cells form small rosettes and micropapillary structures consistent with HGSOC histology (Figure 2.1). In contrast, SKOV3 cells grown in a spindle-like manner with dendritic-like projections.

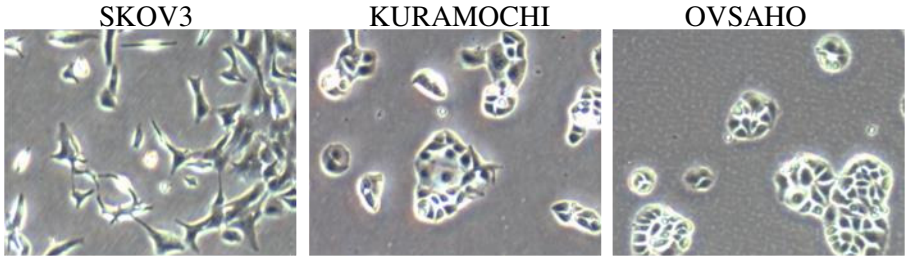

Figure 2.1: Cellular Morphology of Novel Ovarian Cancer Cell Lines
Bright microscope images of SKOV3, KURAMOCHI, and OVSAHO cell lines showing spindle-like growth in SKOV3 cells, cobblestone growth with prominent nucleoli in KURAMOCHI cells, and small rosette like growth with micropapillary structures in OVSAHO cells.

HGSOC is identified clinically by a series of protein markers. This is especially useful in differential diagnoses between müllerian derived malignancies and metastases that preferentially migrate to the ovarian surface epithelium such as colorectal cancer[96]. Novel and traditional ovarian cancer cell

lines as well as various controls were analyzed by western blot for expression of four common markers: PAX8, P53, CK7, and stathmin (Figure 2.2). As expected, PAX8 is expressed exclusively by fallopian tube and ovarian cancer cell lines. Similarly, stathmin, a marker of proliferation and early ovarian cancer pathogenesis, is present in all cultured cell lines[97]. All ovarian cancer cell lines expressed P53, indicating a stabilizing mutation; the exception is SKOV3, which has a known truncation resulting in the deletion of the protein (Table 2.1). The nonsense mutation in tp53 resulting in a premature stop codon previously identified by genetic analysis in OVSAHO (Table 2.1) is confirmed by its smaller molecular weight (Figure 2.2). Surprisingly, neither OVSAHO nor KURAMOCHI expressed CK7, a differential marker for detecting between ovarian cancer and metastases of extra-ovarian origin.

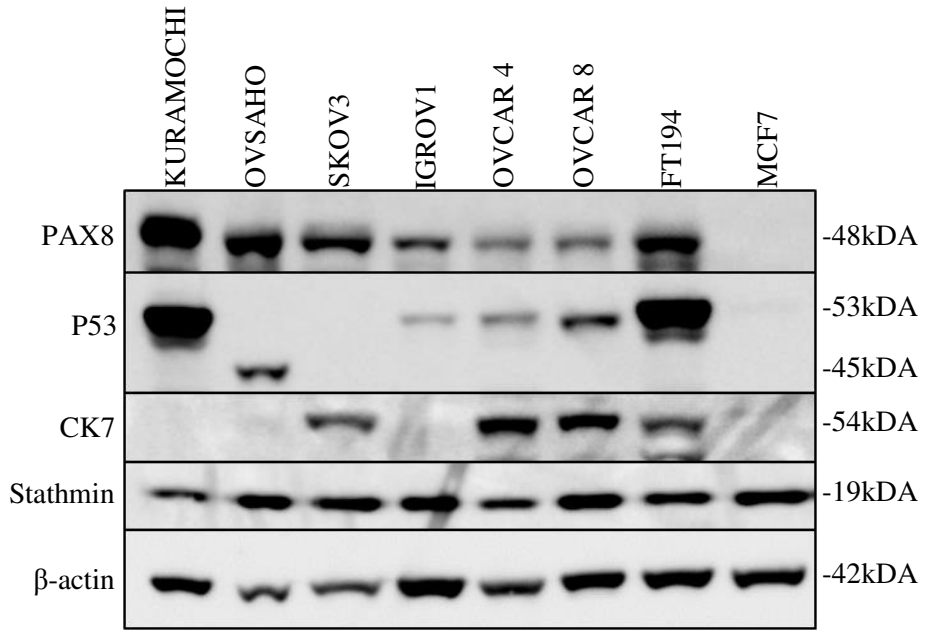

Figure 2.2: Expression of Clinical Markers of Ovarian Cancer in Novel Cell Lines
Western blot analysis of cell lysates measuring relevant markers of ovarian cancer including PAX8, P53, CK7, and Stathmin. Novel ovarian cancer cell lines KURAMOCHI and OVSAHO compared against traditional ovarian cancer cell lines SKOV3, IGROV1, OVCAR4, OVCAR8, immortalized fallopian tube line FT194, and breast cancer contol MCF7.

Levels of secreted protein CA-125 are commonly used as a biomarker clinically to track ovarian cancer recurrence[98]. It is estimated that CA-125 levels are elevated in 75% of ovarian cancers[98]. Concentrated conditioned media was harvested from cell lines and analyzed by ELISA and western blot for CA-125 levels (Figure 2.3). SKOV3 is known not to express CA-125, while S3 HeLa cells served as a positive control[99]. In both ELISA and western blot analysis, S3 HeLa cells were positive for CA-125 while SKOV3, KURAMOCHI, and OVSAHO CA-125 levels were equivalent to RPMI control media.

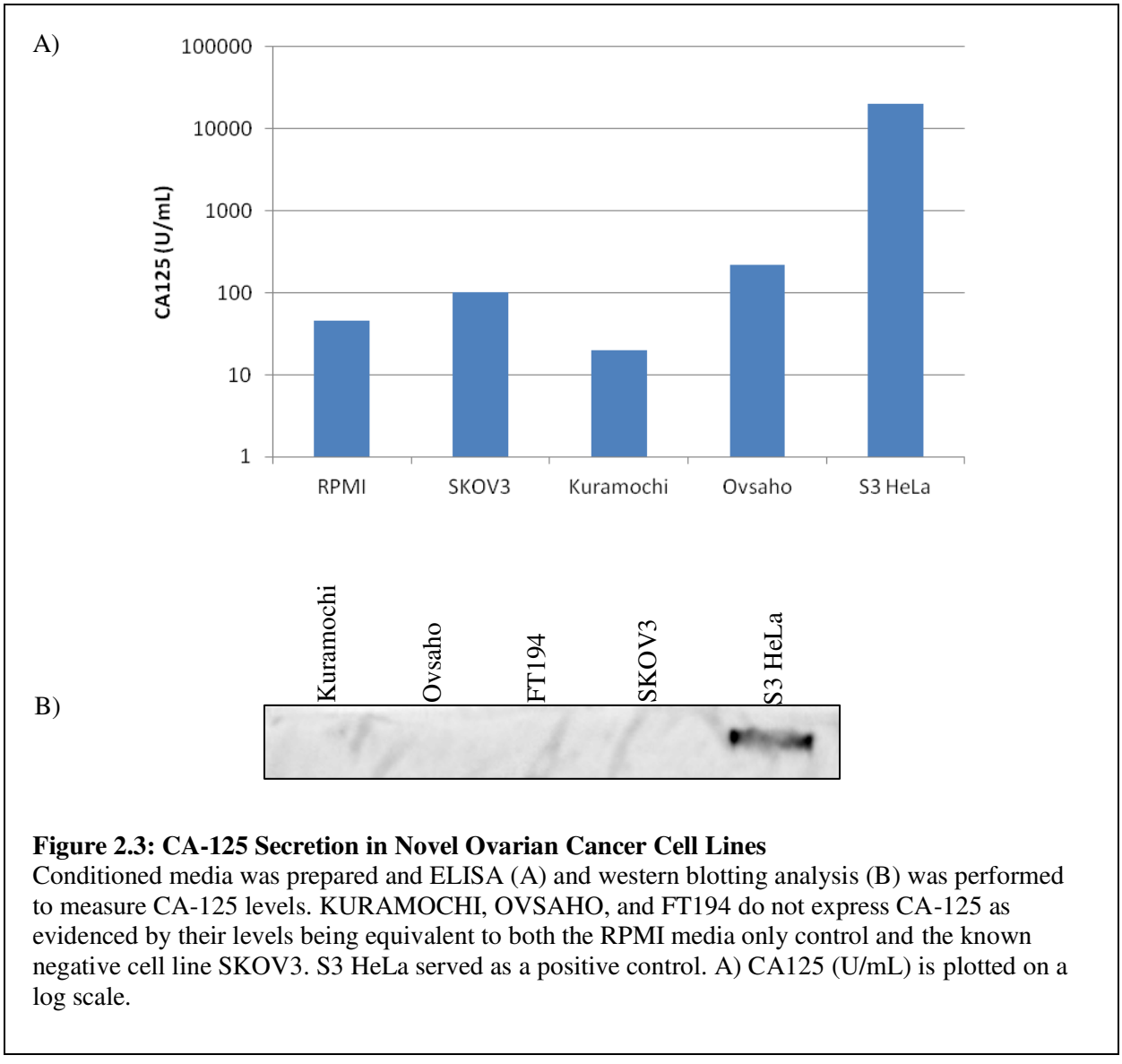

Figure 2.3: CA-125 Secretion in Novel Ovarian Cancer Cell Lines
Conditioned media was prepared and ELISA (A) and western blotting analysis (B) was performed to measure CA-125 levels. KURAMOCHI, OVSAHO, and FT194 do not express CA-125 as evidenced by their levels being equivalent to both the RPMI media only control and the known negative cell line SKOV3. S3 HeLa served as a positive control. A) CA125 (U/mL) is plotted on a log scale.

Platinum Sensitivity in KURAMOCHI and OVSAHO Cells

Ovarian cancer is largely initially sensitive to platinum-based chemotherapy, but tends to develop resistance during recurrence[100–104]. To measure platinum sensitivity in the novel ovarian cancer cell lines, SKOV3, KURAMOCHI, and OVSAHO cells were treated with cisplatin and IC50 concentrations were calculated (Figure 2.4). OVSAHO had a nearly identical IC50 to SKOV3 at 5.450 and 5.986μg/mL, respectively, whereas KURAMOCHI was significantly more sensitive to cisplatin treatment with an IC50 of 3.001 μg/mL ($p<0.0001$).

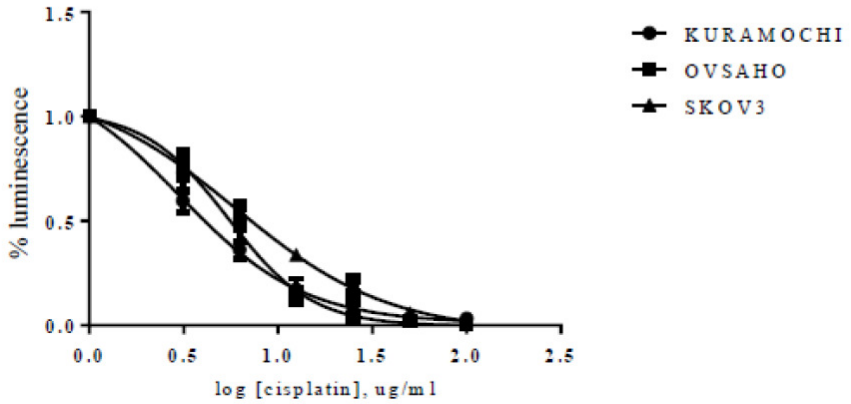

Cell Line	IC50	95% CI	p-value compared to SKOV3	p-value compared to OVSAHO
KURAMOCHI	3.001	2.321 – 3.881	0.0002	<0.0001
OVSAHO	5.450	4.794 – 6.196	0.49	--
SKOV3	5.986	5.075 – 7.059	--	0.49

Figure 2.4: Platinum Sensitivity in Novel Ovarian Cancer Cell Lines
OVSAHO, KURAMOCHI and SKOV3 cells were treated with Cisplatin for 96 hours and cell viability was measured via luminescence. SKOV3 and OVSAHO cells had approximately the same level of cisplatin resistance with IC50s of 5.987 and 5.450, respectively, while KURAMOCHI cells were significantly more sensitive to cisplatin with an IC50 of 3.001 ($p<.0001$)

Tumor Xenografts of KURAMOCHI and OVSAHO in Nude Mice

Athymic (nude) mice are the most common model system for tumor xenografts, with SKOV3 or A2780 cells the most common cell lines used in xenograft models. However, the tumorigenic properties of KURAMOCHI and OVSAHO have not yet been studied. First, cell lines were luciferized with an mCherry-Luc construct to enable bioluminescent imaging. 2.5 million cells were injected intraperitoneally with dPBS injected into control mice. Imaging at 13 days post-injection revealed tumor presence in all mice (Figure 2.5). At 27 days post-injection SKOV3 and KURAMOCHI tumors maintained a significant tumor burden, but OVSAHO tumors remained small. Observation time for OVSAHO was extended to 46 days post-injection, but even this was insufficient to enable tumor growth, and in fact some tumors showed signs of natural clearance (Figure 2.5). No OVSAHO tumors were found upon autopsy, preventing histological analysis.

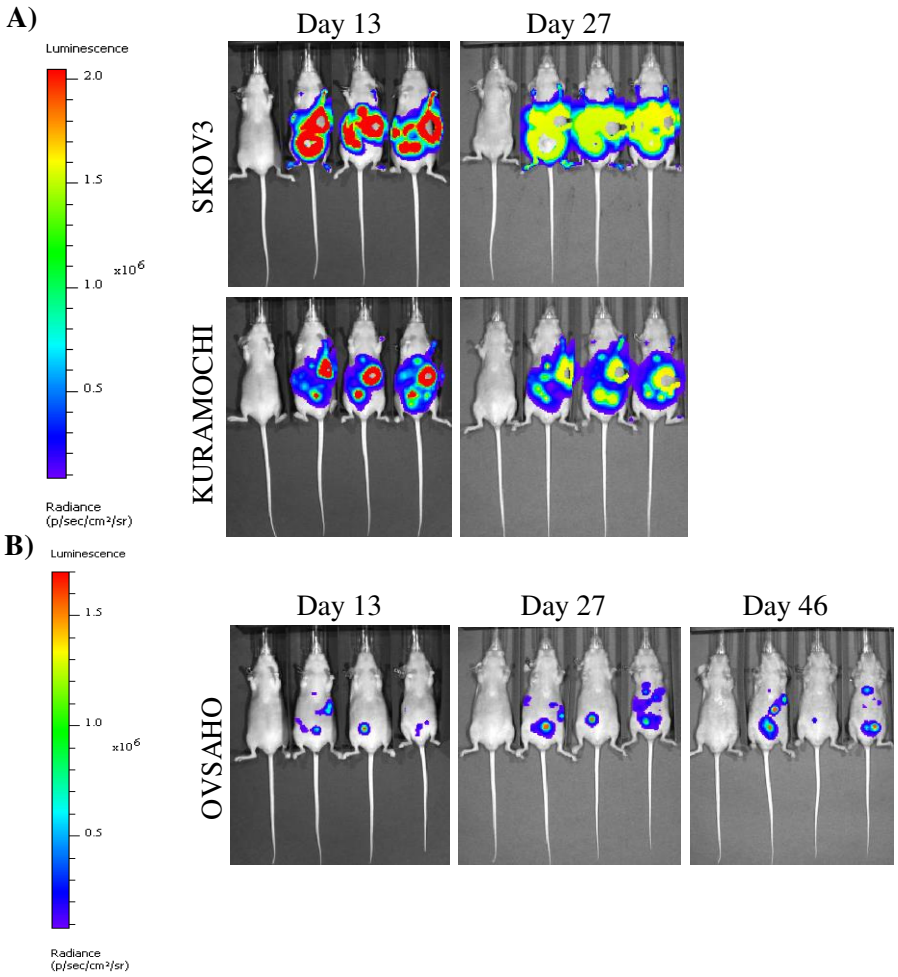

Figure 2.5: Bioluminescent Imaging of IP Xenografts in Nude Mice
Nude mice were injected with 2.5 million cells luciferized SKOV3, KURAMOCHI, or OVSAHO cells. A) SKOV3 and KURAMOHI tumors were imaged at day 13 and 27 and significant tumor burden was observed. B) OVSAHO tumors were imaged at day 13 and 27 with minimal tumor burden. Experiment time was expanded to day 46 but tumor burden did not significantly increase.

Tumor Xenografts of KURAMOCHI and OVSAHO in NSG Mice

Because tumor growth was stagnant in nude mouse models, we sought to test their tumor forming potential in a more severely immunocompromised model, NSG mice. The more compromised the immune system, the less likely the tumors will be cleared by the mouse. Luciferized SKOV3, KURAMOCHI, and OVSAHO tumors were injected at the increased load of 5 million cells intraperitoneally or subcutaneously. Although intraperitoneal tumors are more faithful to the physiology

of ovarian cancer, subcutaneous tumors are well contained and were included to alleviate the previous issues with locating tumors upon autopsy.

Subcutaneous tumors were measured weekly by calipers, and bioluminescent imaging was performed regularly on both intraperitoneal and subcutaneous models (Figure 2.6). Bioluminescent imaging was capable of picking up residual tumor signal even when tumors were no longer detectable via calipers (Figure 2.7). In subcutaneously injected mice, SKOV3 tumors grew continuously, with the largest tumor reaching nearly 250mm^3 by the end of the study. In contrast, KURAMOCHI subcutaneous tumors remained small but detectable after initial injection swelling had decreased and ranged from 4-13mm^3. OVSAHO subcutaneous tumors were the least stable, regressing continuously over the five weeks from an initial volume of nearly 30mm^3 down to nearly 0mm^3 by the third week.

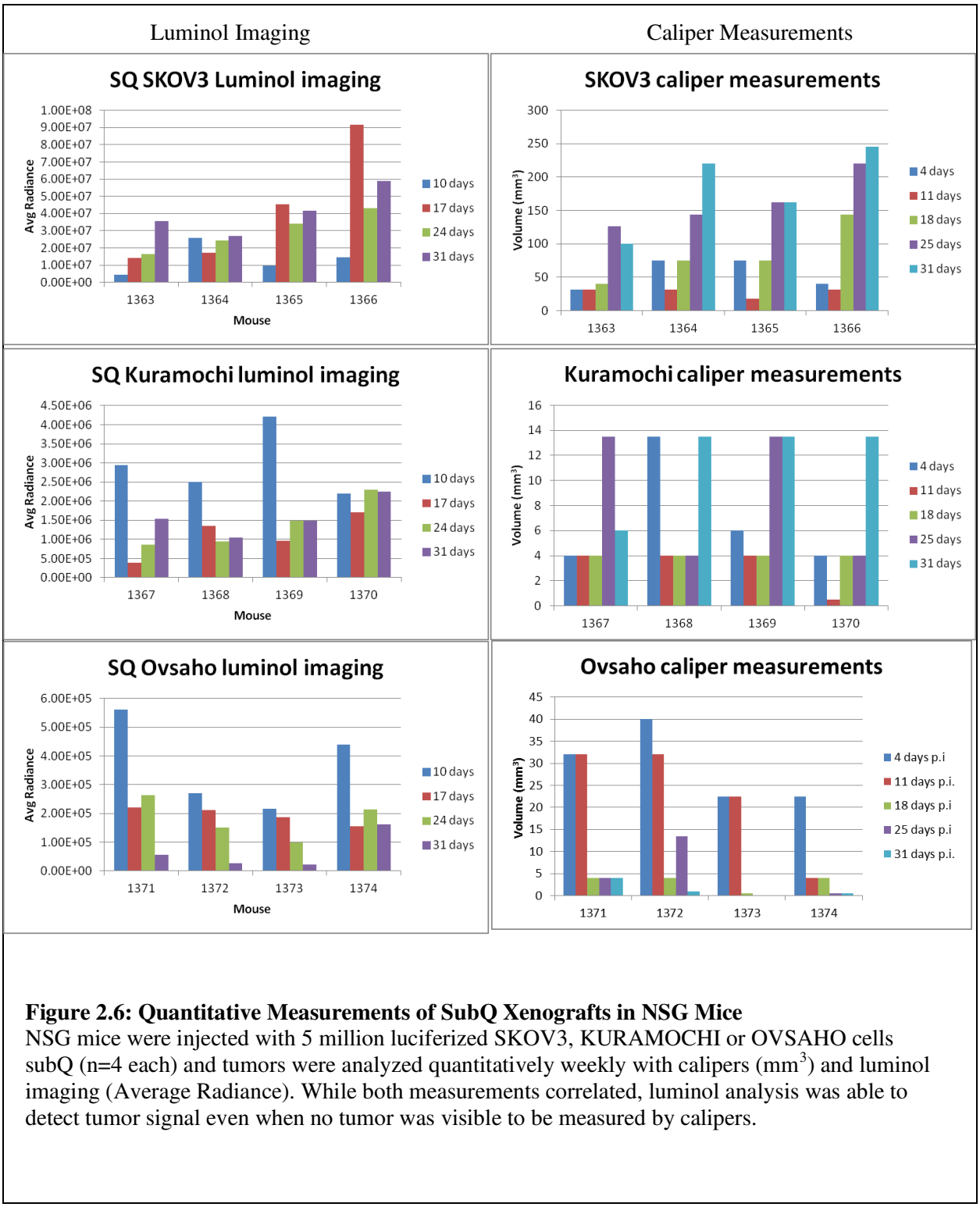

Figure 2.6: Quantitative Measurements of SubQ Xenografts in NSG Mice
NSG mice were injected with 5 million luciferized SKOV3, KURAMOCHI or OVSAHO cells subQ (n=4 each) and tumors were analyzed quantitatively weekly with calipers (mm^3) and luminol imaging (Average Radiance). While both measurements correlated, luminol analysis was able to detect tumor signal even when no tumor was visible to be measured by calipers.

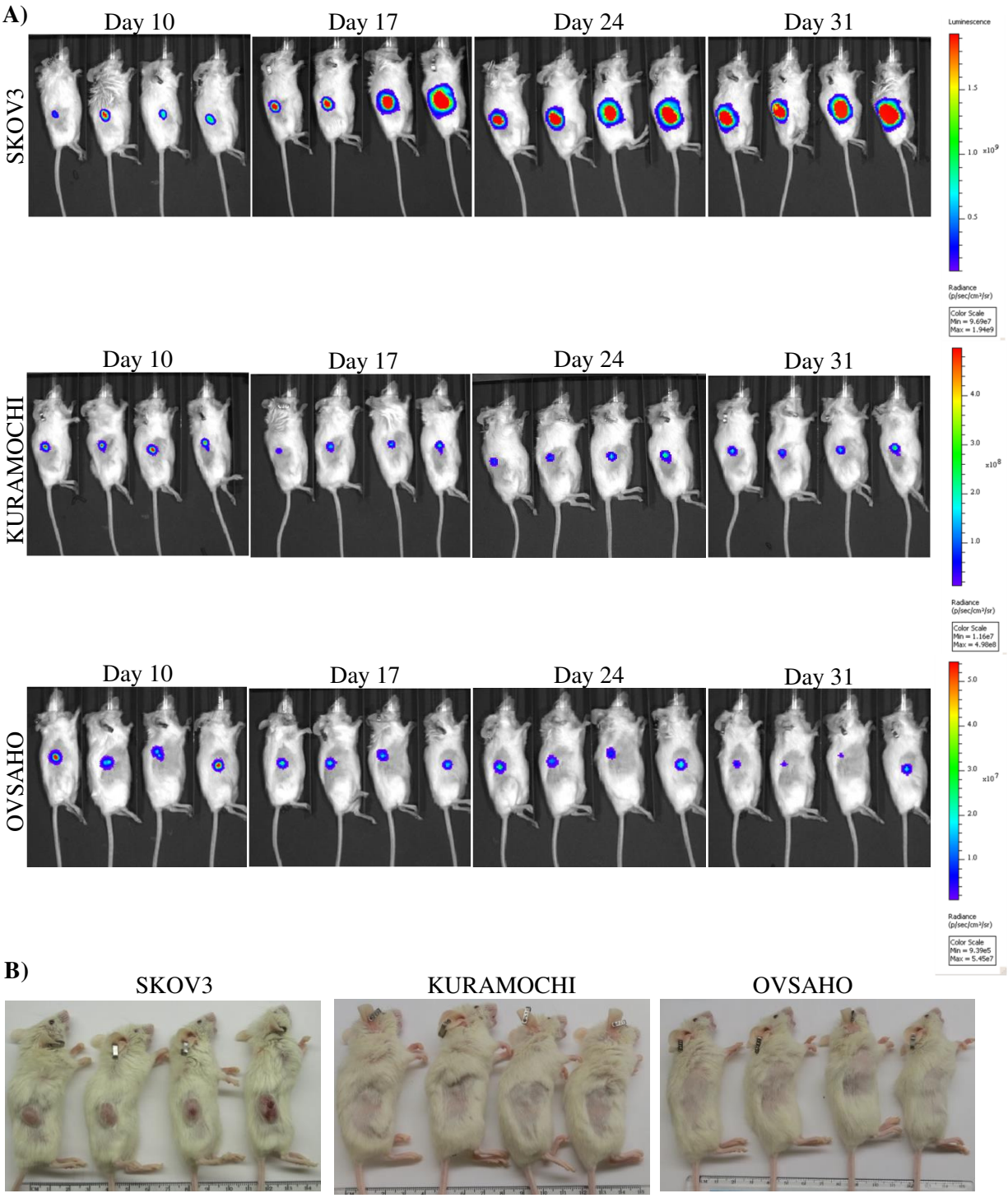

Figure 2.7: Tumor Visualization of SubQ Xenografts in NSG Mice
A) NSG mice were injected with 5 million luciferized SKOV3, KURAMOCHI or OVSAHO cells subQ (n=4 each) and bioluminescent imaging was performed at day 10, 17, 24, and 31. B) At 31 days images were taken to show outwards appearance of xenografts prior to autopsy. SKOV3 mice had large tumors, whereas KURAMOCHI mice had small residual nodules at the injection site and OVSAHO tumors were too small to see or palpate.

Tumors were removed at autopsy and all subcutaneous nodules stained positive for PAX8, confirming bioluminescent imaging (Figure 2.8). On the histological level, SKOV3 tumors were predictably large and expansile, while KURAMOCHI tumors were found to form small, compact nodules. OVSAHO tumors were microscopic and surrounded by fiberous tissue, indicating a desmosplastic response.

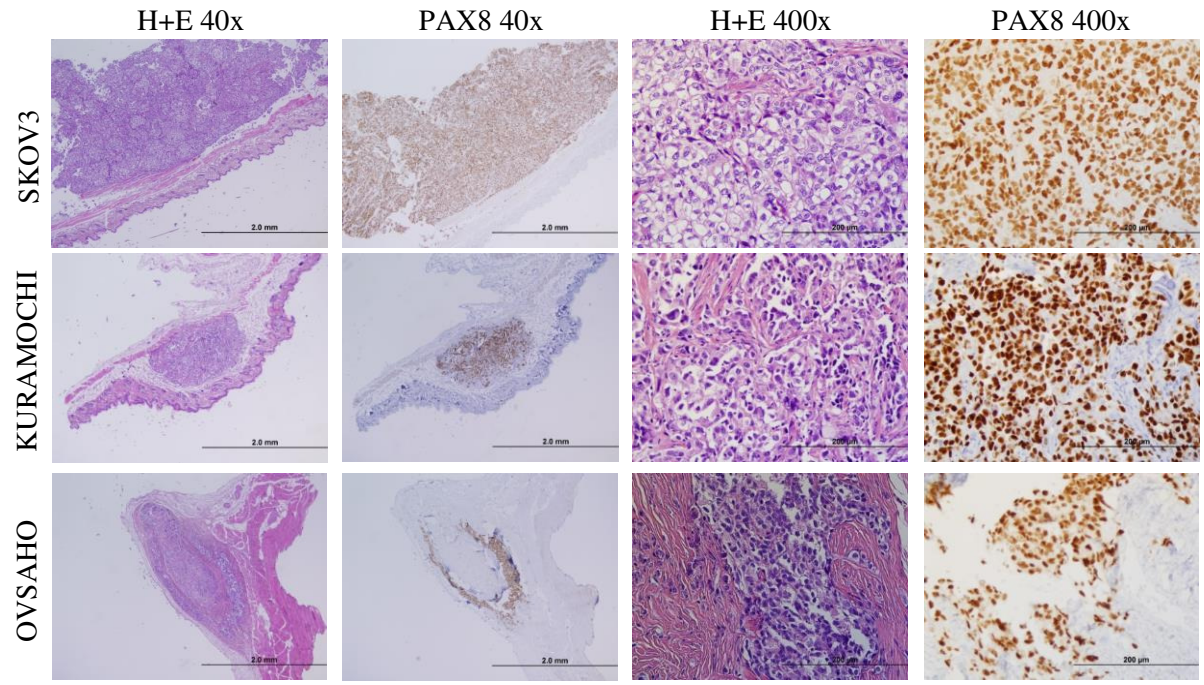

Figure 2.8: PAX8 Expression in NSG SubQ Xenografts
After 31 days of tumor growth in NSG mice injected SubQ with luciferized SKOV3, KURAMOCHI, or OVSAHO cells, tumors were excised and embedded to stain for Hematoxylin and Eosin (H+E) or PAX8 to confirm ovarian tumor lineage. SKOV3 tumors were expansile, while KURAMOCHI tumors formed small nodules and OVSAHO tumors were microscopic and surrounded with fibrous tissue.

The best model system identified for the novel cell lines was the NSG intraperitoneal model. SKOV3 intraperitoneal tumors formed the traditional large, discrete tumors that were easily removed upon autopsy (Figure 2.9).

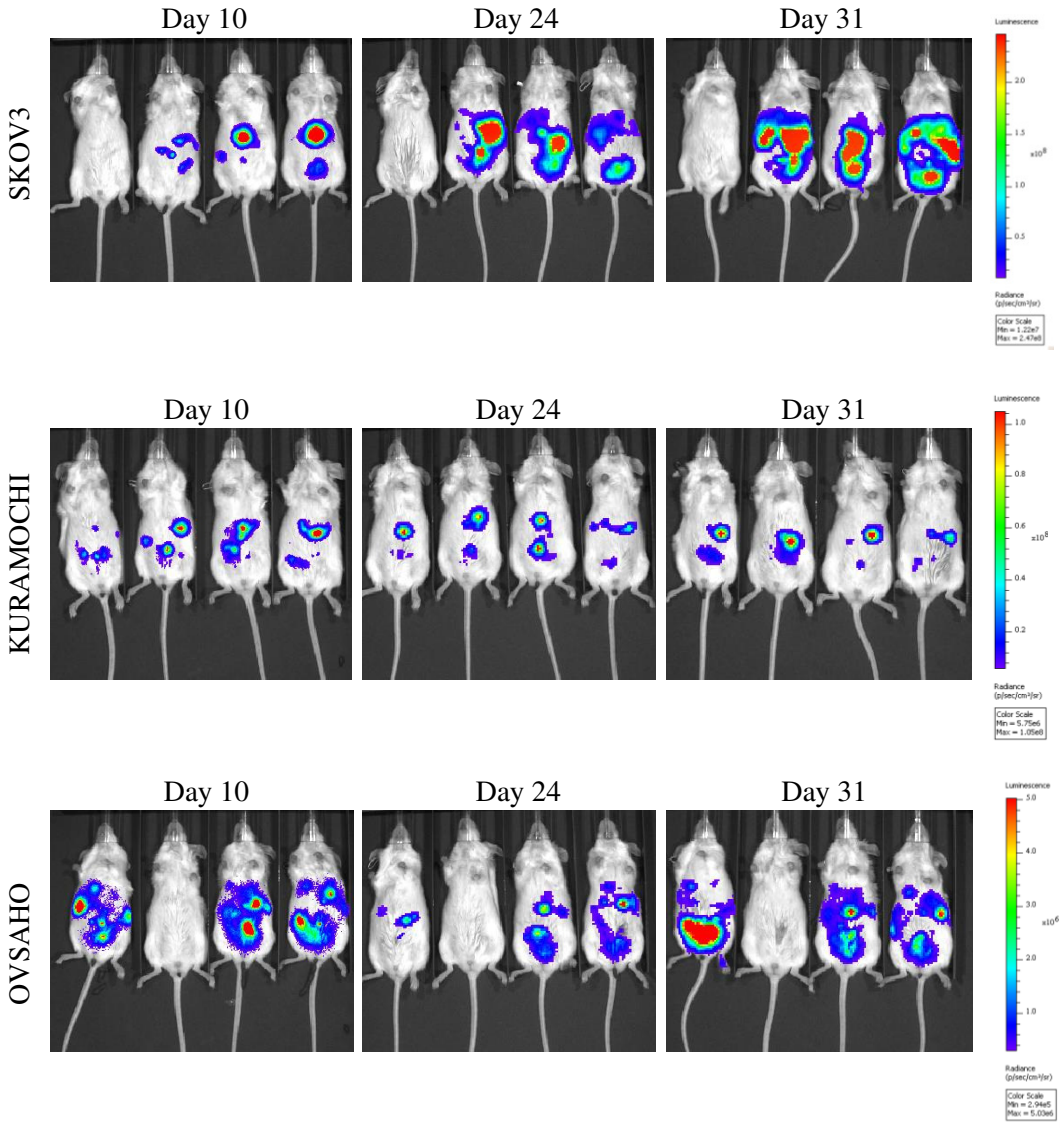

Figure 2.9: Tumor Visualization of IP Xenografts in NSG Mice
NSG mice were injected with 5 million luciferized SKOV3, KURAMOCHI or OVSAHO cells IP (n=4 each) and bioluminescent imaging was performed at day 10, 17, 24, and 31. Tumors failed to take in one SKOV3 mouse and one OVSAHO mouse. SKOV3 tumors had the highest signal, while KURAMOCHI was much lower. OVSAHO tumors put off the least signal and could only by well visualized by measuring tumors on a much smaller luminescence scale.

Both OVSAHO and KURAMOCHI intraperitoneal tumors formed minute implants on the viscera and peritoneum, with OVSAHO implants more diffuse and KURAMOCHI implants slightly larger and therefore more visible (Figure 2.10). The lack of large, solid tumors is a better mimic of the

carcinomatosis common to clinical presentations of HGSOC. None of the mice developed ascites, but all showed minor to significant levels of small bowel obstructions (Figure 2.10).

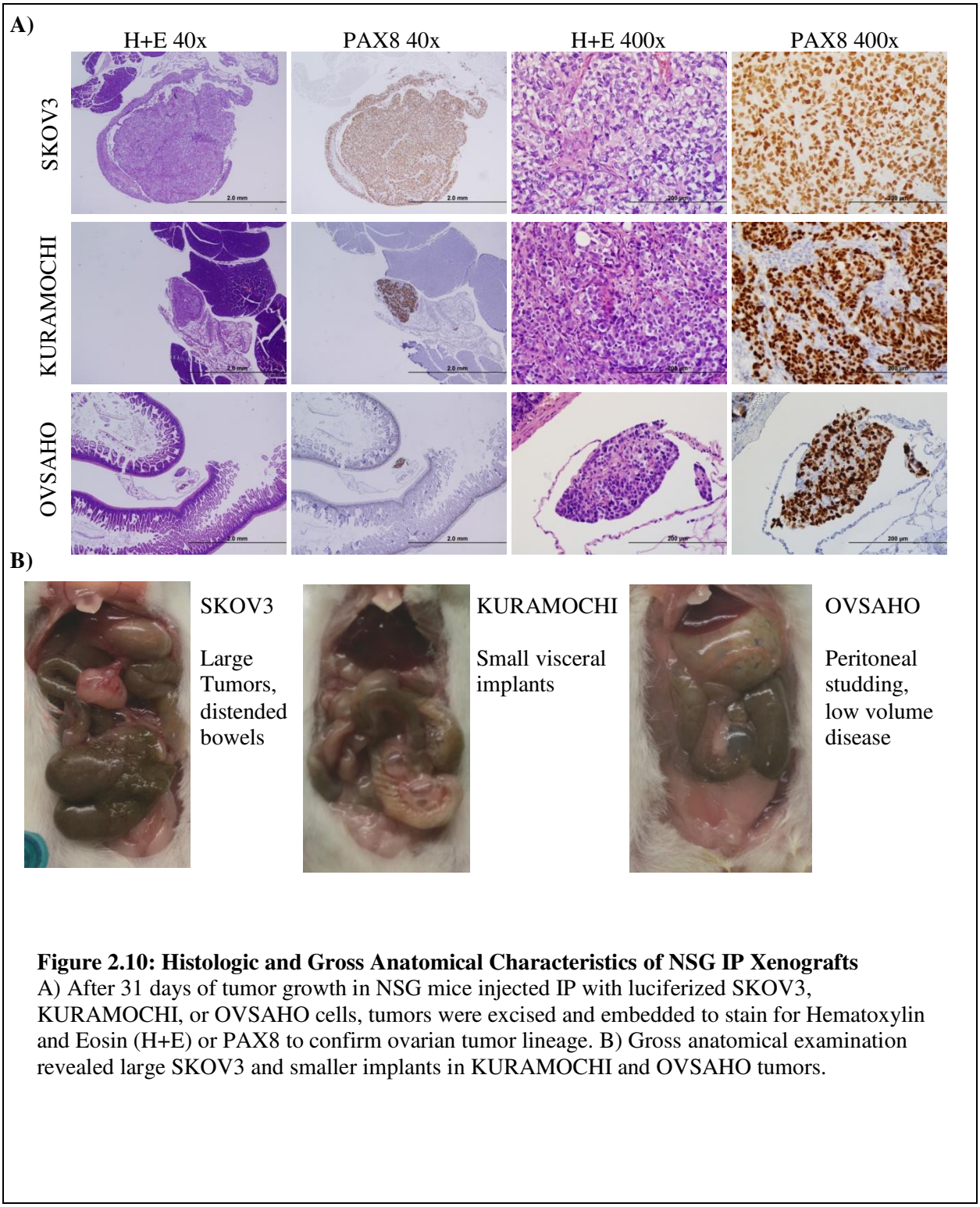

Figure 2.10: Histologic and Gross Anatomical Characteristics of NSG IP Xenografts
A) After 31 days of tumor growth in NSG mice injected IP with luciferized SKOV3, KURAMOCHI, or OVSAHO cells, tumors were excised and embedded to stain for Hematoxylin and Eosin (H+E) or PAX8 to confirm ovarian tumor lineage. B) Gross anatomical examination revealed large SKOV3 and smaller implants in KURAMOCHI and OVSAHO tumors.

Discussion

Ovarian cancer is a heterogenous disease with many subtypes that may be characterized by their genetics, histology, and clinical progression. Recent studies by Domcke et al. comparing the genetics of primary patient tumors from TCGA to the genetics of the most commonly used ovarian cancer cell lines revealed that the most common models of HGSOC are not always the most genetically consistent[7]. However, genetics is only one small part of the larger characterization needed to assess ovarian cancer cell lines. In this study, we sought to expand upon the genetic analysis of the two most genetically faithful ovarian cancer lines identified by Domcke et al, KURAMOCHI and OVSAHO.

In certain phenotypic aspects, KURAMOCHI and OVSAHO better recapitulated advanced ovarian cancer than the traditional ovarian cancer cell line SKOV3. This was especially evident with cell morphology, where KURAMOCHI and OVSAHO formed small cobblestone and micropapillary structures as compared to SKOV3's spindle-like growth, and with tumor formation, where OVSAHO and KURAMOCHI were more likely to form widespread peritoneal implants as opposed to SKOV3's larger, discrete tumors.

In other cases, all three lines equally recapitulated the ovarian cancer phenotype. All three cell lines expressed stathmin, a marker of proliferation and early marker of ovarian cancer pathogenesis, as well as PAX8, a lineage marker for müllerian tissue. Although all three had mutated P53, a mutation common to 99.5% of ovarian cancers, the point mutation found in KURAMOCHI is the most common type of mutation for this cancer[5,6]. OVSAHO and SKOV3 had mutations resulting in truncation and deletion, respectively.

Surprisingly, neither KURAMOCHI nor OVSAHO expressed CK7, a marker used to differentiate ovarian cancer from metastases of extra-ovarian origin in the clinic, and present in approximately 96% of ovarian cancer[96]. It is important to note that lack of CK7 expression was not unique to the novel ovarian cancer lines, as IGROV1 cells were also negative for CK7. Similarly, neither SKOV3, KURAMOCHI or

OVSAHO expressed CA-125, a common biomarker for ovarian cancer and elevated in 75% of tumors[98]. While it is unknown why these tumors do not recapitulate these phenotypes, perhaps extended culturing away from the proper microenvironment could have an impact on normal expression. A larger survey could be done with a broader range of ovarian cancer cell lines to see if this trend is unique to the novel ovarian cancer cell lines or a more widespread problem inherent in cell culture models.

Ultimately, further characterization of the most genetically faithful ovarian cancer lines revealed that none of the lines studied perfectly reproduced all of the phenotypes common to HGSOC as it presents in clinic. This should not be taken as a sign that all cell culture models are bad, but instead should heighten awareness that every cell line is different and careful consideration should be involved prior to choosing a cell line for study. In some cases, this will mean making experimental changes to best leverage the model of choice, such as using NSG mice instead of the traditional nude models so that less aggressive tumor lines can be studied in vivo. While this is more expensive and NSG mice are generally higher maintenance due to their weakened ability to fight off infection, the results are better tumor models that may better bridge the historically broken pipeline between bench and bedside. Ultimately, one cell line alone is no longer sufficient to capture the varied genetic and phenotypic gestalt of clinical ovarian cancer, and greater efforts to characterize and include new cell lines will result in better and more relevant science.

CHAPTER 3

Characterizing PAX8 Expression and Knockdown in Fallopian Tubes and Ovarian Cancer

Acknowledgements

This work was a collaboration between Meg Emori, Kevin Elias, and Emily MacDuffie. Meg Emori and Kevin Elias co-trained and co-supervised Emily MacDuffie, who was responsible for performing the siRNA knockdown for western blot, cell titer glo, and SRB analysis. Meg Emori performed the flow cytometry experiments, and was advised on data analysis by John Daley, head of the Flow Cytometry Core. Kevin Elias and Meg Emori worked together to insert the lentiviral shRNA constructs into cell lines, and Kevin Elias was responsible for luciferizing the shRNA cell lines. Meg Emori performed all the in vitro shRNA experiments. DFCI animal research facility staff injected shRNA xenografts into mice and performed luminol imaging. Meg Emori carried out IPTG treatment, tumor and weight measurements, as well as luminol imaging analysis and quantification. Tumor removal and dissection was performed primarily by Kevin Elias with assistance from Meg Emori. Tumor embedding, sectioning, and staining were outsourced to Mei Zheng.

Introduction

PAX8 is a developmental transcription factor important to the regulation of kidney, thyroid, and Müllerian tract development. When PAX8 is knocked out during development, fallopian tubes and uterus fail to form, resulting in the absence of a functional Müllerian tract and consequently infertility[61]. While PAX8 expression is maintained in mature fallopian tubes and strikingly conserved in 99% of HGSOC, our understanding of the role of PAX8 in these contexts is lacking[67]. Recently, project Achilles, a comprehensive screen to identify genetic weaknesses across cancer lines, identified PAX8 as an essential gene specific to ovarian cancer[73]. A subset of ovarian cancer cell lines treated with PAX8 shRNA showed significant decrease in proliferation, and in these lines PARP cleavage was modestly increased, suggesting an apoptotic mechanism[73].

Given the cytotoxicity of PAX8 knockdown combined with the unique expression of PAX8 in the fallopian tube epithelium, targeting PAX8 could be a novel therapeutic strategy. However, the cell lines

previously used to study PAX8 knockdown (IGROV1, OVCAR3, RMG-1, OVCAR4, OVCAR8, Caov3, COV504, and OV90) do not include the most genetically relevant cell line models[7]. Thus we sought to extend the current understanding of PAX8 knockdown mediated decrease in proliferation in more relevant models of HGSOC, both in vivo and in vitro.

Results

PAX8 is Uniquely Expressed in Fallopian Tubes and Ovarian Cancer

While PAX8 expression is ubiquitous in both fallopian tubes and ovarian cancer, expression levels are known to vary. To compare relative PAX8 expression levels, a western blot was performed on seven ovarian cancer cell lines, one immortalized fallopian tube epithelium line, and one breast adenocarcinoma cell line which served as a negative control. PAX8 expression was present in all of the fallopian tube and ovarian cancer cell lines tested, and negative in the breast adenocarcinoma cell line. PAX8 expression in KURAMOCHI and OVCAR3 cells was exceptionally high, while OVSAHO, OVCAR4 and OVCAR8 expressed much lower levels and were even lower than the expression of PAX8 in the immortalized fallopian tube line (Figure 3.1).

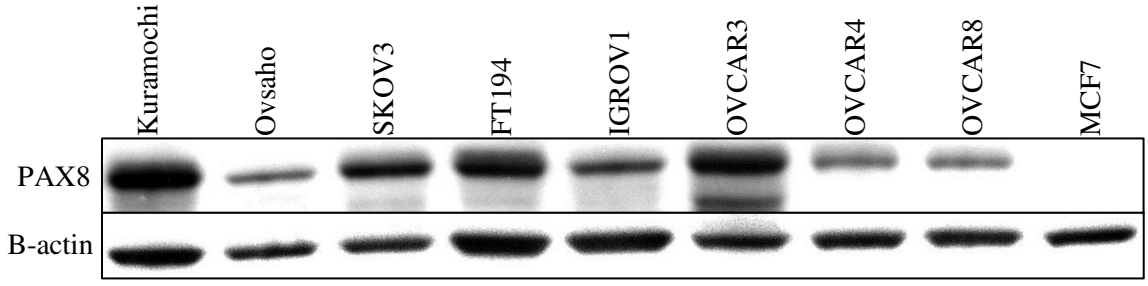

Figure 3.1: PAX8 Expression in Fallopian Tube and Ovarian Cancer Cell Lines
Western blot of PADX8 expression in seven ovarian cancer cell lines, one immortalized fallopian tube (FT194) and negative breast cancer control (MCF7). B-actin served as a loading control.

To ensure antibody specificity to PAX8 and to rule out false identification of another PAX protein, PAX8 expression was validated by siRNA knockdown using 3 individual siRNA constructs and by pooling all three together. A non-targeting sequence of siRNA was used as a negative control to control for the effects of siRNA, while non-treated cells were used as a transfection control. PAX8 knockdown after 72 hours was successful in all cell lines with 10% or less of the original protein levels observed in treated cells (Figure 3.2).

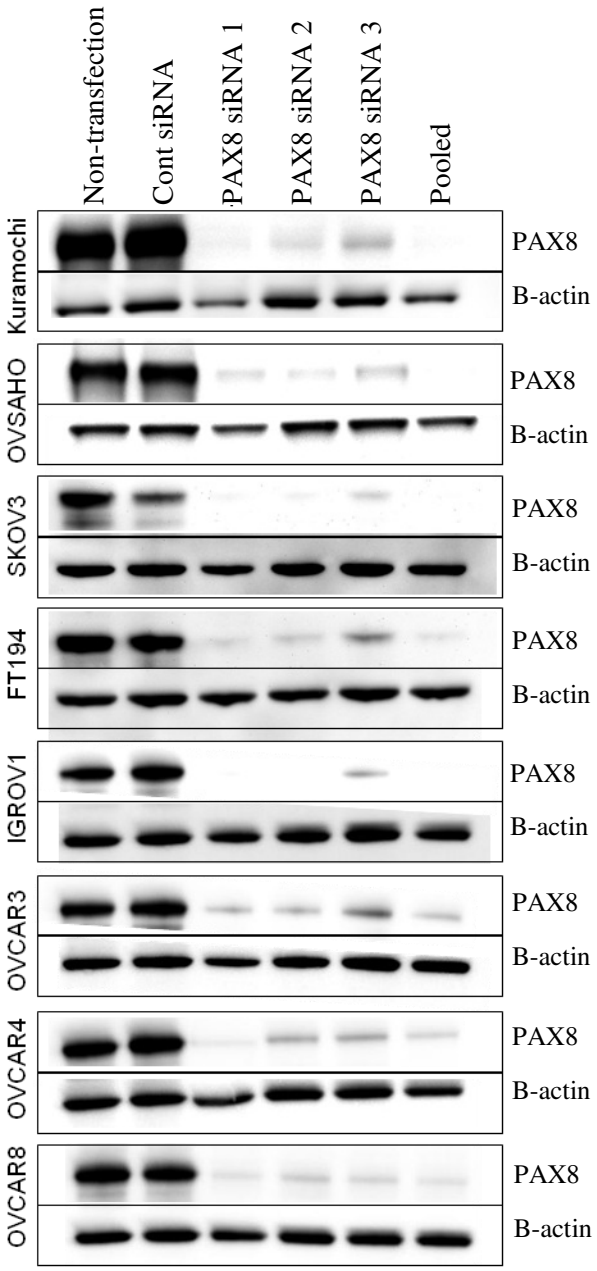

Figure 3.2: PAX8 Knockdown via SiRNA
PAX8 expression was validated by transfection of ovarian cancer and immortalized fallopian tube lines with three PAX8 siRNAs (1,2,3) individually or pooled, and with non-targeting siRNA sequence (Cont siRNA). Untreated cells (Non-Transfection) served as a transfection control. Samples were harvested after 72 hours of reverse transfection. B-actin served as a loading control.

Selective Ovarian Cancer Cell Lines are Sensitive to PAX8 Knockdown with siRNA

To determine the impact of PAX knockdown on proliferation, cells were treated with siRNA for 144 hours and then cell viability was measured by ATP content (cell titer glo) and cell density (SRB analysis). KURAMOCHI, IGROV1, and OVCAR3 cells all exhibited decreased proliferation and cell density, while OVSAHO, SKOV3, FT194, OVCAR4, and OVCAR8 were not affected (Figure 3.3). Thus, although PAX8 knockdown was robust in all samples, only some ovarian cancer cell lines are affected by PAX8 loss.

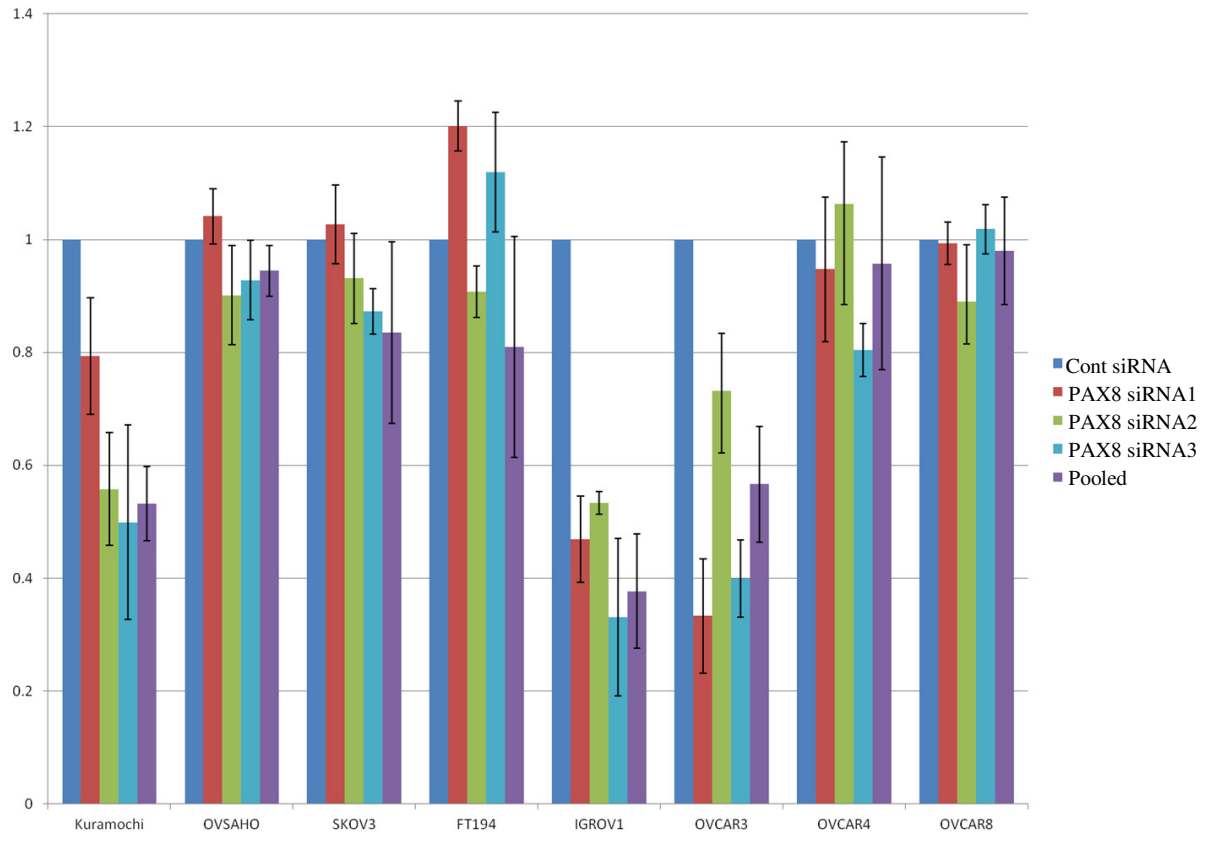

Figure 3.3: Proliferation Defects in a Subset of Fallopian Tube and Ovarian Cancer Cell Lines Treated with PAX8 siRNA
Cell lines were reverse transfected with PAX8 siRNA (1, 2, 3) individually or pooled. Non-targeting siRNA (Cont siRNA) served as a control. Cell-titer glo analysis was performed after 144 hours and Cont siRNA controls normalized to 100% viability with all other lines measured as a fraction of the control. KURAMOCHI, IGROV, and OVCAR3 exhibit decreased proliferation when treated with siRNA whereas no difference is detected in the other cell lines.

PAX8 Knockdown Induced Proliferation Defects are Primarily due to Senescence, not Apoptosis

Reduction in cell viability may be caused by three major mechanisms. The first, and most ideal from a therapeutic approach, is apoptosis. This highly programed mechanism of cell death triggers a closely regulated cascade of events leading to proteolytic lysis and the fragmenting of nuclear DNA, packaging the cellular components into apoptotic bodies which can be identified and absorbed by the surrounding cells. In contrast, necrosis, or uncontrolled cell death, results in cellular swelling, the breakdown of the plasma membrane, and ultimately the expulsion of cellular contents in such a manner that they cannot be properly cleared by surrounding cells. Inducing necrosis is not an optimal treatment strategy for tumor regression as it can lead to inflammation and surrounding tissue damage. Recently, it has become more commonly accepted that apoptosis and necrosis may not be mutually exclusive but rather exist on two ends of a spectrum of possible methods of cell death. In the third major mechanism, senescence, cells are permanently blocked from cell division but not necessarily predisposed to die.

In order to determine which mechanism or combination of mechanisms were behind the decrease in cell number in the subset of ovarian cancer cell lines affected by PAX8 knockdown, flow cytometry with propidium iodide and annexin V staining was performed. Annexin V is a protein known to bind to phosphatidylserine (PS). In healthy cells, PS is located on the inner surface of the cell membrane, but during apoptosis it translocates to the outer surface where it can be detected by exogenous proteins. Fluorescent conjugates of Annexin V thus serve as a highly efficient marker for detecting apoptosis. In combination with propidium iodide (PI), an intercalating agent which binds and stains DNA, it is possible to identify four major stages of cell viability and death. Viable cells do not present PS or DNA, making them negative for both PI and Annexin V. Early apoptotic cells present PS but still have intact DNA, making them positive for Annexin V but negative for PI. Late apoptotic cells present PS and fragmented DNA, making them positive for both Annexin V and PI. Necrotic cells, which do not transpose PS, but do uncontrollably eject their cellular contents, are positive for PI but negative for Annexin V.

KURAMOCHI cells, which had previously been shown to exhibit a proliferation defect as a result of PAX8 knockdown, were treated with PAX8 siRNA and analyzed by flow cytometry after 48, 72, and 96 hours (Figure 3.4). Results for the scramble siRNA treated cells were set as the standard. No difference was observed between siRNA and control treated cells at 72 hours. Two siRNAs and the pooled siRNA showed a slight increase in the late apoptosis population at 48 hours, and the pooled siRNA showed a slight increase in the early apoptosis population at 96 hours. Although these differences were significant with $P>.05$, the data collected over 3 experiments varied widely and the resulting standard deviation was particularly large. Thus it is unlikely that apoptosis plays an important role in the PAX8 knockdown mediated decrease in proliferation. Similarly, no significant increase in the necrotic populations of treated samples at any time point indicates that necrosis is a similarly insignificant factor.

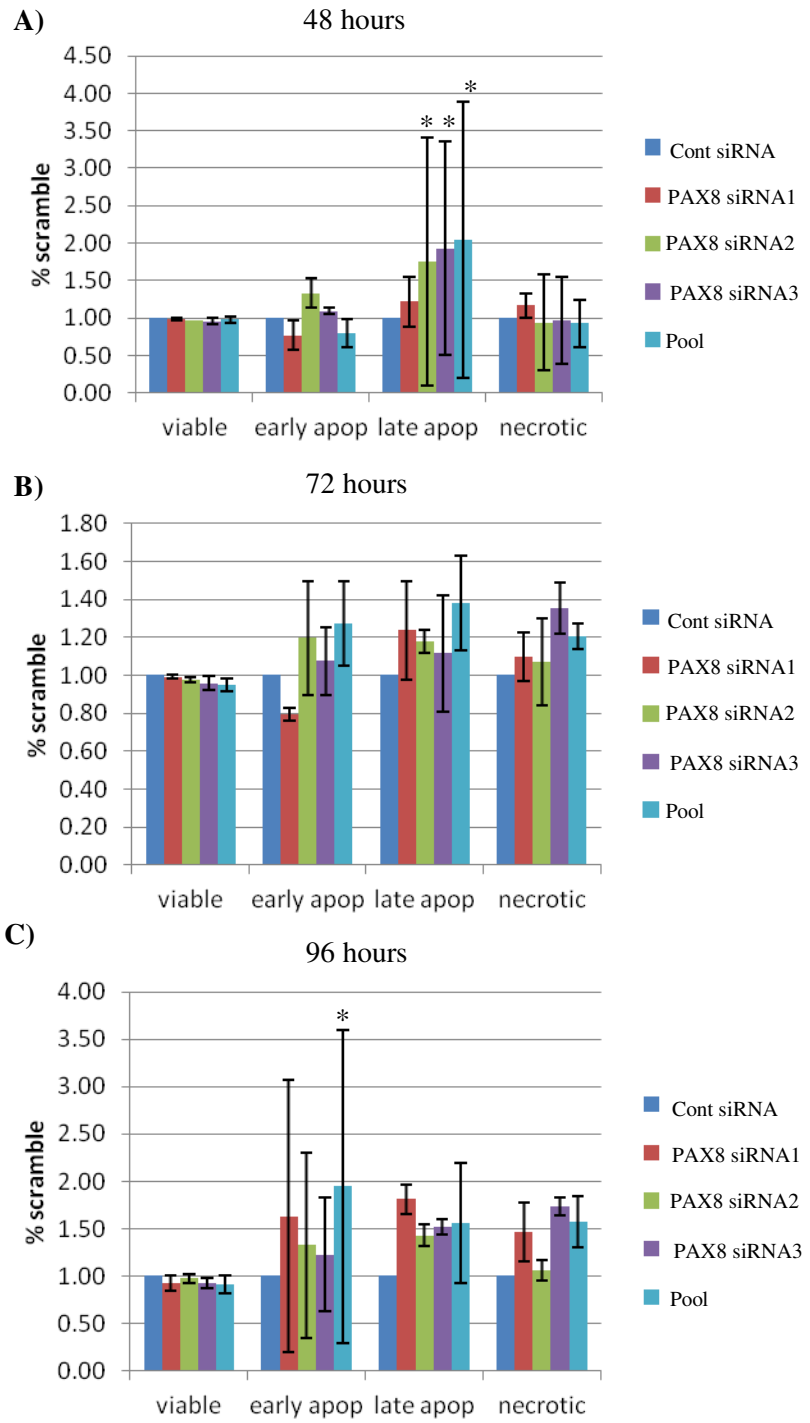

Figure 3.4: Apoptosis in Cells Treated with PAX8 siRNA
KURAMOCHI cells were treated with a non-targeting siRNA control (cont siRNA), 3 PAX8 siRNAs (1,2,3), or pooled PAX8 siRNA (pool). Annexin V analysis was performed via flow cytometry after A) 48 hours, B) 72 hours, and C) 96 hours. Control siRNA populations were normalized to 1 and all other populations (early apoptotic, late apoptotic, and necrotic) were measured as a % of scramble control. Error bars indicate standard deviation. N=3 for each time point. * indicates $P<0.05$

To understand the changes in relative distribution of cell cycle phases as a result of PAX8 knockdown, cells were treated with PAX8 siRNA and analyzed at 72 and 96 hours. Flow cytometry was performed using propidium iodide (PI). In this method, cells are permeabilized with a detergent, allowing the integration of PI into the DNA of all cells. The levels of DNA increase during the cell cycle as the cell duplicates its DNA in preparation for cellular division, such that quantification of PI binding can be used to indicate the cell cycle stage. Compared to control siRNA populations, all PAX8 siRNA treated samples exhibited a large increase in the G0/G1 population and a slighter decrease in both G2M and S-Phase populations, indicating a block in cell cycle progression (Figure 3.5). This was consistent at both 72 and 96 hours.

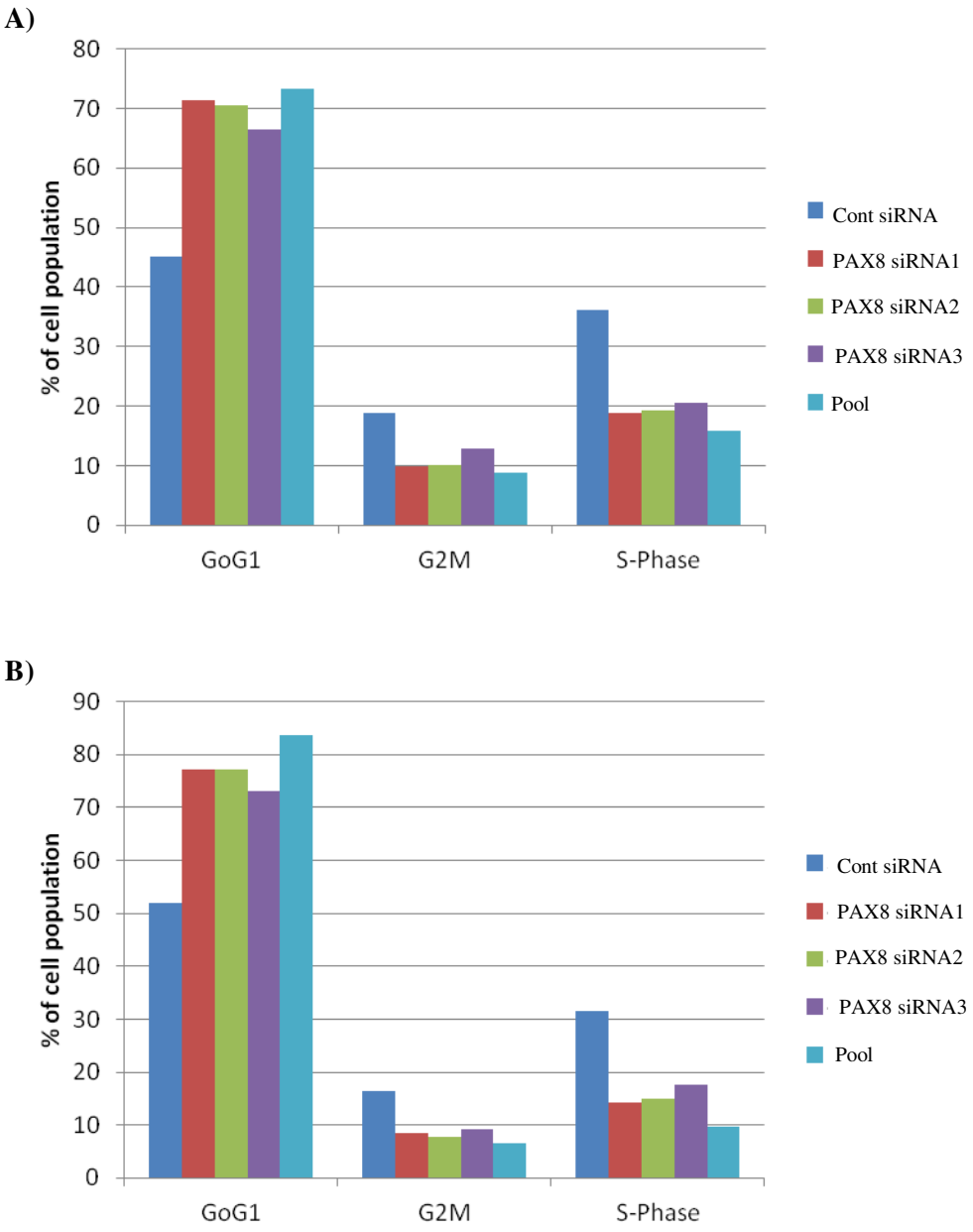

Figure 3.5: **Cell Cycle Analysis of PAX8 knockdown**
KURAMOCHI cells were treated with a non-targeting siRNA control (Cont siRNA), 3 PAX8 siRNAs (1,2,3), or pooled PAX8 siRNA (pool). Annexin V analysis was performed via flow cytometry after A) 72 hours and B) 96 hours. Each treatment group was divided into percentage of cell population in G0/G1, G2M, or S-Phase. N=1

Ovarian Cancer Cells can be Successfully Infected with Inducible PAX8 shRNA Lentiviral Constructs

While shRNA and siRNA work through the same mechanism of RNA interference, siRNA directly delivers pre-cleaved RNA and must be administered via transfection and its effects are transient-lasting on the order of days. In contrast, shRNA is delivered into the cell through a vector backbone and relies on the cell's innate RNAi machinery, including Dicer and Drosha, to process the pre-shRNA into a functional siRNA. ShRNA is particularly advantageous for in vivo experiments as knockdown can be maintained permanently in a cell line of interest, which is essential for long term xenograft studies.

As PAX8 has been shown in vitro to impact cell growth, an inducible PAX8 shRNA construct was used so that cell growth would be uninhibited while cells were maintained in culture. Two different inducible PAX8 shRNA constructs, sh277 and sh278, were introduced into OVSAHO and KURAMOCHI ovarian cancer cell lines via infection with a lentiviral pLKO-puro-IPTG-3xLacO plasmid. Cells containing the PAX8 shRNA constructs were selected for by puromycin. PAX8 shRNA expression was induced with 10mM IPTG dissolved in complete cellular media. After a period of 9 days IPTG treatment, cells were harvested in RIPA buffer and western blot analysis was performed to measure PAX8 expression levels (Figure 3.6). While treatment with IPTG reduced KURAMOCHI PAX8 expression in cells infected with the sh278 construct, IPTG treated KURAMOCHI cells with the sh277 construct and OVSAHO cells containing either construct were not noticeably impacted by IPTG. Control cells containing non-targeting shRNA constructs in the same backbone vector confirmed that treatment with IPTG alone does not impact PAX8 expression. Cell lines were further infected with a second lentiviral construct containing the mCherry-Luc construct to allow for in vivo imaging.

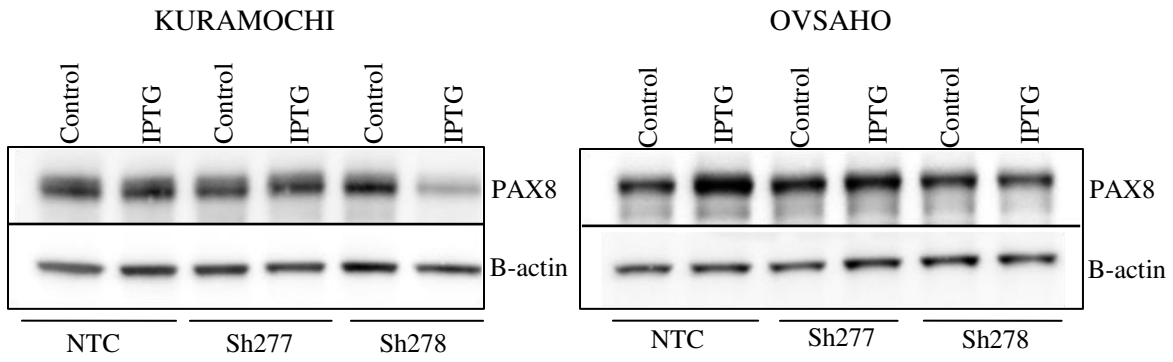

Figure 3.6: ShRNA knockdown of PAX8 in KURAMOCHI and OVSAHO cell lines
KURAMOCHI and OVSAHO cells containing an IPTG inducible shRNA lentiviral construct against PAX8 (sh277 and sh278) or a non-targeting control (NTC) were treated with media containing 10mM IPTG (IPTG) or media alone (Control) for 9 days and western blotting was performed to determine PAX8 expression levels. B-actin was used as a loading control. Knockdown is seen only in KURAMOCHI cells with the Sh278 construct treated with IPTG.

Inducible PAX8 shRNA OVSAHO Intraperitoneal Xenografts are Cleared by the Mouse Model

To test the therapeutic efficacy of knocking down PAX8 in vivo, luciferized OVSAHO cells containing inducible PAX8 sh277 or sh278, or inducible non-targeting shRNA were injected into NU/J (nude) mice intraperitoneally. Because ovarian cancer usually presents at a late stage, the most clinically relevant model must have a well-established tumor present before therapy is initiated. Thus tumors were allowed to grow for 14 days before 10mM IPTG was added to the mice's water, inducing PAX8 knockdown. Mice were imaged 11, 24, and 39 days after injection, and were euthanized at 52 days (Figure 3.7). Autopsy was performed to isolate tumor samples for general histologic analysis and PAX8 expression levels. Unfortunately, although tumors were clearly visible through luminol imaging, the tumors were visually too small to be identified upon autopsy and no histologic analysis could be performed.

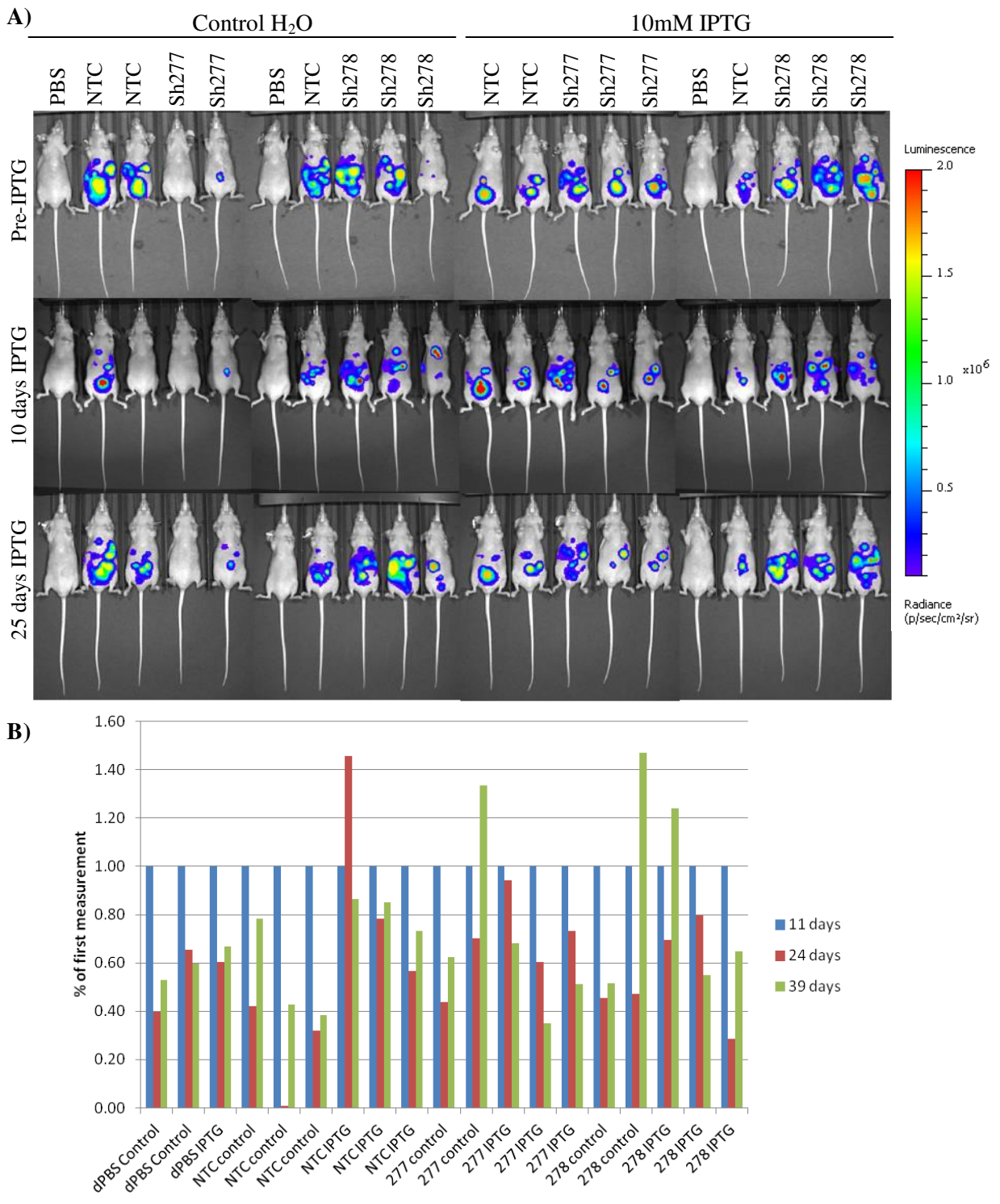

Figure 3.7: OVSAHO PAX8 Inducible shRNA Intraperitoneal Xenografts in Nude Mice
Nude mice were injected intraperitoneally with luciferized OVSAHO cells containing an inducible PAX8 shRNA construct (277 or 278) or a non-targeting control (NTC). Mice were given IPTG or control water (control) after 10 days of tumor growth and imaged with luminol on days 11, 24, and 39 post-injection. Luminol data was quantified and the second two time points presented as a fraction of the first time point for each mouse.

Inducible PAX8 shRNA KURAMOCHI Subcutaneous Xenografts are Cleared by the Mouse Model

As KURAMOCHI shRNA constructs showed successful knockdown and display a faster doubling time in vitro, cells containing inducible PAX8 sh277 or sh278, or inducible non-targeting shRNA were injected into nude mice subcutaneously. Tumors were allowed to grow for 8 days before an increased dose of 25mM IPTG was added to the mice's water to induce PAX8 knockdown. Caliper measurements of subcutaneous tumor volumes were taken weekly. Mice were imaged 3 days prior to and 7 and 14 days after injection (Figure 3.8, Figure 3.9). After the first week tumors were too small to manually measure tumor volume. All mice were euthanized at 29 days. Autopsy was performed to isolate tumor samples for general histologic analysis and PAX8 expression levels. Unfortunately, although tumors were clearly visible through luminol imaging, shrinkage was apparent during the study both by imaging and palpation. Upon autopsy tumors were visible only as small isolated patches of scar tissue at the injection site and histologic analysis was unsuccessful (Figure 3.9).

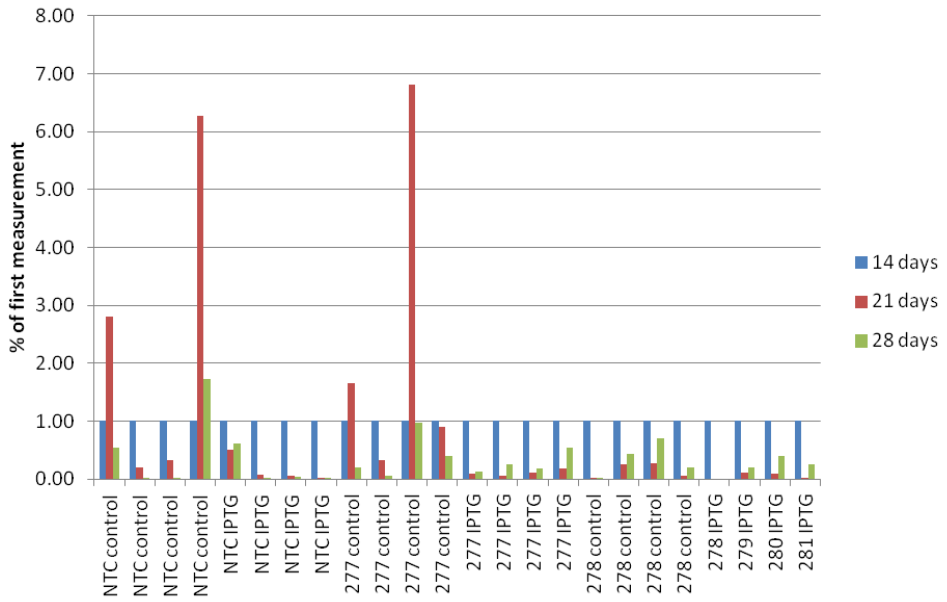

Figure 3.8: Quantification of KURAMOCHI PAX8 Inducible shRNA SubQ Xenografts in Nude Mice
Nude mice were injected subcutaneously with luciferized KURAMOCHI cells containing an inducible PAX8 shRNA construct (277 or 278) or a non-targeting control (NTC). Mice were given IPTG or control water (control) after 14 days and imaged with luminol on days 11, 24, and 39 (14, 21, and 28 days post- IPTG respectively). Luminol data was quantified and the second two time points presented as a fraction of the first time point for each mouse.

Figure 3.9: Imaging of KURAMOCHI PAX8 Inducible shRNA SubQ Xenografts in Nude Mice

Nude mice were injected subcutaneously with luciferized KURAMOCHI cells containing an inducible PAX8 shRNA construct (277 or 278) or a non-targeting control (NTC). **A)** Mice were given IPTG or control water (control) after 14 days and imaged with luminol on days 11, 24, and 39 (3 days pre-IPTG, 7, and 14 days post- IPTG respectively). **B)** At time of autopsy most tumors were visible only as small scar tissue at site of injection. Three representative mice are shown, two with scar tissue and one with no visible mark.

Figure 3.9 (Continued)

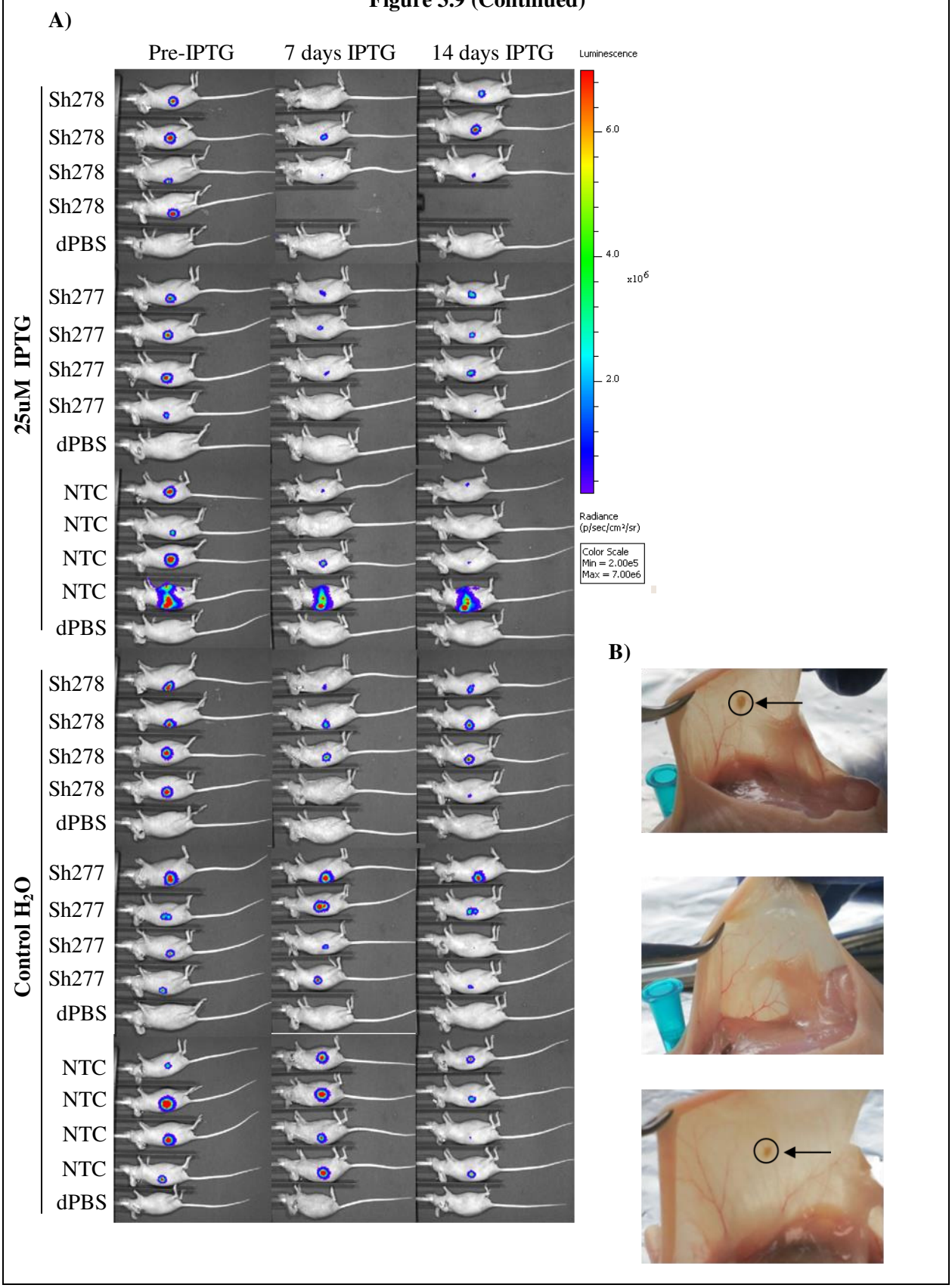

One mouse with a shRNA278 xenograft treated with IPTG developed extensive lymphadenopathy bilaterally in the lymph nodes around its neck, armpits, and groin 10 days after being injected and 2 days after IPTG was added to the water, and had to be euthanized immediately (Figure 3.). No growth abnormalities were observed two days prior, indicating sudden onset, and no tumor was measurable at the injection site. Lymph nodes were removed upon autopsy and histological analysis revealed that they were negative for PAX8, confirming a lymphatic origin rather than a metastatic one. No lymphadenopathy was observed in any other treated or control mouse.

A)

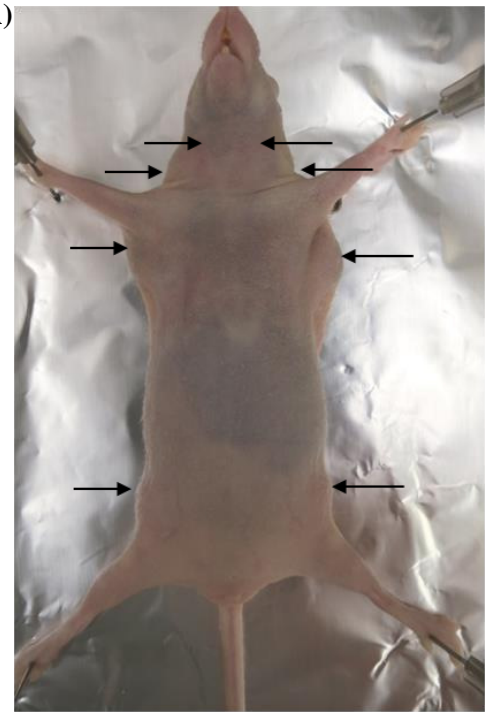

B)

Figure 3.10: Lymphadenopathy in KURAMOCHI PAX8 Inducible shRNA SubQ Xenograft
One mouse injected subcutaneously with luciferized KURAMOCHI cells containing an inducible PAX8 construct (278) exhibited extensive lymphadenopathy 10 days after injection and 2 days after IPTG was added to the water. **A)** Locations of lymph nodes affected indicated by black arrows. **B)** In total, 8 affected lymph nodes were removed.

Discussion

PAX8 is uniquely expressed in fallopian tube epithelium and ovarian cancer cell lines, and can be knocked down successfully with siRNA. However, only a subset of PAX8 expressing lines exhibit proliferation defects when treated with PAX8 siRNA. Detailed analysis of proliferation defects by flow

cytometry indicate very low amounts of apoptosis and significant levels of senescence. Our results confirmed previous experiments showing that both IGROV and OVCAR3 exhibited proliferation defects when PAX8 was knocked down, and found a new ovarian cancer line, KURAMOCHI, that also displayed this phenotype[73]. The previous work by Cheung et al. showed PARP cleavage induced by PAX8 knockdown, which would suggest an apoptotic mechanism, but further analysis with flow cytometry failed to support those findings as low induction of apoptosis was observed with Annexin V staining and a significant increase of cells in the G0/G1 phase via cell cycling analysis indicated a senescent mechanism[73]. While PARP cleavage analyzed by western blot is a useful tool to indicate apoptosis in the whole cell population, cell cycle analysis is a more accurate measure as it quantifies each cell on an individual basis. It is also important to note a slight difference in knockdown techniques, since Wing et al. used PAX8 shRNA while our experiments used siRNA[73]. Both labs transfected cells with either shRNA or siRNA and measured proliferation within similar time frames.

In our hands, stable transfection of OVSAHO and KURAMOCHI cells with PAX8 shRNA was largely unsuccessful. Modest PAX8 knockdown was observed with one PAX8 shRNA construct (278) in KURAMOCHI cells treated with IPTG, but no knockdown was observed in OVSAHO cells. Previous research shows that Dicer and Drosha, the two proteins crucial for the processing of shRNA into siRNA, are decreased in 60% and 51% of ovarian cancer, respectively, and loss of these proteins is directly correlated with worse disease status[105,106]. Further research on ovarian cancer cell lines showed that siRNA techniques worked equally well in cell lines with a variety of Dicer and Drosha levels but shRNA was far more successful in cells with high levels of Dicer and Drosha than in cells with low levels[105]. The levels of Dicer and Drosha in OVSAHO and KURAMOCHI cells are currently unknown, but if they are low it may account for the failure of shRNA in our system. In addition, more recent research has suggested that Dicer and Drosha levels rise as the primary HGSOC tumor progresses to metastatic disease[107]. According to the Japanese Collection of Research Bioresources (JCRB) cell bank, both

KURAMOCHI and OVSAHO were derived from ascites, so that their levels of Dicer and Drosha may be different from their original tumors.

Lastly, our efforts to study the in vivo efficacy of PAX8 knockdown in xenografts were limited by the growth kinetics of our cell lines. While both KURAMOCHI and OVSAHO cells grow aggressively in vitro, both tumor models regressed in vivo, ultimately preventing histologic analysis of PAX8 levels in tumors treated with IPTG or control H_2O. SKOV3 is a well studied ovarian cancer model known to form successful xenografts, but KURAMOCHI and OVSAHO were chosen instead due to recent research which suggests SKOV3 may be a poor genetic model of HGSOC while KURAMOCHI and OVSAHO are among the best representations of HGSOC[7]. Nude mice were chosen for the xenograft studies due to their inability to produce T-cells, leading to a partially immunodeficient state. This allows human-based tumor implantation, but reduces overall cost as mice are cheaper and can be maintained in regular facilities with less risk of infection and other immunodeficient side effects. Future work studying OVSAHO and KURAMOCHI should be conducted in NOD.Cg-Prkdcscid Il2rgtm1Wjl/SzJ (NSG) mice, which are the most highly immunodeficient models and are more susceptible to tumor growth. Alternately, a compromise could be reached by switching to another ovarian cancer cell line that is more reflective of HGSOC than SKOV3 but still known to form tumors in vivo, such as OVCAR3, or by providing the tumor greater support by co-injecting matrigel[7,40].

CHAPTER 4

Identification of PAX8 Binding Sites and Target Genes in Fallopian Tubes and Ovarian Cancer

Acknowledgements

This work was a collaboration between Meg Emori, Kevin Elias, and core facilities at DFCI. Kevin Elias optimized the ChIPseq protocol, Tom Westerling in the Brown lab made the libraries, and peak calling was performed initially by Brian Lawney and Alex Holman in Quackenbush group, and finally by Fugen Li and Henry Long at the Center for Functional Cancer Epigenetics (CFCE). Meg Emori knocked down PAX8 and isolated RNA for RNAseq experiments. Quality control analysis and cDNA library creation was performed by the Center for Cancer Computational Biology (CCCB) with extensive guidance from Prakash Rao. Sequencing and genome mapping was performed by the Molecular Biology Core Facilities (MBCF) at Dana Farber Cancer Institute. Data analysis was performed at the (CFCE) by Henry Long and Fugen Li.

Introduction

Transcription factors work by binding to DNA, often in complexes with other co-factors, and regulating gene expression. They can be regulated both temporally and spatially, and are essential to functions such as development and cell signaling. PAX8 is a member of the Paired Box (PAX) family of nuclear transcription factors. While PAX8 is expressed during development in the brain, metanephros, and Müllerian tract, stable expression in the adult is uniquely observed in kidney, thyroid, and Müllerian tract[59–61].

PAX8 expression is particularly critical to both the thyroid and the fallopian tube, where lack of the protein causes significant developmental defects and can lead to infertility or death[61]. The role of PAX8 has been studied extensively in the context of the rat thyroid, but little is known about PAX8 in the context of human fallopian tube. Given that PAX8 expression is conserved in a striking 99% of HGSOC and has recently been identified as a essential protein in a subset of ovarian cancer cell lines, understanding the changing role of PAX8 from adult fallopian tube epithelium to HGSOC gives insights both into tumorigenesis as well as paving the way for potential targeting of this protein[67].

ChIPseq and RNAseq were performed on three ovarian cancer cell lines with the highest genomic fidelity to HGSOC as well as three immortalized fallopian tube epithelium lines. Fallopian tube lines were intentionally chosen for their differing immortalization methods to minimize the impact of immortalization method on results.

Results

PAX8 Binding to DNA in Fallopian Tube Epithelium and High Grade Serous Ovarian Cancer

To determine where on the genome PAX8 binds, Chromatin Immunoprecipitation sequencing (ChIPseq) was performed on three immortalized fallopian tube secretory cell lines, FT194, FT246, and FT33-Tag, as well as three ovarian cancer cell lines with high genomic fidelity to HGSOC, OVSAHO, KURAMOCHI, and JHOS4. PAX8 was found to bind to DNA at 1,896 peaks found only in fallopian tube (FT), 6,931 peaks found only in HGSOC, and at 2,534 peaks common to both fallopian tube epithelium and HGSOC (Figure 4.1). Only 407 targets were common to all 6 cell lines, suggesting that cell to cell variation is significant.

Approximately 48% of PAX8 binding sites were identified in intergenic regions and approximately 38% in intronic regions, whereas only approximately 4-7% of binding sites were located in known promoter regions (Figure 4.1). Overall, the distribution of peaks across the genomic regions varied minimally between peaks unique to FT lines, peaks unique to HGSOC lines, and peaks conserved across all samples. This distribution is typical of nuclear transcription factors[108,109].

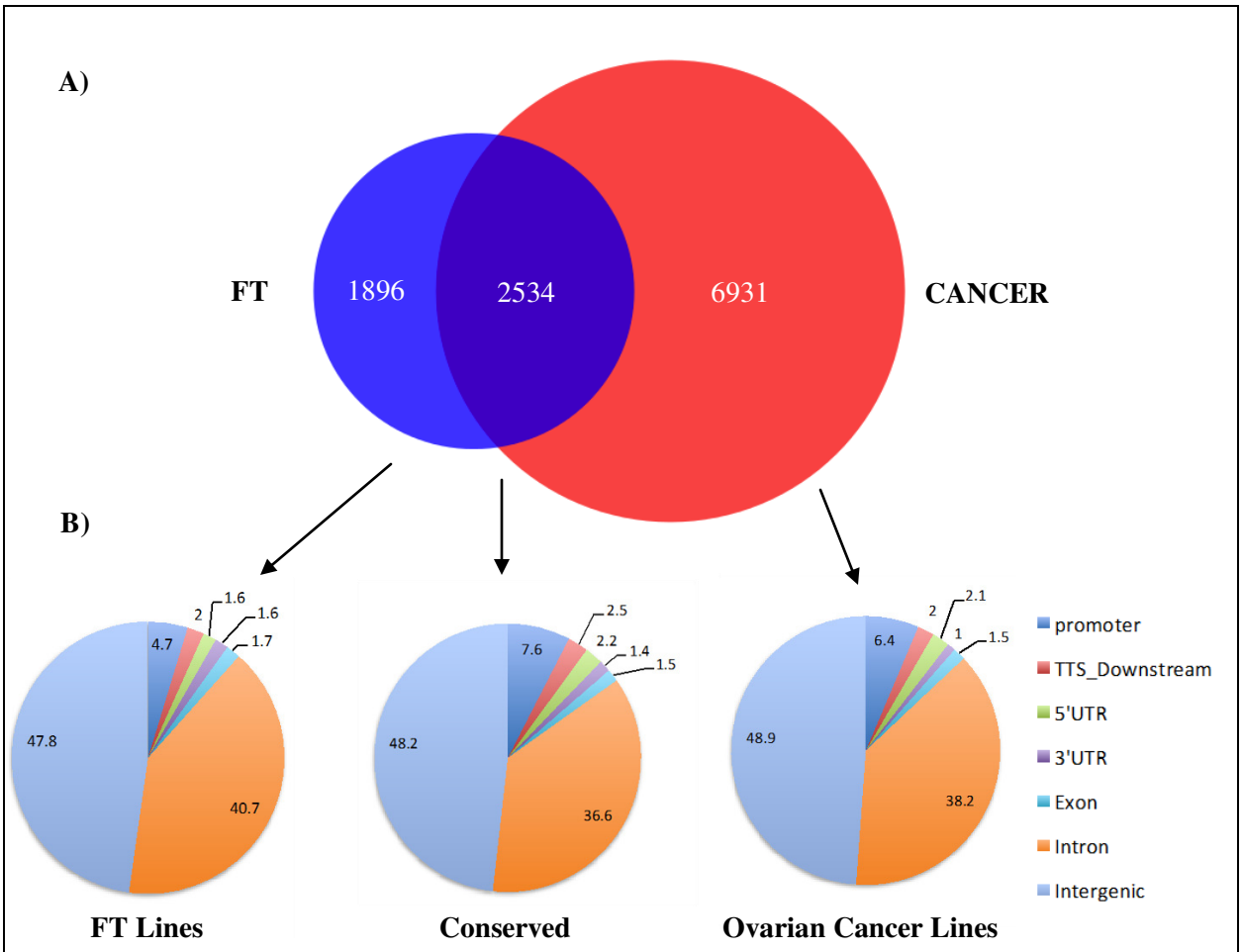

Figure 4.1: Differential PAX8 binding in Fallopian Tube vs. Ovarian Cancer Cell lines
ChIPseq analysis of PAX8 peaks identified in three immortalized fallopian tube lines and three ovarian cancer cell lines. A) Number of PAX8 peaks identified exclusively in fallopian tube (FT) lines, cancer cell lines, or identified in at least one each FT and cancer cell line (Conserved). B) Distribution of identified peaks across various regions of the genome: PAX8 binding favors intergenic and intronic regions.

When individual peaks were compared across cell lines, 558 peaks were identified as conserved across all FT and HGSOC cells and 3,013 peaks were identified as present in FT but lost in HGSOC (Figure 4.2). While FT lines showed striking similarities across samples, cancer cell lines had very unique sets of gained peaks, with KURAMOCHI gaining 3,255 unique peaks and OVSAHO gaining 3,309 unique peaks not previously identified in the setting of the FT. This indicates that fallopian tube peaks are

largely conserved across individuals while individual tumors contain a much wider range of novel binding sites.

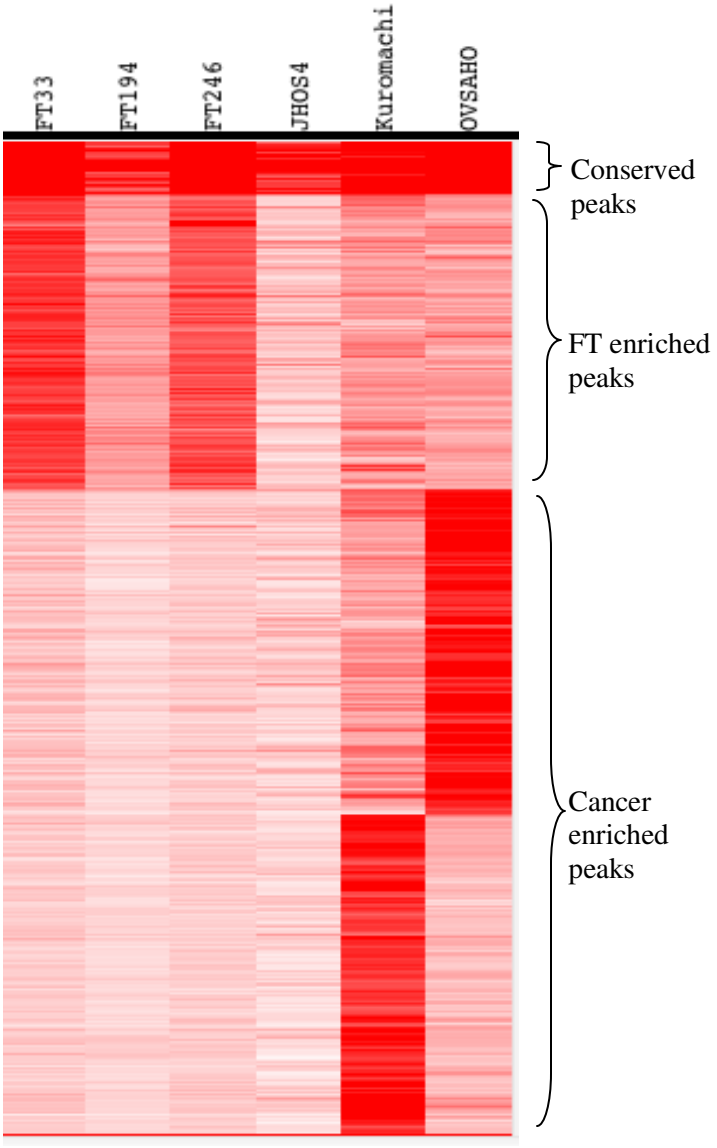

Figure 4.2: PAX8 peak distribution across fallopian tube and ovarian cancer cell lines. PAX8 peaks identified by ChIPseq analysis presented as red bands across each cell line (FT33Tag, FT194, FT246, JHOS4, KURAMOCHI and OVSAHO) Peaks divide into three separate groupings: those conserved across all cell lines, those enriched in the fallopian tube (FT) but lost in cancer, and those which are not present in the fallopian tube but are enriched in at least one ovarian cancer cell line.

De Novo motif analysis of peak summits revealed largely similar motifs for both HGSOC and FT cell lines (Figure 4.3). Both motifs closely matched the previously identified PAX2/5/8 subfamily consensus sequence[84,110] (Figure 4.3). This was also supported by individual known motif analysis of each cell line, where PAX2 was unanimously identified as the most highly conserved published binding sequence (Figure 4.3). For every cell line, the second through fifth top published motifs were also identified as a mixture of PAX1, 5, 9, and 6. As no published PAX8 binding site exists in the motif analysis database, we would therefore expect other PAX binding sequences, specifically PAX2 and 5, which come from the same PAX subfamily, to be the most closely related[48]. As PAX2, 5, and 7 have been previously shown not to be expressed in ovarian cancer, it is unlikely that these binding sites arise as a result of cross-reactivity between other PAX proteins and the antibody[111].

A)

Fallopian Tube Cell Lines

Ovarian Cancer Cell Lines

B)

CACGCTTCACTG –Cancer
CCCGCATGACTG –Fallopian Tube
AAGCGTGAC –PAX2/5/8 consensus

C)

Cell Line	FT33Tag	FT194	FT246	JHOS4	OVSAHO	KURAMOCHI
Top Motif	PAX2	PAX2	PAX2	PAX2	PAX2	PAX2
2nd Motif	PAX1	PAX5	PAX1	PAX5	PAX1	PAX5
3rd Motif	PAX5	PAX1	PAX5	PAX1	PAX5	PAX1
4th Motif	PAX9	PAX9	PAX5	PAX9	PAX9	PAX5
5th Motif	PAX6	PAX5	PAX9	PAX5	PAX6	PAX9

Figure 4.3: PAX8 Motif Analysis. ChIP analysis was performed on three ovarian cancer and three fallopian tube lines. A) De Novo motif analysis was performed on the fallopian tube cell lines and cancer cell lines to determine the highest conserved sequence in each group. B) De Novo PAX8 motif closely matches that of the previously published PAX2/5/8 subfamily consensus sequence[84,110]. C) Motif analysis identifying the most common previously published motifs in the PAX8 peaks universally identified other PAX binding sequences.

PAX8 Gene Regulation in Fallopian Tube Epithelium and High Grade Serous Ovarian Cancer

To determine which genes were regulated by PAX8, RNA Sequencing (RNAseq) was performed on FT194, FT246, and FT33-Tag, HGSOC, OVSAHO, KURAMOCHI, and JHOS4. Cells were treated with four different PAX8 siRNAs, a non transfection control, and non-targeting siRNA control before RNA isolation. Knockdown for each sample was confirmed via western blotting (Figure 4.4).

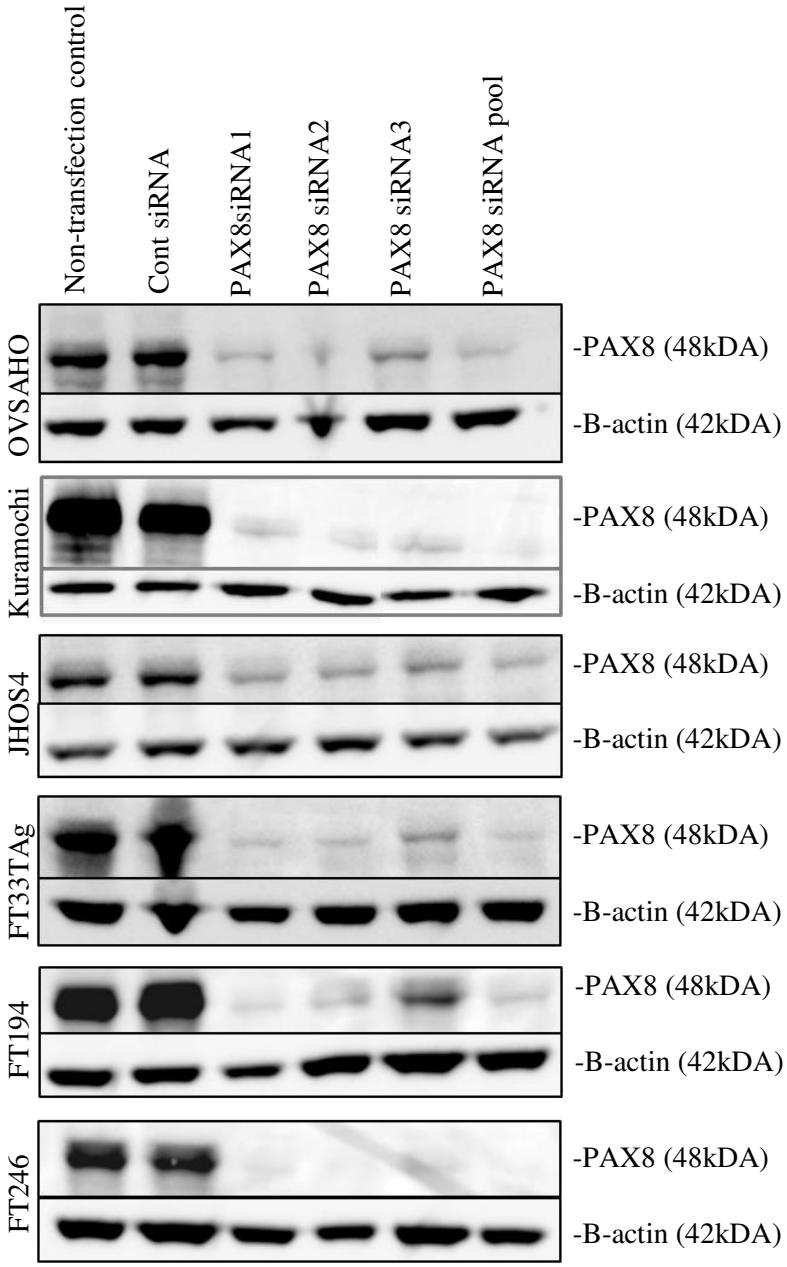

Figure 4.4: Confirmation of PAX8 knockdown
Western blot analysis of each cell line used for RNAseq showing PAX8 knockdown with three unique PAX8 siRNAs (1-3) or pooled PAX8 siRNA. Non transfected cells and cells treated with non-target siRNA (Cont siRNA) served as controls. B-actin was used as a loading control.

Data was initially analyzed in an unbiased manner through selection of the top 1,000 most variable genes across all 36 samples without weighted consideration for cell line or treatment (Figure 4.5). Remarkably, the largest division was between cancer and fallopian tube cell lines. The cancer samples were clearly divided secondly by cell line, with controls and treated samples dividing tertiary groups. Among the fallopian tube cell lines, the general trend was a secondary sorting by cell line, although one FT33Tag sample sorted most closely with FT194 samples. While FT controls tended to group together, no clear tertiary sorting was observed. This supports the idea that fallopian tube gene regulation varies minimally between cell lines, whereas cancer cell line gene regulation varies widely, both from fallopian tube epithelium, but also among individual cancer cell lines.

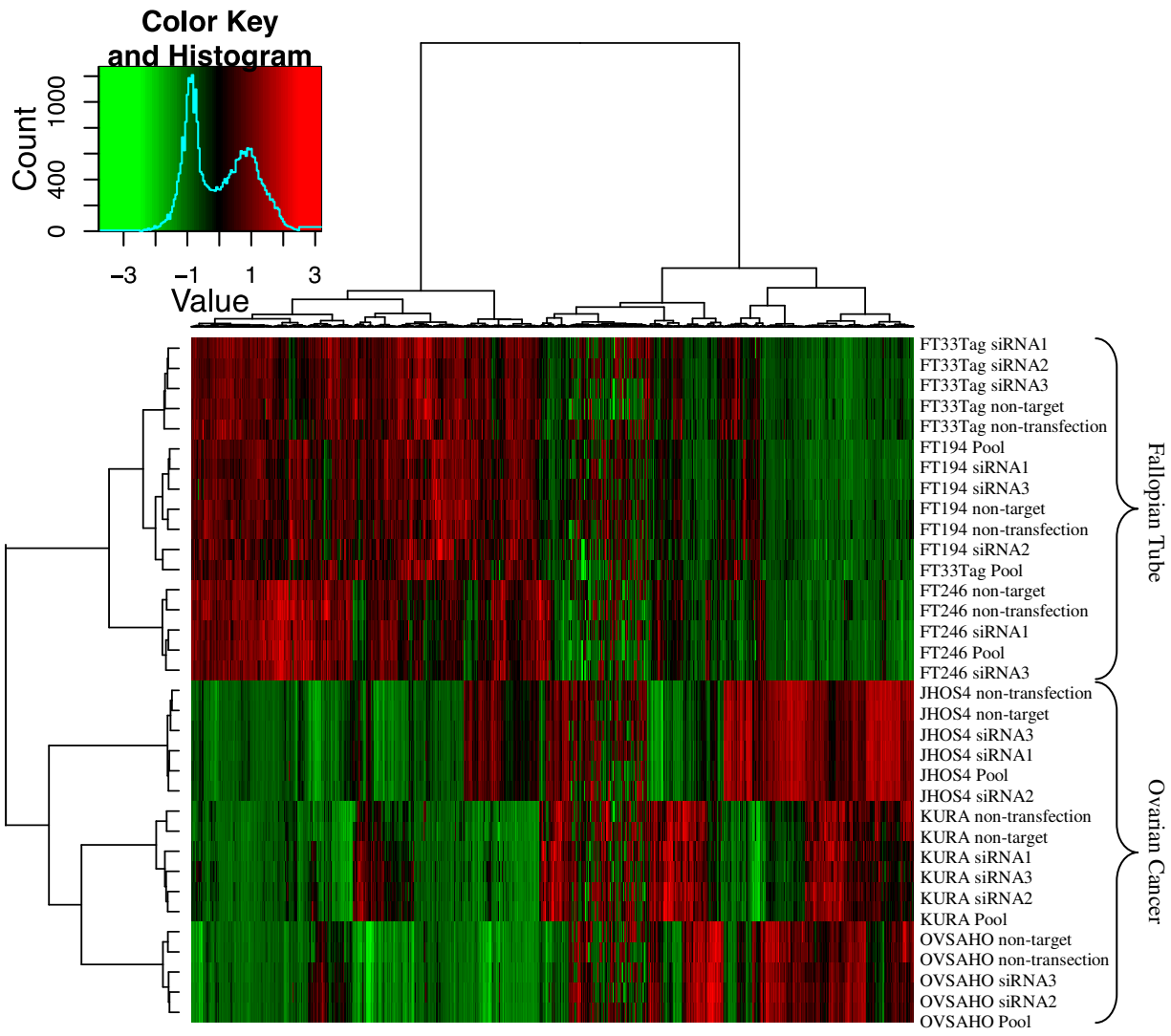

Figure 4.5: RNAseq Analysis of Fallopian Tube and Ovarian Cancer Cell Lines
PAX8 was knocked down with three siRNAs (1-3) and pooled PAX8 siRNA, with two controls, non-transfection and non-target siRNA. The top 1,000 most differential genes across the 36 samples were identified and phylogenetic mapping performed to determine which samples were most closely grouped together.

Strikingly, knocking down PAX8 in FT cells had little impact on gene regulation. Using an adjusted P-value cut off of $P<0.05$, the expression of only 1 gene was altered in FT33Tag cells, 32 in FT246, and 13 in FT194. If a minimum log fold change threshold of >2 is applied, the numbers decrease to 1, 5, and 4 for FT33Tag, FT246, and FT194, respectively. In contrast, 135 and 541 genes were differentially regulated in KURAMOCHI and OVSAHO when PAX8 was knocked down. JHOS4 was an outlier for the cancer cell lines with only 12 genes differentially regulated with an adjusted P-value of $P<0.05$. While very few individual genes overlapped between samples, small nucleolar RNAs and microRNAs as general populations were identified as differently regulated across cell lines.

Gene Ontology (GO) analysis could only be performed on KURAMOCHI and OVSAHO as the FT lines and JHOS4 had too few differentially regulated genes. The expression of 61 genes in OVSAHO cells was enhanced when PAX8 was knocked down, suggesting PAX8 normally downregulates these genes. Through GO analysis, the OVSAHO PAX8 downregulated genes were identified to be involved in cell functions such as cell migration, motility, proliferation, and blood vessel development (Figure 4.6). The expression of 31 genes was suppressed when PAX8 was knocked down in OVSAHO, suggesting PAX8 normally upregulates these genes. Using GO analysis, OVSAHO PAX8 upregulated genes were involved in M phase, mitosis, and other functions involved in cell cycle and cell division. These results differed widely from KURAMOCHI results. In KURAMOCHI, the 30 genes upregulated by PAX8 were identified to be involved in various catabolic and biosynthesis processes, whereas the 28 genes downregulated by PAX8 were involved in cell adhesion, blood vessel development, and interestingly apoptosis and cell death (Figure 4.7). Differences in PAX8 regulation of target genes confirm unique roles of PAX8 in cancer cell lines. Interestingly, apoptosis and cell death was only downregulated by PAX8 in the context of KURAMOCHI, which is known to develop a proliferation defect when PAX8 is knocked down (Figure 3.3).

A) OVSAHO

Term	RT	Genes	Count	%	P-Value
cell cycle	RT		16	12.0	7.6E-4
M phase	RT		10	7.5	9.0E-4
regulation of mitotic cell cycle	RT		7	5.3	1.1E-3
cell cycle phase	RT		11	8.3	1.2E-3
nuclear division	RT		8	6.0	1.4E-3
mitosis	RT		8	6.0	1.4E-3
M phase of mitotic cell cycle	RT		8	6.0	1.6E-3
regulation of cell cycle process	RT		6	4.5	1.8E-3
organelle fission	RT		8	6.0	1.8E-3
cell cycle process	RT		12	9.0	3.8E-3
spindle organization	RT		4	3.0	4.8E-3
rRNA processing	RT		5	3.8	5.3E-3
rRNA metabolic process	RT		5	3.8	6.2E-3
regulation of S phase of mitotic cell cycle	RT		3	2.3	6.4E-3

B) KURAMOCHI

Term	RT	Genes	Count	%	P-Value
cellular amino acid catabolic process	RT		6	3.8	3.8E-4
carboxylic acid catabolic process	RT		7	4.4	5.2E-4
organic acid catabolic process	RT		7	4.4	5.2E-4
carboxylic acid biosynthetic process	RT		8	5.0	5.3E-4
organic acid biosynthetic process	RT		8	5.0	5.3E-4
amine catabolic process	RT		6	3.8	7.1E-4
cellular amino acid biosynthetic process	RT		5	3.1	1.2E-3
ribonucleoprotein complex biogenesis	RT		8	5.0	1.3E-3
serine family amino acid metabolic process	RT		4	2.5	1.6E-3
oxidation reduction	RT		15	9.4	2.0E-3
nitrogen compound biosynthetic process	RT		10	6.2	2.9E-3
serine family amino acid biosynthetic process	RT		3	1.9	4.3E-3
serine family amino acid catabolic process	RT		3	1.9	4.3E-3

Figure 4.6: Gene Ontology Analysis of Genes Upregulated by PAX8.
Gene Ontology (GO) analysis was applied to RNAseq data comparing gene expression before and after PAX8 knockdown. Pathways were identified involving genes which were decreased when PAX8 was knocked down, and therefore upregulated by PAX8 in A) OVSAHO and B) KURAMOCHI cells.

A) OVSAHO

Term	RT	Genes	Count	%	P-Value
cell motion	RT		16	13.1	6.7E-7
cell migration	RT		11	9.0	1.8E-5
localization of cell	RT		11	9.0	4.4E-5
cell motility	RT		11	9.0	4.4E-5
regulation of cell proliferation	RT		17	13.9	7.3E-5
positive regulation of immune system process	RT		8	6.6	1.2E-3
blood vessel development	RT		8	6.6	1.4E-3
vasculature development	RT		8	6.6	1.6E-3
regulation of locomotion	RT		7	5.7	2.0E-3

B) KURAMOCHI

Term	RT	Genes	Count	%	P-Value
homophilic cell adhesion	RT		8	5.7	7.0E-5
cell-cell adhesion	RT		10	7.1	2.9E-4
response to hypoxia	RT		7	5.0	6.1E-4
blood vessel development	RT		9	6.4	6.3E-4
vasculature development	RT		9	6.4	7.4E-4
apoptosis	RT		14	10.0	7.6E-4
response to oxygen levels	RT		7	5.0	8.0E-4
induction of apoptosis	RT		10	7.1	8.5E-4
induction of programmed cell death	RT		10	7.1	8.7E-4
programmed cell death	RT		14	10.0	8.8E-4
cell adhesion	RT		15	10.7	1.0E-3
biological adhesion	RT		15	10.7	1.0E-3
angiogenesis	RT		7	5.0	1.0E-3
positive regulation of cell-substrate adhesion	RT		4	2.9	1.3E-3
cell death	RT		14	10.0	3.7E-3
death	RT		14	10.0	3.9E-3

Figure 4.7: Gene Ontology Analysis of Genes Suppressed by PAX8.
Gene Ontology (GO) analysis was applied to RNAseq data comparing gene expression before and after PAX8 knockdown. Pathways were identified involving genes which were increased when PAX8 was knocked down, and therefore suppressed by PAX8 in A) OVSAHO and B) KURAMOCHI cells.

PAX8 Dependent Gene Regulation in Ovarian Cancer Cell Lines

Merging of ChIPseq and RNAseq data was only possible in KURAMOCHI and OVSAHO cell lines where both data sets were large enough to facilitate analysis. Gene transcripts significantly impacted by PAX8 knockdown as determined through RNAseq by an adjusted P value of $P<0.05$ and a Log fold change threshold of 1.5 were merged with ChIPseq data to identify any regulated gene containing a PAX8 binding site within 50K bp of the gene start sight. Through this method, 20 and 22 genes were identified in OVSAHO and KURAMOCHI cells, respectively, that were not only regulated by PAX8 but also had unique PAX8 binding sites not present in the FT setting (Figure 4.8). All genes showed a decrease in expression when PAX8 was knocked down, therefore indicating a gain of PAX8 dependent regulation in the setting of ovarian cancer.

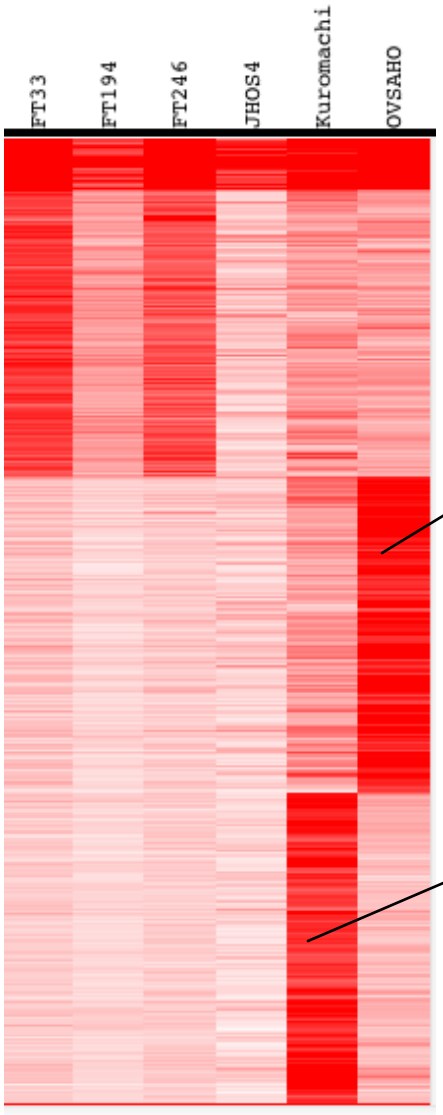

A)

Gene	LogFC	Gene	LogFC
LMO3	-2.1190436	CBS	-0.8702479
RAP1GAP	-2.0816155	ILVBL	-0.7966206
AFAP1L2	-1.9790826	POR	-0.7879854
COMTD1	-1.3039289	ATP2B2	-0.7788407
GDF11	-1.2781106	FAM20A	-0.7355449
RAI2	-1.2547991	AIMP2	-0.6995449
PKNOX1	-1.1552406	ENO1	-0.6653121
LRRK1	-1.0226624	ASF1B	-0.6184003
SLC25A29	-0.9223729	CNTFR	-0.6115579
MCU	-0.8878575	COX5B	-0.5834022

B)

Gene	LogFC	Gene	LogFC
SEMA5B	-4.0694354	SYK	-1.3968394
RAP1GAP	-2.8790656	TP53AIP1	-1.3216462
SLC26A7	-2.8033031	SERTM1	-1.2882428
KLRG2	-2.6853322	EVA1A	-1.2581869
GLDC	-2.3629285	SMAD9	-1.2517365
ABCA4	-2.0724722	GPD1L	-1.1603745
KCNJ16	-1.9549945	CBS	-1.0341532
REN	-1.7057131	PECR	-1.0292801
PLXNA4	-1.6770386	BHLHE41	-1.010406
LGR5	-1.6565063	AIMP2	-0.6002974
FAT2	-1.397614	DMRT1	-0.5801427

Figure 4.8: PAX8 Dependent Gains in Ovarian Cancer Cell Lines
Gene transcripts significantly impacted by PAX8 knockdown as determined through RNAseq by an adjusted P value of P<0,05 and a Log fold change threshold of 1.5 were merged with ChIPseq data to identify any regulated gene containing a PAX8 binding site within 50K bp of the gene start sight. In A) OVSAHO cells, this resulted in 20 PAX8 dependent genes with PAX8 binding sites, and in B) KURAMOCHI cells, this resulted in 22 PAX8 dependent genes with

Discussion

PAX8 is expressed in both the fallopian tube and HGSOC, but gene regulation and PAX8 binding sites differ widely between the normal and cancer settings. Fallopian tube cell lines remarkably preserve similar binding sites across individuals and immortalization methods, while cancer cell line PAX8 binding sites overlap minimally with fallopian tube samples, losing many binding sites previously identified and gaining many novel binding sites. Lost binding sites in the context of ovarian cancer seem to be similar across cell lines, while novel binding sites differ widely from ovarian cancer cell line to cell line.

With only three ovarian cancer cell lines in the data set, it is unknown whether the diversity of distinct binding site patterns would be preserved across a larger sample size, or whether we would begin to see groups of binding site patterns emerge. Specifically of interest is the JHOS4 ChIPseq data which produced a scarcity of binding sites as compared to the other two cancer cell lines. Originally, this was thought to be due to a technical error, but independent RNAseq data also identified relatively few genes differentially regulated by PAX8 knockdown. Similarly, ChIPseq peaks were scarce in the FT194 cell line, yet all FT lines produced few differentially regulated genes by PAX8 knockdown. This may suggest that the JHOS4 pattern of PAX8 regulation most closely mimics that of the FT lines rather than other ovarian cancers.

By GO analysis of RNAseq data, PAX8 was found to uniquely downregulate cell functions including apoptosis and cell death in KURAMOCHI cells. Analysis of the genes involved in these pathways could help us develop a mechanistic explanation for why PAX8 knockdown significantly inhibits proliferation in KURAMOCHI cells but not OVSAHO cells. Unfortunately, proliferation assays were not performed on JHOS4 so we are unable to draw similar conclusions from its gene expression analysis. Expanding RNAseq data to include several cell lines previously identified as sensitive and insensitive to PAX8 knockdown would further help develop a gene signature relating to PAX8 sensitivity.

It currently remains unclear why PAX8 binding sites are so different between the fallopian tube and ovarian cancer. One possible explanation is a difference in methylation whereby access to certain binding sites is restricted or exposed in the setting of the fallopian tube vs. ovarian cancer. Patient methylation data available from the TCGA could be used to further explore this hypothesis. Another possibility is that a cofactor or tandem transcription factor is required for PAX8 binding at certain sites, which is gained or lost as the cell undergoes pathogenesis. A more detailed analysis of the ChIPseq data would be required to tease out conserved binding sites close to PAX8 peaks which might suggest potential cofactors or co-transcription factors.

Peak identification from the ChIPseq data revealed that the most common PAX8 binding sites very closely matched the motifs of other PAX proteins. While theoretically possible that this is due to antibody cross reactivity picking up non-PAX8 proteins, this is unlikely due to the fact that PAX8 has previously been identified as the only PAX protein expressed in ovarian cancer[111]. This is further supported by the developmental role of PAX proteins which are closely regulated both spatially and temporally[48]. Thus, from previous data showing similar binding sites for the PAX2/5/8 subfamily, we would expect the differential role of these proteins to come primarily from the contextual expression level of each PAX protein rather than their binding location[84,110] It should be noted, however, that not all PAX protein expression is mutually exclusive. Specifically, PAX2 and 8 are co-expressed in the kidney, which is not significantly impacted in PAX8 knockout models as compared to the fallopian tube and thyroid[61]. This suggests that when multiple PAX proteins are co-expressed, one can at least partially compensate for the other's loss.

CHAPTER 5

Materials and Methods

Materials and Methods

Cell Culture

All cell lines were grown at 37°C with 5% Co_2. SKOV3, OVCAR3, OVCAR4, and OVCAR8 cells were cultured in RPMI 1640 with L-glutamine supplemented with 10% fetal bovine serum and 1% Penicillin/ Steptomycin (Mediatech, Atlanta Biologicals, and Gibco). IGROV1, MCF7, S3 HeLa, and S3 HeLa derived cell lines were cultured in DMEM media supplemented with 10% fetal bovine serum and 1% Penicillin/ Steptomycin (Mediatech, Atlanta Biologicals, and Gibco). JHOS4, OVSAHO, KURAMOCHI, and OVSAHO and KURAMOCHI derived cell lines were cultured in DMEM:F12 media supplemented with 10% fetal bovine serum and 1% Penicillin/ Steptomycin (Mediatech inc, Atlanta Biologicals, and Gibco). FT33Tag, FT194, FT246, and FT189 were derived from primary fallopian tube epithelium as described previously[40,112] and were cultured in DMEM:F12 media supplemented with 2% Ultraser^{tm}G and 1% Penicillin/ Streptomycin (Mediatech inc, Pall Biosera, and Gibco). 293T cells were cultured in DMEM media supplemented with 10% FBS and 5mM HEPES (Mediatech inc, and Gibco).

Western Blotting

Cell pellets were lysed in RIPA buffer (Boston BioProducts) containing protease and phosphotase inhibitors for 20 min on ice, and then cleared by centrifugation for 10 minutes at 15,000 rpm at 4°C. Protein concentration was determined by DC Protein Assay (Bio-Rad). Between 10-20ug of cell lysate were loaded onto NuPage 4-12% BisTris Gels (Novex) and proteins were separated by electrophoresis in MOPS-SDS running buffer. Proteins were transferred to nitrocellulose membranes (Novex) using the iBlot semi dry transfer system (Invitrogen, Life Technologies). Blots were blocked for an hour at room temperature in 5% nonfat milk in PBS-Tween-20 (Westnet Inc.) and probed with the antibody of interest diluted in blocking buffer overnight at 4°C (Table 5.1). B-actin was used as a loading control. HRP-linked anti-mouse and anti-rabbit secondary antibodies (GE Healthcare) were applied at 1:4,000 dilution for 1

hour at room temperature and proteins were detected with ECL2 western blotting substrate kit or Supersignal sensitivity substrate (Thermo scientific).

Table 5.1: Antibodies and Dilutions used for Western Blotting

Antibody	Type	Company	Product #	Dilution used
PAX8	Rabbit poly	Proteintec	10336-1-AP	1:1,000
PAX8	Mouse mono	Abcam	Ab53490	1:500
BACH1	Rabbit poly	Sigma Aldrich	B1310	1:500
BRCA1	Rabbit poly	Millipore	07-434	1:500
BRCA1	Mouse mono	Sigma Aldrich	SAB2702136	1:500
B-actin	Mouse	Sigma	A2228	1:4,000
HA	Mouse	Cell Signaling	2367S	1:4,000
P53 (DO-1)	Mouse mono	Santa Cruz	Sc-126	1:500
CK7	Rabbit poly	Cell Signaling	4898s	1:1,000
Stathmin	Rabbit poly	Cell Signaling	3352	1:500
CA-125	Rabbit mono	Abcam	Ab168360	1:500

SiRNA Reverse Transfection

RNAi knockdown was performed by reverse transfection using standard siRNA oligonucleotides (Ambion, Life Technologies). Oligonucleotides targeting PAX8 (Life Technologies #439240 IDs 15403, 15404, or 15405) or a non-targeting control oligonucleotide (Life Technologies #4390843) were diluted to achieve a final concentration of 30pmol in serum-free Opti-MEM®I media (Life Technologies) before being combined with Lipofectamine®RNAiMAX (Life Technologies) for 10 min at room temperature. For pooled samples, 10pmol each of the three PA8 siRNAs were combined. Cells in antibiotic free media were then combined with siRNA complexes. An aliquot of non-treated cells served as a transfection control. Western blot analysis of siRNA was performed at 72hrs and Cell Titer Glo analysis after an appropriate time period depending on experimental design, ranging from 72-168 hours.

Massively Parallel Paired-End Sequencing and Somatic Mutation Identificaiton

Sample library construction, targeted capture, next generation sequencing, and bioinformatic analyses of cell lines were performed as previously described[112]. In brief, fragmented genomic DNA from cell lines were used for targeted regions using the Agilent SureSelect 50 Mb kit according to the manufacturer's instructions (Agilent). Captured DNA libraries were sequenced with Illumina MiSeq System (Illumina). Sequence reads were analyzed and aligned to the human genome sequence (hg18) with the Eland v.2 algorithm in CASAVA 1.7 software (Illumina). Potential somatic mutations and copy number alterations were identified as described previously[113,114].

Conditioned Media

Cell lines were grown to 80-90% confluency on 15cm plates and then washed three times in serum free media without antibiotics. Cells were then cultured for 3 days in serum free and antibiotic free media to produced conditioned media. The conditioned media was centrifuged at 3,000 rpm for 10 min to pellet debris, then the supernatant was concentrated using a 3kDa centrifugal filter (EMD Millipore) to a volume of 500 ml.

CA-125 ELISA

CA-125 levels were quantitated from conditioned media using a CA-125 ELISA kit (Thermo Fisher Scientific) according to the manufacturer's instructions. Conditioned media from HeLa cells served as a positive control.

Platinum Sensitivity Assay

Luciferized KURAMOCHI, OVSAHO, and SKOV3 cells were plated in sextuplicate on a 96 well plate and treated with cis-diamminedichloroplatinum (II) (cisplatin, Sigma-Aldrich) at indicated concentrations in complete media. Cells were incubated for 96 hours, and cell number was quantified by luciferase activity. Log dose response curves were constructed, and the mean IC50 values compared using the extra sum-of-squares F test (GraphPad). A p-value of less than 0.05 was considered significant.

Cell Titer Glo Analysis

Cell Titer Glo analysis was performed according to the kit manufacturer's instuctions (Promega) with the following minor alteration for experiments including cells treated with follicular fluid: Instead of adding an equal amount of Cell Titer Glo reagent directly to the cells and culture media, treatment media was first aspirated and replaced with 1%RPMI immediately before the addition of Cell Titer Glo reagent. This was to prevent clotting of follicular fluid and consequent obscuring of cellular signal. Luminescence was quantified on a modulus microplate reader (Turner Biosystems).

SRB Analysis

Cells were plated in 96 well plates at sufficient density to reach approximately 80% confluence at end time point. At end time point all media was aspirated and cells were incubated in equal parts PBS and freshly prepared 10% trichloroacetic acid (Sigma) overnight at 4°C. Plates were then rinsed with tap water 3x and allowed to dry overnight at room temperature. When plates were completely dry, 100uL of 0.12% SRB in 1% acetic acid (Fischer Scientific) was added to each well and plates were incubated for 30 min at room temperature. Samples were then rinsed with 1% acetic acid 4x until all unbound dye had been removed. Plates were then dried completely at room temperature. Once plates were dry, 200uL 10mM Trizma Base solution (Sigma) was added to each well and incubated rocking at room temperature 10 min to allow all dye to dissolve. OD was measured at a wavelength of 510nm on a Modulus microplate reader (Turner Biosystems, Promega).

Flow Cytometry

Annexin V analysis was performed to analyze levels of apoptosis in KURAMOCHI cells treated with PAX8 siRNA after 48, 72, and 96 hours using the TACS® Annexin V-FITC kit (Trevigen) following the manufacturer's instructions. Cell cycle analysis was performed to analyze levels of cellular arrest at 72 and 96 hours in KURAMOCHI cells treated with PAX8 siRNA using the BD Cycletest™ Plus DNA Reagent Kit (BD) following the manufacturer's instructions but excluding the filtration final step since KURAMOCHI cells are larger than the cells used to optimize the protocol and therefore do not

pass through the filter. All flow cytometry results were read on a BD LSRFortessa™ cell analyzer (BD) with the support of the DFCI Flow Cytometry Core.

Generation of IPTG Inducible PAX8 shRNA Expressing Lines

E.Coli was first transformed with vector plasmid. 30pg plasmid DNA (Mission®pLKO-puro-IPTG-3xLacO containing PAX8 specific shRNAs as previously described[73]: RTRCN0000021277 5′-CCCAGTGTCAGCTCCATTAAT-3′ (277) or TRCN0000021278 5′-CCGACTAAGCATTGACTCACA-3′ (278), or non target control, Sigma Aldrich) or control P-UC19 plasmid were combined with E. coli and incubated in ice for 30 min prior to heat shock at 42°C for 45 seconds. Samples were replaced on ice and rescued with SOC media (Invitrogen) before being shaken at 37°C for 1 hour. E.Coli was spread on selection plates and incubated overnight at 37°C at which point mini-preps were prepared and restriction digest performed using PST1 and Kpn1 restriction enzymes to confirm proper sequence alignment. Maxipreps of validated bacterial clones were generated and DNA was purified with an endotoxin free maxiprep kit (Qiagen).

Next, 293T cells were transfected with DNA to generate packaged lentiviral constructs. Lentiviral packaging mix (Sigma Aldrich) was combined with 2.6ug transfer vector (generated in E.Coli) on ice before being combined with Xtremegene and Optimem at room temperature for 15 min. Transfection cocktails were added dropwise to 10cm plates of 293T cells in antibiotic free media and incubated at 37°C. Three days later the media was replaced and virus was harvested on the 4th and 5th days. Viral harvest was performed by collecting media from lenti-viral plates and centrifuging at 500g for 10 minutes to remove dead 293T cells. Viral containing supernatent was combined with 1 volume Lenti-X concentrator (Clontech) to 3 volumes supernatent and incubated at 4°C for 30 min before centrifugation to pellet viral constructs. Virus aliquots were quantified using the QuickTiterHIV Lentivirus Quantitation Kit (Cell Biolabs) following manufacturer's instructions and stored at -80°C.

OVSAHO and KURAMOCHI cells were infected with viral constructs. 100,000 cells were plated per well on a 6 well plate and incubated overnight at 37°C with complete, antibody containing media. The next day Hexadimethrine (Polybrene, Sigma Aldrich) was combined with media for a final concentration of 8ug/mL and combined with virus at concentrations of 1, 5, 10, and 20MOI. Cells and virus containing media were incubated together overnight at 37°C and media was replaced the following day. On the second day after infection, fresh media containing 0.5ug/mL puromycin was added to cells to induce selection. Selection was maintained until non-virally infected control cells were all dead. To induce shRNA in vitro, cells were treated with 10mM IPTG fresh daily.

Luciferization of Cell Lines

Cell lines were combined with mCherry-luc containing lentiviral particles (generously provided by Dr. Sangeetha Palakurthi, Belfer Center, DFCI, with permission from Dr. Andrew Kung, Columbia University) at several multiples of infection (MOI) along with 8ug/mL Hexadimethrine Bromide (Polybrene, Sigma-Aldrich). After 24 hours standard complete media replaced viral media. 48 hours after start of infection, 0.5ug/mL puromycin (Sigma Aldrich) was added to select for successfully infected cells. Selection was maintained until non-infected control cells had died, at which point positive selection was performed via flow cytometry selecting for mCherry expression. Luciferase activity confirmed selection success.

Xenografts

All animal work was performed with approval from the Institutional Animal Care and Use Committee (IACUC) under protocol 13-043: Establishment of murine serous ovarian carcinoma xenografts from ovarian cancer cell lines. All cells were confirmed to be pathogen free via Mouse Antibody Production (MAP) testing (Charles River Research Animal Diagnostic Services) prior to experimentation. Athymic (nude) and NOD.Cg-Prkdc^{scid} Il2rg^{tm1Wjl}/SzJ (NSG) mice were provided by the Jackson Laboratory. Mice were given food and water ad libitum and maintained in compliance with

standard IACUC protocol. Body conditioning scores and weight were assessed weekly to ensure colony health.

Subcutaneous tumors were measured with calipers and tumor volume calculated using the standard formula 0.5 x (length x width^2)[115,116]. PAX8shRNA xenograft tumors were treated with Isopropyl β-D-1-thiogalactopyranoside (IPTG, Fisher Scientific) dissolved in ultrapure water and filtered with a 0.2uM filter. IPTG water was replaced at least every 3 days for maximal drug potency.

Luminol Imaging

Mice were anesthetized with isoflurane and injected with luciferin intraperitoneally or subcutaneously in accordance with tumor location (Gold Biotechnology). After 5 min, mice were imaged via the IVIS® in vivo imaging system (PerkinElmer). All images were taken at F-stop1 with medium binning. Exposure time was optimized for each cell line. Post-image processing and quantification of bioluminescence was performed with Living Image software® (PerkinElmer). Intensity scales were normalized across time points for each cell line prior to quantitative analysis of average radiance measured in p/s/cm²/sr.

Histology

After euthanasia, necropsies were immediately performed, and tissues were placed in cassettes. Tissues were fixed for 24 hours at room temperature in 10% neutral buffered formalin, then transferred to 70% ethanol. Tissues were embedded in paraffin blocks, and histologic sections were stained with hematoxylin and eosin.

Immunohistochemistry

Immunohistochemistry was performed using the Envision Plus/Horseradish Peroxidase system (Dako) and a polyclonal antibody to PAX8 (Proteintech, 1:200 dilution). Paraffin embedded sections were incubated in hydrogen peroxidase and absolute alcohol for 30 minutes to block endogenous peroxidase activity. Antigen retrieval was performed using pressure cooker pretreatment in citrate buffer

(pH=6.0). Tissue sections were subsequently incubated with the primary antibody for 40 minutes at 25°C. Following Tris-Buffered Saline (TBS) rinses, the tissue was incubated using the Envision Plus secondary antibody (Dako) for 30 minutes followed by diaminobenzidine for 5 minutes. Appropriate positive (prostate) and negative (incubation with secondary antibody only) controls were stained in parallel for each round of immunohistochemistry. Strong nuclear staining PAX8 was considered positive.

RNA Sequencing

SiRNA was used to knockdown PAX8 expression in duplicate cell cultures of the cell lines FT33TAg, FT194, FT246, JHOS4, KURAMOCHI, and OVSAHO via a reverse transfection (as described above). Cells were harvested after 72 hours with one culture designated for RNA extraction and the other for western blot confirmation of knockdown. RNA was extracted by homogenization with a QIAshredder and purified following the manufacturer's instructions in the RNeasy mini prep kit (Qiagen). Samples were further purified by DNAse treatment via the Turbo DNA-free^{TM} Kit following manufacturer's instructions (Ambion) and final RNA concentration measured using a Nanodrop system (Thermo Scientific). RNA sample quality was validated by the Center for Cancer Computational Biology (CCCB) at Dana Farber Cancer Institute (DFCI). RNA-seq libraries were generated via Illumina Truseq HT (Illumina) and validated by the Center for Functional Cancer Epigenetics (CFCE) at DFCI. Libraries were sequenced via the single-end 75bp method on a Illumina NextSeq 500 system (Illumina) at the Molecular Biology Core Facilities (MBCF) at DFCI. Reads were aligned using human reference genome hg19 via TopHat software[117]. Post-sequencing analysis was performed by the CFCE at DFCI.

Chromatin Immunoprecipitation Sequencing

FT33TAg, FT194, FT246, JHOS4, KURAMOCHI, and OVSAHO cells were grown to confluency. Transcription factors were crosslinked to DNA by incubating cells in 1% Formaldehyde in full media for 10 min at 37°C. The crosslinking reaction was quenched with ice cold PBS containing 0.125M glycine and 5mg/mL BSA. Cells were then rinsed in ice cold PBS and harvested by scraping. Cells were spun down at 2,000rpm for 5 min at 4°C before being resuspended in 15 mL of the first lysis

buffer LB1 (50mM Hepes-KOH pH 7.5, 140mM NaCl, 1mM EDTA, 10% Glycerol, 0.5% NP-40, 0.25% TritonX-100) for 10 min rotating. Cells were pelleted at 2,000rpm for 5 min at 4°C and resuspended in 15 mL of the second lysis buffer LB2 (10mM Tris-HCL pH 8.0, 200mM NaCl, 1mM EDTA, 0.5mM EGTA) for 5 min rotating. Cells were pelleted as in previous step and resuspended in 350uL of the third lysis buffer LB3 (10mM Tris-HCL pH 8.0, 200mM NaCl, 1mM EDTA, 0.5mM EGTA, 0.1% Na-Deocycholate, 0.5% N-Laurylsarcosine) before sonication at setting 2, 21 minutes pulsing with 30 seconds on and 30 seconds off. 40uL 10% TritonX was added to each sonicated sample and samples were centrifuged for an additional 13,000 rpm for 10 min at 4°C. The supernatant was then transferred to a new tube for immunoprecipitation.

10uL of the chromatin solution was set aside as input from each sample. 1mL of ChIP dilution buffer (20mM Tris-HCL, 150mM NaCL, 2mM EDTA, 1% TritonX-100) was added to the remainder of the sample and incubated overnight with 10ug of PAX8 antibody (Novus) at 4°C rotating. Protein G beads washed in PBS with 5% BSA and then resuspended in ChIP dilution buffer. Beads were then added to the antibody-bound samples and incubated for 45 min at 4°C with rotation. The beads were then captured on a magnent. Supernatant was removed and samples washed 4x with RIPA-LiCl wash buffer (50mM HEPES pH 7.6, 1mM EDTA, 0.7% Na-Deoxycholate, 1% NP-40, 0.5M LiCl), then washed 2x with ice-cold TE before resuspension in ice-cold TE.

Input and antibody bound fractions were treated with 0.5ug/uL RNase in 1x TE for 1 hour at 37°C. ProteinaseK at 0.5ug/uL was added and crosslinking was immediately reversed by incubating at 65°C overnight in 1% SDS and 0.1M NaBicarbonate NaHCO3. DNA fragments were purified via Qiaquick PCR purification columns (Qiagen) and quantified to ensure a concentration between 50-200pg/uL. DNA fragments were confirmed to be between 200-800bps via E-gel. For ChIP-Seq, after repairing the DNA ends, sequencing adaptors (Illumina) were ligated to the purified chromatin and the DNA was amplified for sequencing.

Libraries were sequenced on a HiSeq2000 instrument (Illumina) by the Center for Functional Cancer Epigenetics (CFCE) at DFCI and aligned to human genome 19 (hg19). Post-sequencing analysis was performed by the CFCE at DFCI.

Generation of Stable S3 HeLa and KURAMOCHI Cell Lines Expressing Empty and PAX8 TAP TAG Vectors

PAX8 cDNA was inserted into the TAPTAG vector via PCR cloning so that the TAPTAG vector attached to the C terminus of PAX8. S3 HeLa and KURAMOCHI cells were grown to 40% confluence in 6cm plates and infected with virus containing the PAX8 or empty-TAPTAG vector and combined with 5ug/mL polybrene (Sigma-Aldrich). After 3 days, cells infected with the virus were selected via incubation with Dynabeads (Invitrogen) bound to anti-IL-2 Receptor alpha antibody (Millipore) for 1 hour. Bound cells were rinsed and examined under a microscope until cells in the non-infected control group were no longer visible, and infected cells finally resuspended in media to expand infected population. Reselection was performed as necessary when western blotting indicated a decrease in expression of TAP-TAG construct.

Re-Selection of TAP TAG Cells

To increase TAP-Tag expression, KURAMOCHI cells were dissociated with enzyme free, PBS based cell dissociation buffer (Gibco) and cell pellet resuspended with 20uL of magnetic Dynabeads (Invitrogen) bound to anti-IL-2 Receptor alpha (Millipore) for every 1.5million cells. Samples were incubated rocking at room temperature for 1 hour. Cells bound to magnetic beads were selected and re-plated in normal cell culture conditions to expand desired population and obtain a higher expression of TAP-Tag construct.

Immunoprecipitation

Nuclear extracts were obtained from S3 HeLa taptag PAX8 and S3 HeLa taptag empty cells as previously described[118]. Briefly, cells were manually removed from plate and resuspended in hypotonic

buffer prior to cell lysis via dounce. Centrifugation separated out the chromatin pellet, and the solubilized nuclear fraction was further digested with micrococcal nuclease. For KURAMOCHI taptag PAX8 and KURAMOCHI taptag empty cells, IP input was whole cell extracts harvested via manual dissociation.

Immunoprecipitation was performed described by Adelmant et al[118]. Briefly, cellular inputs were incubated with Flag-agarose conjugate (Sigma-Aldrich) and eluted with FLAG peptide (Sigma-Aldrich). Flag eluates were filtered with a PVDF 0.45um centrifuge filter (Millipore) before being re-selected with HA-agrose conjugate and eluted with HA peptide (Marto Lab, DFCI). Silverstains were performed to validate eluates using the Silverquest Staining Kit (Invitrogen), and western blots were probed with anti-HA to confirm purification.

Mass Spectroscopy

LC-MS/MS was performed by the BLAIS proteomics center as previously described[118]. Briefly, tryptic digest peptides from IP elutions were analyzed via LC-MS/MS, and data was further filtered using an internal database to rule out proteins with a false detection rate of >1%. Proteins identified in the empty vector control samples were removed from finalized list of potential interacting proteins.

Co-Immunoprecipitation

Two confluent 10cm plates per Co-IP sample were manually dissociated and lysed in the same lysis buffer used for IP (150mM NaCl, 50mM Tris pH 7.5, 1mM EDTA, 0.5% NP40, 10% Glycerol and EDTA-free protease inhibitors (Roche)) for 20 min at 4°C. Cell debris was spun down for 10 min full speed and supernatent cleared for 1 hour at 4°C with unbound protein-G sepharose beads (Sigma Aldrich). Cleared lysate was then incubated with 5ug antibody of interest (PAX8, Abcam, BACH1, Sigma Aldrich, BRCA1, Sigma Aldrich) or 5 ug of IgG control antibody (IgG Rabbit, Cell Signalling, or IgG Mouse, Jackson Antibodies) for 3 hours rocking at room temperature. Unbound protein-G sepharose beads were added to solutions and incubation continued for 30 more minutes. Bound antibody and protein

complexes were eluted with Laemmli buffer (Boston BioProducts) and interactions validated by western blot.

Immunofluorescence

Cells were grown and treated on either transwell membranes (Corning) or glass coverslips before being fixed with 4% PFA for 20 min at room temperature. Cells were permeabilized with 0.5% Triton X-100 for 5 min and blocked for 1 hour at room temperature with superblock blocking buffer (Life Technologies). Primary antibody (p-H2AX, Millipore, 53Bp1, Bethyl) at 1:500 concentration diluted in 3% superblock blocking buffer was incubated with cells overnight at 4°C followed by a one hour incubation with Alexa Fluor 568 (red) or 488 (green) conjugated secondary antibody (Life Technologies) diluted 1:500 in PBS at room temperature. For TAP-Tag construct localization studies, cells were co-stained with PAX8 (1:500, Proteintech) and HA (1:100, Cell Signaling). Samples were mounted onto glass slides using DAPI-containing Vectashield mounting medium (Vector Laboratories, Inc.). Images were acquired at 40x using an Olympus BX51 fluorescence microscope with attached DP71 camera and DP Manager Software.

Comet Assay

Cells were grown in standard culture or treatment conditions before being scraped in ice cold PBS and centrifuged at 1,000rpm for 5 min at 4°C to remove residual media. Cells were resuspended in ice cold PBS at $1x10^5$ cells/mL. Cells were processed via the Alkaline protocol as outlined in the Trevigen Comet Assay kit (Trevigen). A 30cm long electrophoresis chamber was used to elongate DNA at 30V for 30 min in compliance with the 1V/cm guidelines. Lastly, slides were stained with SYBR Gold (Life Technologies) and imaged with an Olympus BX51 fluorescence microscope with attached DP71 camera and DP Manager Software. Percent DNA in comet tail was analyzed via Comet Score software (TriTek Corporation) by analyzing 100 cells per treatment group and filtering out the 5 highest and lowest values to decrease outliers.

Ex Vivo Fallopian Tube Culture

Primary fallopian tubes were collected from Brigham and Women's Hospital in compliance with IRB protocol 02-051: Collection of Tissue and Blood Specimens and Clinical Data from Patients with Suspected Gynecological Neoplasms and Patients with Gynecological Cancers. Tissues were dissociated and cultured on collagen IV-coated Costar polyester Transwell-clear inserts placed in 24-well tissue culture plates (Corning) and cultured in DMEM:F12 media supplemented with 2% Ultraser^{tm}G and 1% Penicillin/ Streptomycin (Mediatech inc, Pall Biosera, and Gibco) as previously described[37].

Processing of Follicular Fluid

Frozen human follicular fluid samples were obtained from the Brigham and Women's Hospital In Vitro Fertilization clinic in pre-processed, frozen aliquots. Samples were thawed on ice and used immediately. Repeat freezing and thawing was limited.

Bovine follicular fluid was generously donated by the Tsang lab from research cows at the University of New Hampshire in pre-processed, frozen aliquots. Samples were thawed on ice and used immediately. Repeat freezing and thawing was limited.

Fresh human follicular fluid was obtained from the Brigham and Women's Hospital In Vitro Fertilization clinic in compliance with IRB protocol 2013P000771: Effect of Ovulation on Ovarian Cancer. Follicular fluid was harvested along with mature follicles via transvaginal ultrasound aspiration. Once eggs had been removed, discarded follicular fluid was stored briefly at 4°C until it could be picked up by researchers for further experimentation (less than 20 min). Follicular fluid samples were transferred to ice and immediately centrifuged at 1,500g for 10 min at 4°C as per standard follicular fluid processing guidelines[119]. This separated the blood cells and the straw-colored follicular fluid. The bloody pellet was discarded and the supernatant containing follicular fluid was then used for experimental purposes within the next hour. For paired samples comparing frozen fresh follicular fluid to fresh follicular fluid, a fresh sample was divided and one half kept on ice breifly while the second half was flash frozen in ethanol and

dry ice and transferred to -80°C for 15 min before being thawed on ice. Both samples were then immediately used to treat cell cultures.

Chemiluminescent Analysis of Follicular Fluid

Frozen, pre-spun follicular fluids were thawed on ice and immediately measured. Fresh Ascites samples were spun down at 1,000rpm to remove blood cells, fat cells, and other debris, and the supernatant was immediately measured. Titrated H2O2 samples were made by combining 10uL of the labeled molarity with 390uL of PBS. 400uL of sample was combined with 10uL luminol and, when noted, 2uL of catalyzing reagent horseradish peroxidase (HRP). All samples were measured on a Berthold Sirius Luminometer (ver. 3.2, Berthold Detection Systems, Titertek) using the single kinetics program. Initial start time was delayed for 5 seconds to prevent variation in start time, with 2 second measurements taken every 5 seconds over the course of 15 minutes. Background RLU/s was set at 0 and RLU/s factor was kept at 1 as per manufacturer instructions, so that 1 RLU/s was equivalent to 1 cps.

CHAPTER 6

Discussion

Modeling Ovarian Cancer

Over the past few decades, our understanding of ovarian cancer has grown exponentially. We now understand that ovarian cancer is not just one disease arising from the ovarian surface epithelium, but a heterogenous disease with origins across the female reproductive tract[3,4,24]. In particular, research over the last several years looking at precursors of HGSOC in BRCA1 and BRCA2 patients has led to the discovery that the high grade serous subtype of ovarian cancer arises from the fallopian tube[19–21]. This has revolutionized the way we study HGSOC pathogenesis, and has led to the development of several novel models, including immortalized fallopian tube epithelium, ex vivo cultures of fallopian tube epithelium, and mouse models with targeted Brca, Tp53, and Pten genes in the fallopian tube epithelium[37,42,112].

While new models of early pathogenesis have flourished, the overwhelming majority of published research on ovarian cancer still comes from two cell lines, SKOV3 and A2780[7]. Recent large scale sequencing efforts, including the TCGA, allow us to get an intimate view of ovarian cancer genetics at the patient level[120]. Surprisingly, when a detailed comparison was made of a large panel of available ovarian cancer cell lines and the TCGA data for ovarian cancer, the majority of cell lines with high genetic fidelity to HGSOC were virtually unused, whereas SKOV3 and A2780 were two of the cell lines found most unlikely to be high grade serous in origin[7]. As mass scale genetic data becomes available not only for ovarian cancer, but for other diseases as well, we expect that similar disconnects will be found between the most commonly used cell lines and the diseases they represent. Thus we set out to characterize both genetically and experimentally two ovarian cancer lines, OVSAHO and KURAMOCHI, with the highest reported genetic fidelity to HGSOC.

Genetics of Ovarian Cancer Cell Lines

In Chapter 2, we identified OVSAHO and KURAMOCHI cell lines as having fewer mutations than SKOV3, a finding consistent with the low mutation rates and high copy number changes of HGSOC[7]. All cell lines had mutations in TP53, which is thought to be the earliest mutated and most

ubiquitous oncogene in this cancer, and KURAMOCHI had an additional mutation in BRCA2 (Table 2.1). BRCA1 and BRCA2 mutations are common in ovarian cancer cell line models as women who inherit these mutations are predisposed to develop HGSOC. As it is currently unknown how BRCA1/2 mutations drive the rise of breast and ovarian cancer at the molecular level, it is also unknown how much disease progression overlaps between BRCA1/2 mutation carriers and the general population. Thus studying a population of HGSOC cell lines that includes cells both with and without BRCA1/2 mutations is vital to getting a clear picture of ovarian cancer.

While end stage tumors are readily accessible to develop both hereditary and spontaneous models of ovarian cancer, carrying this diversity through models of early progression presents a significant challenge to researchers. Rates of prophylactic salpingo-oophorectomy are high in BRCA1/2 patients, whose lifetime risk may be as high as 56% and 27%, respectively, and best practice protocols for this population require the total sectioning of the fallopian tube to identify early tumor lesions, making these samples unavailable for further experimentation[14,121,18]. Because early lesions with BRCA1/2 mutations are unavailable to researchers, most early lesion models are derived from women without a family history of ovarian cancer, resulting in a skewed model population[7]. Balancing the need for rigorous screening in the high risk BRCA1/2 populations at the time of salpingectomy and the need to understand how BRCA1/2 impacts early pathogenesis on the molecular level will be key to the development of early precursor models.

Molecular Characterization of Ovarian Cancer Cell Lines

While genetic relevance plays an important role in ensuring the ultimate goal of successfully translating therapies from bench to bedside, many other factors are equally essential to selecting a relevant and useful ovarian cancer cell line. In chapter 2, we discovered that the cobblestone and rosette forming morphologies of KURAMOCHI and OVSAHO cells were much more consistent with HGSOC than the spindle-like growth of SKOV3 (Figure 2.1). However, KURAMOCHI and OVSAHO failed to

express two common markers of HGSOC, CK7 and CA-125. Thus a more complex picture of ovarian cancer cell lines begins to emerge, suggesting that no one cell line can completely recapitulate the common biomarker phenotypes of HGSOC and that cell line selection should be based on characteristics most relevant to a particular study. For example, for a study on a more sensitive method to detect CA-125 levels to be tested in xenograft models, a cell line such as NIHOVCAR3 would be ideal as it both forms robust tumors and expresses CA-125[122,123]. Thus a careful examination of cell lines before they are widely used is a useful tool to ensure the highest probability of translational success.

In Vivo Tumor Formation

The ability to form xenografts in vivo is also important to leveraging cell lines for pre-clinical research. While SKOV3 cells have long been known to robustly form tumors in nude mice, we found that KURAMOCHI and OVSAHO tumor growth was weak and often cleared by the mouse's partial immune system. Moving to the more immunocompromised NSG mouse model enabled better intraperitoneal tumor growth for both OVSAHO and KURAMOCHI, but subcutaneous tumors in this model regressed or remained static for both lines. This suggests that optimal xenograft growth may be achieved in the environment most closely associated with that of the original tumor. Given recent research showing the metabolic dependence of ovarian tumors on the omentum, it is probable that proximity to this tissue may be one of the many growth advantages of intraperitoneal tumor growth[124,125].

Another factor that may impact xenograft growth in vivo is the origin of the cell line. The two cell lines that grew most robustly when injected intraperitoneally, SKOV3 and KURAMOCHI, were both derived from the ascites of women with ovarian cancer. In contrast, OVSAHO, which formed microscopic tumor implants and that failed to grow over extended periods of time, was derived from an abdominal metastasis. The most common sources of ovarian cancer derived cell models include tumors, metastases, or tumor cells found in ascites, all of which are differently adapted to best fit their biological niche[45]. When records are clearly kept, cell line origin can be clearly identified from ATCC records.

However, often the records of a cell line's origin are ambiguous or unavailable, and this is especially true of cell lines developed several decades ago before we understood the complexity of the disease. We now know that clinically ovarian cancer may have many different faces during its different reincarnations, especially after recurrence when it develops drug resistance[126,127]. Thus it may be overly simplistic to choose a cell line only based on its drug resistance status, when a primary tumor resistant to platinum treatment may have a different resistance mechanism than ascites from a recurrent tumor where secondary resistance has developed[126–128].

Going forward, better records of tumor origins and patient history can help better select cell lines from tumors that more closely reflect the intended treatment population and may inform the optimal environment for in vivo modeling of a particular cell line. To further explore the differences between primary and recurring tumors, one group has recently developed ovarian cancer cell lines from three ovarian cancer patients, with matched samples derived from primary tumor, recurrent tumor, and ascites[128]. Further studies of matched samples would elucidate the differences and similarities between tumors from different sources and time points within the same patient, ultimately giving us a better idea of how much location and timing matters in cell line selection and the ability of the tumors to form xenografts.

Microenvironment and Ovarian Cancer Models

Our work in supplemental chapter 8 focused on modeling the impact of ovulation on fallopian tube epithelium. In order to model the microenvironmental impact of ovulation ex vivo, a special transwell membrane had to be employed to maintain fallopian tube polarization as well as both cilliated and secretory sub-populations in culture. Using this model, we were able to establish that follicular fluid had a similar proliferatory phenotype to serum containing media, which is unsurprising as follicular fluid is primarily derived from thecal capillary serum[129–131]. However, we were unable to establish a novel phenotype for follicular fluid beyond that of the serum. These results are at odds with another lab which

has since used a similar set up and successfully identified moderate DNA damage and an increase in inflammatory pathways as measured by microarray[132]. A possible reason for this discrepancy is the heavy reliance on small volumes of follicular fluid and brief viability ex vivo of fallopian tubes, necessitating new samples from different women for virtually every experiment.

While follicular fluid is known to vary from woman to woman and even within the same woman over the course of follicle development, it is unknown how widely fallopian tube epithelium varies between individuals[133–135]. The consistency of our RNAseq and ChIP data between immortalized fallopian tube samples in chapter 3 supports the idea that tissue variability between women is minimal. However, it is important to note that comparison is limited as RNAseq and ChIP results focused on one specific protein, PAX8, in immortalized cell lines preserving only the secretory cell sub-population.

In general, 2-D cell culture does little to preserve the original environment of the cells being modeled. Our primary fallopian tube epithelium ex vivo cultures as well as similar methods by others seeks to preserve cellular polarization and in rare cases even stroma in order to better recapitulate the original biological setting[37,39,136]. Although novel culturing methods are common to fallopian tube models, tumor models are still overwhelmingly 2-D. Given our newfound understanding of the importance of tumor microenvironment, several labs are seeking to change this bias and to develop equally novel methods to make microenvironmentally relevant insights into late stage ovarian cancer. Promising new studies have focused on the communication and metabolic dependency of ovarian cancer cells on the adipose tissue of the omentum, using similar transwell plates as in supplementary chapter 8, which allow the co-culture of cancer cells above and adipose tissue below to measure signaling interactions [124,125]. Applying already familiar techniques used to model fallopian tube epithelium to end stage ovarian cancer models could offer additional opportunities to further characterize cell lines in vitro.

Other labs, led by ground breaking methods developed in the Brugge lab, seek to model the initiation of metastasis in ovarian cancer by modeling the clearing of the mesothelium. This is done by

spheroid assays that allow the tumor cells to interact with each other in a more organic matter, resulting in decreased drug sensitivity and increased malignancy. They also employ an elegant system of dual fluorescent labeling where RFP tumor cells can be imaged in real time invading the GFP labeled mesothelial layer[137–139]. The future of ovarian cancer research is likely to be driven by similar novel modeling techniques that go beyond traditional 2-D cell culture in an effort better understand and treat this disease in the context of its unique environment.

Tumor heterogeneity

One last important characteristic of clinical ovarian cancer that is often overlooked at the lab bench is tumor heterogeneity. Even with ovarian cancer being broken down into histologic subtypes, studies on the Australian Ovarian Cancer Study led by David Bowtell suggest that HGSOC, the most lethal and common subtype, can be further divided into 4 distinctive molecular subtypes[140]. Perhaps even more startling is a recent study with a small but powerful data set which took 11 spatially separated samples from across the primary tumor and metastases of a patient with ovarian cancer during cytoreductive surgery and performed whole exome sequencing to determine the similarities and differences of each sample[141]. Surprisingly, only 6% of somatic mutations were present across all samples, and TP53 was the only unifying mutation. Further evolutionary mapping of the mutations implied that ovarian cancer is not only a heterogenous disease, but also one whose genomic instability under a single TP53 mutation enables quick adaption to new environments[7,141]. In Chapter 3, our ChIPseq and RNAseq data suggests that while similarities exist between tumors, gene regulation can vary widely. However, this work was performed on tumor derived cell lines that are heavily selected under the pressures of 2D culture and may underestimate variation within the same tumor. Further studies could be conducted performing similar ChIPseq and RNAseq experiments on primary patient samples to determine how much DNA binding and gene regulation is differentially regulated across the same patient. Understanding ovarian cancer as a quickly evolving and heterogenous entity is daunting and raises many challenges both in modeling and treatment. However, better models, as evidenced by the work of the

Brugge lab and others, are the first step to understanding the underlying mechanisms and potential weaknesses of this deadly disease.

PAX8

One of the most significant challenges in treating ovarian cancer clinically is the frequent rate of tumor recurrence and drug resistance. While most ovarian tumors are initially sensitive to standard taxane and platinum-based chemotherapy, recurrent tumors are much more likely to be resistant, leading to limited treatment options and ultimately a mere 44% 5 year survival rate[126,127]. Novel drug targeting strategies offer one way to overcome this unmet clinical challenge. In particular, we examined PAX8, a developmental transcription factor which is amplified and essential for a subset of ovarian cancers, with the ultimate goal of targeting it therapeutically[7].

PAX8 Knockdown

The first step to understanding PAX8 as a drug target is to better characterize its knockdown. Our research knocking down PAX8 in multiple ovarian cancer cell lines confirmed previous work by Project Achilles showing that PAX8 knockdown only impacts proliferation in a subset of cell lines[73]. We found that sensitivity to PAX8 knockdown does not correlate with genetic fidelity to HGSOC, nor does it correlate directly with PAX8 expression levels[7,73]. Interestingly, immortalized fallopian tube lines appear resistant to proliferation defects when PAX8 is knocked down, whereas ovarian cancer lines are evenly split between sensitivity and resistance to PAX8 knockdown (Figure 3.3). However, only one fallopian tube line, FT194, was tested in triplicate, so this data could be further strengthened by testing more immortalized fallopian tube lines.

We hypothesized that sensitivity to PAX8 knockdown could be attributed to molecular differences between cell lines. This was supported by our ChIPseq and RNAseq data, which showed that KURAMOCHI cells, which are sensitive to PAX8 knockdown, had very different DNA binding sites and regulated different genes than OVSAHO cells, which are resistant to the effects PAX8 knockdown.

Specifically, Gene Ontology analysis showed apoptosis and cell death pathways were suppressed by PAX8 in the context of KURAMOCHI cells but not OVSAHO (Figure 4.7), which could explain why PAX8 knockdown only impacts the proliferation of the former cell line and not the latter. A third cell line, JHOS4, was included, but was shown to have limited PAX8 binding sites and few genes regulated by PAX8. It is also unknown if JHOS4 is sensitive to PAX8 knockdown. Ideally, further ChIPseq and RNAseq experiments including sensitive and resistant to PAX8 knockdown would reveal differences at the molecular level that could explain why some cell lines become dependent on PAX8 at the cancer level. Our current data sets have insufficient power to answer this question as KURAMOCHI cells were the only PAX8 sensitive line included.

Targeting a Transcription Factor

One major challenge of targeting PAX8 is that it belongs to the family of transcription factors, which are largely considered "undruggable". While transcription factors are often in the center of cancer dysegulation and present attractive targets in theory, very few have successfully been targeted in practice, largely because of their broad, flat DNA binding regions[142]. To overcome difficulties targeting the protein itself, researchers have recently sought to inhibit interacting proteins[142]. While PAX8 interacting proteins have been studied heavily in the context of the thyroid, very little is known about PAX8 interactions in the context of the fallopian tube. We sought to identify PAX8 binding partners through immunoprecipitation and mass spectrometry in supplemental chapter 7. Unfortunately, low yield made it necessary to perform the immunoprecipitation experiments in the context of S3 HeLa cells rather than ovarian cancer cell lines. Thirteen potential PAX8 binding proteins were identified in S3 HeLa cells (Table 7.1). Of these, several proteins were non-nuclear, decreasing their likelihood of physiological relevance given that PAX8 has been shown to be exclusively nuclear (Figure 7.6). One nuclear protein identified was BRIP1, which has particular relevance to ovarian cancer as it interacts with BRCA1, a protein which is mutated in patients with high genetic risk for HGSOC. However, we were unable to validate the BRIP1/PAX8 interaction in the context of ovarian cancer. This suggests that interacting

proteins may vary across cell types, and any drug targeting PAX8 interactions would need to be carefully validated in the target cell population before use.

Another way researchers target transcription factors indirectly is by inhibiting DNA binding[142]. We identified PAX8 binding sites through ChIPseq in three ovarian cancer lines and three immortalized fallopian tube lines. While the fallopian tube lines had strikingly similar PAX8 binding sites, PAX8 binding sites varied widely among cancer cell lines (Figure 4.1). Like most transcription factors, PAX8 binding heavily favored intronic and intergenic regions. Unfortunately, our understanding of how binding in these regions impacts cellular function is extremely limited, making PAX8 binding in these regions an unlikely target for drug purposes. In KURAMOCHI cells, where knocking down PAX8 induces a decrease in proliferation, 22 genes were identified with PAX8 binding sites within 50K bp of the start site whose expression was significantly impacted by PAX8 knockdown (Figure 4.8). Further research validating PAX8 binding at these individual sites, as well as looking into the impact of regulating these genes would be essential to developing a successful target for inhibiting PAX8 DNA binding.

Lastly, inhibiting dimerization of transcription factors is a promising way to inhibit their function. While PAX8 has been suggested to autoregulate by binding to its own promoter region in mouse thyroid, no dimerization of PAX8 proteins has been previously reported[83]. In support of this, our immunoprecipitation experiments pulling down TAP-Tag PAX8 constructs and probing with a PAX8 antibody recognizing both native and tagged PAX8 failed to identify a band at the molecular weight of native PAX8. Thus, this suggests that this may not be a tractable strategy for PAX8 inhibition.

Clinical Implications of Targeting PAX8

In the event that a successful drug targeting PAX8 is developed for ovarian cancer patients in the preclinical setting, the transition to humans could reveal previously unaddressed side effects. Because PAX8 is primarily expressed in adult thyroid, kidney, and fallopian tube, these are the primary tissues we would expect to be impacted by PAX8 inhibition[57–60,62]. Although PAX8 is important to kidney

development, PAX8 knockout mice showed no noticeable defects in their kidneys, leading to the assumption that PAX8 expression is not essential to that organ[59–61]. This may be due in part to overlapping expression of PAX8 and PAX2 in the kidney, one of which could be sufficient for organ maintenance in the other's absence[143]. Conversely, PAX8 knockout in mice as well as naturally occurring PAX8 mutations in humans leads to severe hypothyroidism[61,65]. If left untreated the side effects are severe and may result in growth deficits and intellectual disabilities. However, these symptoms are primarily incurred as a result of lacking PAX8 during critical early developmental stages and would likely be much less severe if PAX8 loss occurred during adulthood[63,66]. Fortunately, even hypothyroidism induced by the complete lack of PAX8 is easily treatable with synthetic thyroid hormone[64,65]. Hypothyroidism is much more common in females than males, and incidence is particularly high in older females. Various studies of Japanese, European, and American populations estimate that between 10-20% of women over 55 years of age will develop hypothyroidism, with the highest prevalence seen in Caucasian women[144,145]. While synthetic thyroid hormone is generally well tolerated, side effects are primarily due to overcompensation, resulting in hyperthyroid symptoms including anxiety, weight loss, and osteoporosis[145]. Since the average age of onset for ovarian cancer is 63[146], it is likely that some women with ovarian cancer already take thyroid replacement hormones. Thus, with careful management, the addition of synthetic thyroid hormone to targeted PAX8 treatment should ameliorate any impact on thyroid function with minimal adverse side effects.

It is currently unknown what impact PAX8 inhibition would have on a human patient's fallopian tubes and female reproductive tract. We know that PAX8 is essential to Müllerian tract in mice as without PAX8 both the uterus and fallopian tubes fail to form, but it is unclear if PAX8 expression is required for tubal maintenance in humans[61]. In our hands, PAX8 knockdown induced no proliferation defects in immortalized fallopian epithelium (Figure 3.3), supporting a non-essential role for PAX8 in fully developed tubes. While treatment would ideally exclusively impact the proliferation of the tumor, in the case of most ovarian cancer patients, whose diagnosis is typically post-menopause, ovulation has already

ceased and thus the fallopian tubes and even uterus are unnecessary to survival and quality of life[146]. In addition, HGSOC is typically diagnosed at late stage when tumor burden is significant, and thus the fallopian tubes are often indistinguishable from the tumor at the time of diagnosis, and would be removed during standard debulking procedures in any case[12]. Finally, even in the rare cases of younger women diagnosed with HGSOC, maintaining fertility after aggressive disease progression and treatment would be unlikely, and is a relatively small cost to pay for increased chances of survival[126,127].

Mechanism of PAX8 Proliferation Defects

Although a cancer drug may target tumor growth through many different mechanisms, apoptosis is the most ideal mechanism of cell death. Less ideal are necrosis, which can cause inflammation and damage the surrounding tissue, and senescence, where cells are blocked from proliferating but not necessarily primed to die. The mechanism by which PAX8 knockdown causes a proliferation defect is currently debated, with some research supporting apoptosis and others senescence. Data from Project Achilles performed in ovarian cancer cells as well as from Di Palma et al performed in rat thyroid cells indicates that PAX8 inhibition induces apoptosis by P53 dependent activation of caspase 3 and subsequent PARP cleavage[73,82]. In contrast, our research using cell cycle analysis and Annexin V staining found little apoptosis but significant cell cycle arrest (Figure 3.4, Figure 3.5), suggesting senescence. PARP cleavage as measured by western blot is a slightly less accurate measurement of apoptosis than flow cytometry as the former looks at the whole sample and a positive signal may come from a small subset of the whole population. In contrast, flow cytometry is considered to be a more robust technique as the levels of apoptosis can be measured in each cell individually. Differences in measurement techniques may account for the differences observed, and cell populations tested may impact the results as well. One set of data was collected from rat thyroid cells, and the two experiments using human ovarian cancer cell lines used different cell lines. While large tumor burden is a significant clinical challenge for ovarian cancer patients and tumor debulking is a frequently employed strategy for palliative care, an ideal ovarian cancer treatment would cause the cells to undergo apoptosis and not merely arrest. Thus defining the

mechanism by which PAX8 inhibition causes a decrease in cell population is an important issue to resolve prior to therapy development.

In conclusion, this thesis provides a detailed characterization of ovarian cancer cell lines with high genetic fidelity to HGSOC, showing that each ovarian cancer cell line has different strengths and weaknesses in recapitulating the HGSOC phenotype in vitro and in vivo. It is therefore highly advantageous to carefully examine cell lines before choosing which to include in an individual study. Using these ovarian cancer cell lines with high genetic fidelity to HGSOC, we sought to elucidate the role of a developmental transcription factor, PAX8, which is ubiquitous to fallopian tube epithelium and HGSOC and which has been previously identified as essential to a subset of ovarian cancer cell lines. We found that PAX8 DNA binding sites are similar across fallopian tube epithelium, but vary highly among ovarian cancer cell lines. In addition, while PAX8 gene regulation is uniformly low in fallopian tube epithelium, gene regulation varies significantly among ovarian cancer cell lines. In one cell line sensitive to PAX8 knockdown, flow cytometry suggested that PAX8 knockdown inhibits proliferation via cell arrest rather than apoptosis. Our data suggests that sensitivity to PAX8 knockdown may be driven in part by underlying molecular differences between cell lines. Ultimately, this body of research seeks to improve ovarian cancer modeling techniques and to better understand fallopian tube pathogenesis, leading to more effective translation of ovarian cancer research from bench to bedside.

REFERENCES

References

1. Vaughan, S. et al. Rethinking ovarian cancer: new recommendations for improving outcomes. Nature Reviews Cancer. **11** (2011).

2. Levanon, K., Crum, C. & Drapkin, R. New insights into the pathogenesis of serous ovarian cancer and its clinical impact. J. Clin. Oncol. **26,** 5284–93 (2008).

3. Karst, A. M. & Drapkin, R. Ovarian cancer pathogenesis: a model in evolution. J. Oncol. **2010,** 932371 (2010).

4. Kurman, R. J. & Shih, I.-M. The origin and pathogenesis of epithelial ovarian cancer: a proposed unifying theory. Am. J. Surg. Pathol. **34,** 433–443 (2010).

5. Ahmed, A. A. et al. Driver mutations in TP53 are ubiquitous in high grade serous carcinoma of the ovary. J. Pathol. **221,** 49–56 (2010).

6. Bell, D. et al. Integrated genomic analyses of ovarian carcinoma. Nature **474,** 609–615 (2011).

7. Domcke, S., Sinha, R., Levine, D. a, Sander, C. & Schultz, N. Evaluating cell lines as tumour models by comparison of genomic profiles. Nat. Commun. **4,** 2126 (2013).

8. Nutu, M. et al. Distribution and hormonal regulation of membrane progesterone receptors beta and gamma in ciliated epithelial cells of mouse and human fallopian tubes. Reprod. Biol. Endocrinol. **7,** 89 (2009).

9. Comer, M. T., Leese, H. J. & Southgate, J. Induction of a differentiated ciliated cell phenotype in primary cultures of Fallopian tube epithelium. Hum. Reprod. **13,** 3114–20 (1998).

10. Snegovskikh, V., Mutlu, L., Massasa, E. & Taylor, H. S. Identification of Putative Fallopian Tube Stem Cells. Reprod. Sci. **21,** 1460–1464 (2014).

11. Köbel, M. et al. Differences in tumor type in low-stage versus high-stage ovarian carcinomas. Int. J. Gynecol. Pathol. **29,** 203–211 (2010).

12. Bowtell, D. D. L. The genesis and evolution of high-grade serous ovarian cancer. Nat. Rev. Cancer **10,** 803–8 (2010).

13. Jackman, R. & Mayo, C. The adenoma-carcinoma sequence in cancer of the colon. Surgery, Gynecol. Obstet. **93,** 327–30 (1951).

14. Crum, C. P. et al. Lessons from BRCA: the tubal fimbria emerges as an origin for pelvic serous cancer. Clin. Med. Res. **5,** 35–44 (2007).

15. Leeper, K. et al. Pathologic Findings in Prophylactic Oophorectomy Specimens in High-Risk Women. Gynecol. Oncol. **87,** 52–56 (2002).

16. Powell, C. B. et al. Risk-reducing salpingo-oophorectomy in BRCA mutation carriers: role of serial sectioning in the detection of occult malignancy. J. Clin. Oncol. **23,** 127–32 (2005).

17. Finch, A. et al. Clinical and pathologic findings of prophylactic salpingo-oophorectomies in 159 BRCA1 and BRCA2 carriers. Gynecol. Oncol. **100,** 58–64 (2006).

18. Medeiros, F. et al. The Tubal Fimbria Is a Preferred Site for Early Adenocarcinoma in Women With Familial Ovarian Cancer Syndrome. Cancer **30,** 230–236 (2006).

19. Lee, Y. et al. A candidate precursor to serous carcinoma that originates in the distal fallopian tube. J. Pathol. 26–35 (2007).

20. Leonhardt, K., Einenkel, J., Sohr, S., Engeland, K. & Horn, L.C. P53 Signature and Serous Tubal In-situ Carcinoma in Cases of Primary Tubal and Peritoneal Carcinomas and Serous Borderline Tumors of the Ovary. Int. J. Gynecol. Pathol. **30,** 417–24 (2011).

21. Carlson, J. W. et al. Serous tubal intraepithelial carcinoma: its potential role in primary peritoneal serous carcinoma and serous cancer prevention. J. Clin. Oncol. **26,** 4160–5 (2008).

22. Tone, A. a, Virtanen, C., Shaw, P. a & Brown, T. J. Decreased progesterone receptor isoform expression in luteal phase fallopian tube epithelium and high-grade serous carcinoma. Endocr. Relat. Cancer **18,** 221–34 (2011).

23. Tone, A. a et al. Gene expression profiles of luteal phase fallopian tube epithelium from BRCA mutation carriers resemble high-grade serous carcinoma. Clin. Cancer Res. **14,** 4067–78 (2008).

24. Levanon, K., Crum, C. & Drapkin, R. New insights into the pathogenesis of serous ovarian cancer and its clinical impact. J. Clin. Oncol. **26,** 5284–5293 (2008).

25. Yates, M. S. et al. Microscopic and early-stage ovarian cancers in BRCA1/2 mutation carriers: building a model for early BRCA-associated tumorigenesis. Cancer Prev. Res. (Phila). **4,** 463–70 (2011).

26. Mehra, K. et al. STICS, SCOUTs and p53 signatures; a new language for pelvic serous carcinogenesis. Front Biosci. **3,** 625-34 (2011).

27. Bast, R. C., Hennessy, B. & Mills, G. B. The biology of ovarian cancer: new opportunities for translation. Nat. Rev. Cancer **9,** 415–28 (2009).

28. Norquist, B. M. et al. The molecular pathogenesis of hereditary ovarian carcinoma: alterations in the tubal epithelium of women with BRCA1 and BRCA2 mutations. Cancer **116,** 5261–71 (2010).

29. Fathalla, M. Incessant ovulation- a factor in ovarian neoplasia? Lancet **2,** 163 (1971).

30. Cramer, D. & Welch, W. Determinants of ovarian cancer risk II Inferences regarding pathogenesis. J. Natl. Cancer Inst. **71,** 717–721 (1983).

31. McCartney, C., Eagleson, C. & Marshall, J. Regulation of gonadotropin secretion: implications for polycystic ovary syndrome. Semin. Reprod. Med. **20,** 317–326 (2002).

32. Emori, M. M. & Drapkin, R. The hormonal composition of follicular fluid and its implications for ovarian cancer pathogenesis. Reprod. Biol. Endocrinol. **12,** 60 (2014).

33. Vercellini, P. et al. The 'incessant menstruation' hypothesis: a mechanistic ovarian cancer model with implications for prevention. Hum. Reprod. **26,** 2262–73 (2011).

34. Lau, A. et al. Altered expression of inflammation-associated genes in oviductal cells following follicular fluid exposure: Implications for ovarian carcinogenesis. Exp. Biol. Med. (Maywood). **239,** 24–32 (2014).

35. Backman, S., Kollara, A., Haw, R., Stein, L. & Brown, T. J. Glucocorticoid-induced reversal of interleukin-1β-stimulated inflammatory gene expression in human oviductal cells. PLoS One **9,** (2014).

36. Levanon, K. et al. Primary ex vivo cultures of human fallopian tube epithelium as a model for serous ovarian carcinogenesis. Oncogene **29,** 1103–13 (2010).

37. Fotheringham, S., Levanon, K. & Drapkin, R. Ex vivo culture of primary human fallopian tube epithelial cells. J. Vis. Exp. 3–7 (2011). doi:10.3791/2728

38. Lawrenson, K. et al. In vitro three-dimensional modeling of fallopian tube secretory epithelial cells. BMC Cell Biol. **14,** 43 (2013).

39. King, S. M. et al. The impact of ovulation on fallopian tube epithelial cells: evaluating three hypotheses connecting ovulation and serous ovarian cancer. Endocr. Relat. Cancer 627–642 (2011). doi:10.1530/ERC-11-0107

40. Karst, A. M., Levanon, K. & Drapkin, R. Modeling high-grade serous ovarian carcinogenesis from the fallopian tube. Proc. Natl. Acad. Sci. U. S. A. **108,** 7547–52 (2011).

41. Jazaeri, A.A. et al. Molecular Requirements for Transformation of Fallopian Tube Epithelial Cells into. Neoplasia **13,** 899–911 (2011).

42. Perets, R. et al. Transformation of the fallopian tube secretory epithelium leads to high-grade serous ovarian cancer in Brca;Tp53;Pten models. Cancer Cell **24,** 751–765 (2013).

43. The Cancer Genome Atlas Network. Integrated genomic analyses of ovarian carcinoma. Nature **474,** 609–615 (2011).

44. Anglesio, M. S. et al. Type-Specific Cell Line Models for Type-Specific Ovarian Cancer Research. PLoS One **8,** (2013).

45. Yanagibashi, T. et al. Complexity of expression of the intermediate filaments of six new human ovarian carcinoma cell lines: new expression of cytokeratin 20. Br. J. Cancer **76,** 829–835 (1997).

46. Motoyama, T. [Quantitative analysis on in vitro drug sensitivity of cultured human ovarian cancer cell lines]. Nihon Sanka Fujinka Gakkai Zasshi **34,** 308–314 (1982).

47. Deutsch, U. et al. Pax1, a member of a paired box homologous murine gene family, is expressed in segmented structures during development. Cell. **53,** 617-625 (1988).

48. Balczarek, K. a, Lai, Z. C. & Kumar, S. Evolution of functional diversification of the paired box (Pax) DNA-binding domains. Mol. Biol. Evol. **14,** 829–842 (1997).

49. Chi, N., Epstein, J.A. Getting your Pax straight: PAX proteins in development and disease. Trends Genet. **18,** 41-47 (2002).

50. Poleev, A. et al. Determination of functional domains of the human transcription factor PAX8 responsible for its nuclear localization and ransactivating potential. Eur J Biochem. **247,** 860-890 (1997).

51. Kozmik, Z., Kurzbauer, R., Dörfler, P. & Busslinger, M. Alternative splicing of Pax-8 gene transcripts is developmentally regulated and generates isoforms with different transactivation properties. Mol. Cell. Biol. **13,** 6024–6035 (1993).

52. Poleev, a. et al. Distinct functional properties of three human paired-box-protein, PAX8, isoforms generated by alternative splicing in thyroid, kidney and Wilms' tumors. Eur. J. Biochem. **228,** 899–911 (1995).

53. De Cristofaro, T. et al. Pax8 protein stability is controlled by sumoylation. J. Mol. Endocrinol. **42,** 35–46 (2009).

54. Cao, X., Kambe, F., Ohmori, S. & Seo, H. Oxidoreductive modification of two cysteine residues in paired domain by Ref-1 regulates DNA-binding activity of Pax-8. Biochem. Biophys. Res. Commun. **297,** 288–293 (2002).

55. Cao, X. et al. Glutathionylation of two cysteine residues in paired domain regulates DNA binding activity of Pax-8. J. Biol. Chem. **280,** 25901–25906 (2005).

56. Stoykova, a & Gruss, P. Roles of Pax-genes in developing and adult brain as suggested by expression patterns. J. Neurosci. **14,** 1395–1412 (1994).

57. Plachov, D. et al. Pax8, a murine paired box gene expressed in the developing excretory system and thyroid gland. Development **110,** 643–651 (1990).

58. Filippone, M. G., Palma, T. Di, Lucci, V. & Zannini, M. Pax8 modulates the expression of Wnt4 that is necessary for the maintenance of the epithelial phenotype of thyroid cells. **15,** 1–11 (2014).

59. Narlis, M., Grote, D., Gaitan, Y., Boualia, S. K. & Bouchard, M. Pax2 and pax8 regulate branching morphogenesis and nephron differentiation in the developing kidney. J. Am. Soc. Nephrol. **18,** 1121–1129 (2007).

60. Bouchard, M., Souabni, A., Mandler, M., Neubüser, A. & Busslinger, M. Nephric lineage specification by Pax2 and Pax8. Genes Dev. **16,** 2958–2970 (2002).

61. Mittag, J., Winterhager, E., Bauer, K. & Grümmer, R. Congenital hypothyroid female Pax8-deficient mice are infertile despite thyroid hormone replacement therapy. Endocrinology **148,** 719–725 (2007).

62. Bowen, N. J. et al. Emerging roles for PAX8 in ovarian cancer and endosalpingeal development. Gynecol. Oncol. **104,** 331–337 (2007).

63. Mittag, J. et al. Athyroid Pax8-/- mice cannot be rescued by the inactivation of thyroid hormone receptor α1. Endocrinology **146,** 3179–3184 (2005).

64. Wistuba, J. et al. Male congenital hypothyroid Pax8-/- mice are infertile despite adequate treatment with thyroid hormone. J. Endocrinol. **192,** 99–109 (2007).

65. Ramos, HE., Carré, A., Chevrier, L., Szinnai, G., Tron, E., Oliveira, TL., Léger, J., Cabrol., Puel, O., Queinnec, C., De Roux, N., Guillot, L., Castanet, M., Polak, M. Extreme phenotypic variability of thyroid dysgenesis in six new cases of congenital hypothyroidism due to PAX8 gene loss-of-function mutations. Eur. J. Endocrinol. 1–10 (2014).

66. Macchia, P. E. et al. PAX8 mutations associated with congenital hypothyroidism caused by thyroid dysgenesis. Nat. Genet. **19,** 83–86 (1998).

67. Laury, A. R. et al. A comprehensive analysis of PAX8 expression in human epithelial tumors. Am. J. Surg. Pathol. **35,** 816–826 (2011).

68. Castro, P. et al. PAX8-PPARγ rearrangement is frequently detected in the follicular variant of papillary thyroid carcinoma. J. Clin. Endocrinol. Metab. **91,** 213–220 (2006).

69. Giordano, T. J. et al. Delineation, functional validation, and bioinformatic evaluation of gene expression in thyroid follicular carcinomas with the PAX8-PPARG translocation. Clin. Cancer Res. **12,** 1983–1993 (2006).

70. Tong, G.-X. et al. Expression of PAX8 in nephrogenic adenoma and clear cell adenocarcinoma of the lower urinary tract: evidence of related histogenesis? Am. J. Surg. Pathol. **32,** 1380–1387 (2008).

71. Tamimi, Y., Dietrich, K., Stone, K. & Grundy, P. Paired box genes, PAX-2 and PAX-8, are not frequently mutated in Wilms tumor. Mutat. Res. - Fundam. Mol. Mech. Mutagen. **601,** 46–50 (2006).

72. Hung, N. et al. Increased paired box transcription factor 8 has a survival function in Glioma. BMC Cancer **14,** 159 (2014).

73. Cheung, H. et al. Systematic investigation of genetic vulnerabilities across cancer cell lines reveals lineage-specific dependencies in ovarian cancer. (2011).

74. Laury, A. R. et al. PAX8 reliably distinguishes ovarian serous tumors from malignant mesothelioma. Am. J. Surg. Pathol. **34,** 627–635 (2010).

75. Wang , Y. et al. PAX8: a sensitive and specific marker to identify cancer cells of ovarian cancer origin for patients prior to neoadjuvant chemotherapy. J Hematol Oncol. **6** (2013).

76. Di Palma, T. et al. The paired domain-containing factor Pax8 and the homeodomain-containing factor TTF-1 directly interact and synergistically activate transcription. J. Biol. Chem. **278,** 3395–3402 (2003).

77. Miccadei, S., Provenzano, C., Mojzisek, M., Natali, P. G. & Civitareale, D. Retinoblastoma protein acts as Pax 8 transcriptional coactivator. Oncogene **24,** 6993–7001 (2005).

78. Di Palma, T. et al. TAZ is a coactivator for Pax8 and TTF-1, two transcription factors involved in thyroid differentiation. Exp. Cell Res. **315,** 162–175 (2009).

79. Di Palma, T. et al. Poly(ADP-ribose) polymerase 1 binds to Pax8 and inhibits its transcriptional activity. J. Mol. Endocrinol. **41,** 379–388 (2008).

80. Costamagna, E., García, B. & Santisteban, P. The Functional Interaction between the Paired Domain Transcription Factor Pax8 and Smad3 Is Involved in Transforming Growth Factor-β Repression of the Sodium/Iodide Symporter Gene. J. Biol. Chem. **279,** 3439–3446 (2004).

81. Roberts, E. C. et al. Id Helix-Loop-Helix Proteins Antagonize Pax Transcription Factor Activity by Inhibiting DNA Binding Id Helix-Loop-Helix Proteins Antagonize Pax Transcription Factor Activity by Inhibiting DNA Binding. **21,** 524–533 (2001).

82. Di Palma, T. et al. Pax8 has a critical role in epithelial cell survival and proliferation. Cell Death Dis. **4** (2013).

83. Di Gennaro, A., Spadaro, O., Baratta, M. G., Di Lauro, R. & De Felice, M. Functional Analysis of the Pax8 Promoter Reveals Autoregulation and the Presence of a Novel Thyroid-Specific Dna Binding Activity. Thyroid **23,** 121018093034001 (2012).

84. Ruiz-Llorente, S. et al. Genome-wide analysis of Pax8 binding provides new insights into thyroid functions. BMC Genomics **13,** 147 (2012).

85. Di Palma, T. et al. Identification of novel Pax8 targets in FRTL-5 thyroid cells by gene silencing and expression microarray analysis. PLoS One **6,** (2011).

86. Grote, D., Souabni, A., Busslinger, M. & Bouchard, M. Pax 2/8-regulated Gata 3 expression is necessary for morphogenesis and guidance of the nephric duct in the developing kidney. Development **133,** 53–61 (2006).

87. Fraizer, G. C., Shimamura, R., Zhang, X. & Saunders, G. F. PAX 8 regulates human WT1 transcription through a novel DNA binding site. J. Biol. Chem. **272,** 30678–30687 (1997).

88. Dehbi, M. & Pelletier, J. PAX8-mediated activation of the wt1 tumor suppressor gene. EMBO J. **15,** 4297–4306 (1996).

89. Chen, Y. J. et al. PAX8 regulates telomerase reverse transcriptase and telomerase RNA component in glioma. Cancer Res. **68,** 5724–5732 (2008).

90. Barretina, J. et al. The Cancer Cell Line Encyclopedia enables predictive modelling of anticancer drug sensitivity. Nature **483,** 603–307 (2012).

91. Chan, K. K. L. et al. Targeting estrogen receptor subtypes (ERα and ERβ) with selective ER modulators in ovarian cancer. J. Endocrinol. **221,** 325–336 (2014).

92. Horio, M. et al. Expression of RET finger protein predicts chemoresistance in epithelial ovarian cancer. Cancer Med. **1,** 218–29 (2012).

93. Mikuła-Pietrasik, J. et al. Peritoneal mesothelium promotes the progression of ovarian cancer cells in vitro and in a mice xenograft model in vivo. Cancer Lett. **355,** 310–315 (2014).

94. Seino, M. et al. Requirement of JNK Signaling for Self-renewal and Tumor-initiating Capacity of Ovarian Cancer Stem Cells. **4732,** 4723–4731 (2014).

95. Zhu, X. et al. MiR-145 sensitizes ovarian cancer cells to paclitaxel by targeting Sp1 and Cdk6. Int. J. Cancer **135,** 1286–1296 (2014).

96. Kriplani, D. & Patel, M. Immunohistochemistry: A diagnostic aid in differentiating primary epithelial ovarian tumors and tumors metastatic to the ovary. South Asian J. Cancer **2,** 254 (2013).

97. Karst, A. M. et al. Stathmin 1, a marker of PI3K pathway activation and regulator of microtubule dynamics, is expressed in early pelvic serous carcinomas. Gynecol. Oncol. **123,** 5–12 (2011).

98. Scholler, N., Urban, N. & Gene, C. CA125 in ovarian cancer. Biomark Med. **1,** 513–523 (2010).

99. Boivin, M., Lane, D., Piché, A. & Rancourt, C. CA125 (MUC16) tumor antigen selectively modulates the sensitivity of ovarian cancer cells to genotoxic drug-induced apoptosis. Gynecol. Oncol. **115,** 407–413 (2009).

100. Bookman, M. a et al. Carboplatin and paclitaxel in ovarian carcinoma: a phase I study of the Gynecologic Oncology Group. J. Clin. Oncol. **14,** 1895–1902 (1996).

101. Liu, F. S. et al. Triplet combination of gemcitabine, carboplatin, and paclitaxel in previously treated, relapsed ovarian and peritoneal carcinoma: An experience in Taiwan. Gynecol. Oncol. **94,** 393–397 (2004).

102. Markman, M. & Bookman, M.A. Second-Line Treatment of Ovarian Cancer. The Oncologist. **5,** 26–35 (2000).

103. McGuire, W.P. et al. Cyclophosphamide and cisplatin compared with paclitaxel and cisplatin in patients With Stage Iii and Stage Iv Ovarian Cancer. The New England Journal of Medicine. **334,** 1–6 (1996).

104. Ozgul, N. et al. Addition of epirubicin to conventional chemotherapy in patients with advanced ovarian cancer: Sequential therapy - A retrospective evaluation. Turkish J. Med. Sci. **44,** 212–219 (2014).

105. Merritt, W. M. et al. Dicer, Drosha, and Outcomes in Patients with Ovarian Cancer. N. Engl. J. Med. **359,** 2641–2650 (2008).

106. Pampalakis, G., Diamandis, E. P., Katsaros, D. & Sotiropoulou, G. Down-regulation of dicer expression in ovarian cancer tissues. Clin. Biochem. **43,** 324–327 (2010).

107. Vaksman, O., Hetland, T. E., Trope', C. G., Reich, R. & Davidson, B. Argonaute, Dicer, and Drosha are up-regulated along tumor progression in serous ovarian carcinoma. Hum. Pathol. **43,** 2062–2069 (2012).

108. Walker, S. R. et al. The transcriptional modulator BCL6 as a molecular target for breast cancer therapy. Oncogene **34,** 1–10 (2014).

109. Carroll, J. S. et al. Genome-wide analysis of estrogen receptor binding sites. Nat. Genet. **38,** 1289–1297 (2006).

110. Czerny, T., Schaffner, G. & Busslinger, M. DNA sequence recognition by Pax proteins: Bipartite structure of the paired domain and its binding site. Genes Dev. **7,** 2048–2061 (1993).

111. Adler, E., Mhawech-Fauceglia, P., Gayther, S. a. & Lawrenson, K. PAX8 expression in ovarian surface epithelial cells. Hum. Pathol. **46,** 948–956 (2015).

112. Karst, A. M. & Drapkin, R. Primary culture and immortalization of human fallopian tube secretory epithelial cells. Nat. Protoc. **7,** 1755–1764 (2012).

113. Sausen, M. et al. Integrated genomic analyses identify ARID1A and ARID1B alterations in the childhood cancer neuroblastoma. Nat. Genet. **45,** 12–7 (2013).

114. Jones, S. et al. Personalized genomic analyses for cancer mutation discovery and interpretation. Sci Transl Med. **7,** (2015).

115. Euhus, D., Hudd, C., LaRegina, M. & Johnson, F. Tumor measurement in the nude mouse. J Surg Oncol **31,** 229–234 (1986).

116. Tomayko, M. M. & Reynolds, C. P. Determination of subcutaneous tumor size in athymic (nude) mice. Cancer Chemother. Pharmacol. **24,** 148–154 (1989).

117. Trapnell, C., Pachter, L. & Salzberg, S. L. TopHat: Discovering splice junctions with RNA-Seq. Bioinformatics **25,** 1105–1111 (2009).

118. Adelmant, G. et al. DNA Ends Alter the Molecular Composition and Localization of Ku Multicomponent Complexes. Mol. Cell. Proteomics **11,** 411–421 (2012).

119. De Los Santos, M. J. et al. Hormonal and molecular characterization of follicular fluid, cumulus cells and oocytes from pre-ovulatory follicles in stimulated and unstimulated cycles. Hum. Reprod. **27,** 1596–1605 (2012).

120. Bell, D. et al. Integrated genomic analyses of ovarian carcinoma. Nature **474,** 609–615 (2011).

121. Obermair, A., Youlden, D. R., Baade, P. D. & Janda, M. The impact of risk-reducing hysterectomy and bilateral salpingo-oophorectomy on survival in patients with a history of breast cancer--a population-based data linkage study. Int. J. Cancer **134,** 2211–22 (2014).

122. Mitra, A. et al. In vivo tumor growth of high-grade serous ovarian cancer cell lines. Gynecol. Oncol. (2015).

123. Comamala, M. et al. Downregulation of cell surface CA125/MUC16 induces epithelial-to-mesenchymal transition and restores EGFR signalling in NIH:OVCAR3 ovarian carcinoma cells. Br. J. Cancer **104,** 989–999 (2011).

124. Salimian Rizi, B. et al. Nitric Oxide Mediates Metabolic Coupling of Omentum-Derived Adipose Stroma to Ovarian and Endometrial Cancer Cells. Cancer Res. **75,** 456–471 (2014).

125. Leinster, D. A. et al. The peritoneal tumour microenvironment of high-grade serous ovarian cancer. J. Pathol. **227,** 136–145 (2012).

126. Cannistra, S. a. Cancer of the ovary. N. Engl. J. Med. **351,** 2519–29 (2004).

127. Van Nagell, J. R. et al. Ultrasound and assessment of ovarian cancer risk. Cancer **37,** 408–14 (2013).

128. Letourneau, I. et al. Derivation and characterization of matched cell lines from primary and recurrent serous ovarian cancer. BMC Cancer **12,** 379 (2012).

129. Jiang, J., Macchiarelli, G., Miyabayashi, K. & Sato, E. Follicular microvasculature in the porcine ovary. Cell Tissue Res. **310,** 93–101 (2002).

130. Carson, R., Findlay, J., Mattner, P. & Brown, B. Relative levels of thecal blood flow in atretic and non-atretic ovarian follicles of the consious sheep. Aust J Exp Biol Med Sci. **64,** 381–387 (1986).

131. Rodgers, R. J. & Irving-rodgers, H. F. Formation of the Ovarian Follicular Antrum and Follicular Fluid Minireview Formation of the Ovarian Follicular Antrum and Follicular Fluid 1. Biol. Reprod. **82,** 1021–1029 (2010).

132. Bahar-Shany, K. et al. Exposure of fallopian tube epithelium to follicular fluid mimics carcinogenic changes in precursor lesions of serous papillary carcinoma. Gynecol. Oncol. **132,** 322–327 (2014).

133. Shalgi, R., Kracier, P., Rimon, A., Pinto, M. & Soferman, N. Proteins of human follicular fluid: the blood-follicle barrier. Fertil. Steril. **24,** 429–434 (1973).

134. Garzo, V. & Dorrington, J. Aromatase activity in human granulosa cells during follicular development and the blood-follicle barrier. Am. J. Obstet. Gynecol. **148,** 657–62 (1984).

135. Jana, S. K., K, N. B., Chattopadhyay, R., Chakravarty, B. & Chaudhury, K. Upper control limit of reactive oxygen species in follicular fluid beyond which viable embryo formation is not favorable. Reprod. Toxicol. **29,** 447–51 (2010).

136. Eddie, S. L. et al. Three-dimensional modeling of the human fallopian tube fimbriae. Gynecol. Oncol. **136,** 348–354 (2015).

137. Iwanicki, M. P. et al. Ovarian cancer spheroids use myosin-generated force to clear the mesothelium. Cancer Discov. **1,** 144–157 (2011).

138. Fischbach, C. et al. Engineering tumors with 3D scaffolds. Nat. Methods **4,** 855–860 (2007).

139. Davidowitz, R. a., Iwanicki, M. P. & Brugge, J. S. In Vitro Mesothelial Clearance Assay that Models the Early Steps of Ovarian Cancer Metastasis. J. Vis. Exp. 1–7 (2012).

140. Leong, H. S. et al. Efficient molecular subtype classification of high-grade serous ovarian cancer. J. Pathol. **1,** n/a–n/a (2015).

141. Lee, J.-Y. et al. Tumor evolution and intratumor heterogeneity of an epithelial ovarian cancer investigated using next-generation sequencing. BMC Cancer **15,** 1–9 (2015).

142. Johnston, S. J. & Carroll, J. S. Transcription factors and chromatin proteins as therapeutic targets in cancer. Biochim. Biophys. Acta - Rev. Cancer **1855,** 183–192 (2015).

143. Mansouri, a, Chowdhury, K. & Gruss, P. Follicular cells of the thyroid gland require Pax8 gene function. Nat. Genet. **19,** 87–90 (1998).

144. Vanderpump, M. P. J. & Tunbridge, W. M. G. Epidemiology and prevention of clinical and subclinical hypothyroidism. Thyroid **12,** 839–847 (2002).

145. Laurberg, P., Andersen, S., Inge, B. & Carl, A. Hypothyroidism in the Elderly : Pathophysiology , Diagnosis. **22,** 23–38 (2005).

146. Yancik, R., Reis, L. & Yates, J. Ovarian cancer in the elderly: an analysis of Surveillance, Epidemiology, and End Results Program data. Am. J. Obstet. Gynecol. **154,** 639–47 (1986).

147. Pal, T. et al. BRCA1 and BRCA2 mutations account for a large proportion of ovarian carcinoma cases. Cancer **104,** 2807–2816 (2005).

148. De Los Santos, M. J. et al. The follicular hormonal profile in low-responder patients undergoing unstimulated cycles: Is it hypoandrogenic? Hum. Reprod. **28,** 224–229 (2013).

149. Agarwal, A., Allamaneni, S. S. R. & Said, T. M. Chemiluminescence technique for measuring reactive oxygen species. Reprod. Biomed. Online **9,** 466–8 (2004).

150. Bächler, M., Menshykau, D., De Geyter, C. & Iber, D. Species-specific differences in follicular antral sizes result from diffusion-based limitations on the thickness of the granulosa cell layer. Mol. Hum. Reprod. **20,** 208–221 (2014).

151. Muasher, S. J., Abdallah, R. T. & Hubayter, Z. R. Optimal stimulation protocols for in vitro fertilization. Fertil. Steril. **86,** 267–273 (2006).

152. Ghoneim, I. M., Waheed, M. M., El-Bahr, S. M., Alhaider, a. K. & Al-Eknah, M. M. Comparison of some biochemical and hormonal constituents of oversized follicles and preovulatory follicles in camels (Camelus dromedarius). Theriogenology **79,** 647–652 (2013).

153. Walsh, S. W. et al. Acute dietary restriction in heifers alters expression of genes regulating exposure and response to gonadotrophins and IGF in dominant follicles. Anim. Reprod. Sci. **133,** 43–51 (2012).

154. Johnson, P. a & Giles, J. R. The hen as a model of ovarian cancer. Nat. Rev. Cancer **13,** 432–436 (2013).

155. De Bont, R. & van Larebeke, N. Endogenous DNA damage in humans: A review of quantitative data. Mutagenesis **19,** 169–185 (2004).

156. Bonner, W. M. et al. γH2AX and cancer. Nat Rev Cancer **8,** 957-67 (2008).

157. Shkolnik, K. et al. Reactive oxygen species are indispensable in ovulation. PNAS **2010,** 1–6 (2010).

158. Bridge, G. et al. DNA mismatch repair and oxidative DNA damage: implications for cancer biology and treatment. Cancers (Basel). **5,** 1597-614 (2014).

159. Attaran, M. et al. The effect of follicular fluid reactive oxygen species on the outcome of in vitro fertilization. Int. J. Fertil. Womens Med. **45,** 314–320 (2000).

160. Shekarriz, M., Sharma, R. K., Thomas, a J. & Agarwal, a. Positive myeloperoxidase staining (Endtz test) as an indicator of excessive reactive oxygen species formation in semen. J. Assist. Reprod. Genet. **12,** 70–4 (1995).

161. Venkatesh, S. et al. Clinical significance of reactive oxygen species in semen of infertile Indian men. Andrologia **41,** 251–256 (2009).

162. Imam, S.N. et al. Idiopathic recurrent pregnancy loss: role of paternal factors; a pilot study. J Reprod Infertil. **12,** 267-76 (2011).

163. Dada, R. et al. A comprehensive work up for an asthenozoospermic man with repeated intracytoplasmic sperm injection (ICSI) failure. Andrologia **43,** 368–372 (2011).

164. Kolettis, P. N. et al. Effect of seminal oxidative stress on fertility after vasectomy reversal. Fertil. Steril. **71,** 249–55 (1999).

165. Rodgers, R. J. & Irving-Rodgers, H. F. Formation of the ovarian follicular antrum and follicular fluid. Biol. Reprod. **82,** 1021–1029 (2010).

166. D'Autréaux, B. & Toledano, M. B. ROS as signalling molecules: mechanisms that generate specificity in ROS homeostasis. Nat. Rev. Mol. Cell Biol. **8,** 813–824 (2007).

167. Tamura, H. et al. Melatonin as a free radical scavenger in the ovarian follicle. Endocr. J. **60,** 1–13 (2013).

SUPPLEMENTAL CHAPTER 7

Identifying Potential PAX8

Interacting Proteins through Immunoprecipitation

Acknowledgements

Kevin Elias created the PAX8-Flag-HA taptag constructs and inserted them retrovirally into KURAMOCHI and S3 HeLa cells. Meg Emori cultured, harvested, and performed all IP experiments on KURAMOCHI and S3 HeLa cells. IP elutions were validated by silverstain and western blot by Meg Emori, and mass spectroscopy analysis was performed by Guillaume Adelmant at the Blais Proteomics Center at DFCI.

Introduction

PAX8 is a transcription factor involved in the development of the fallopian tube, thyroid, and kidney. While the role of PAX8 has been well established in the thyroid, where it has been shown to interact with thyroid transcription factor 1 (TTF-1), tafazzin (TAZ), Smad3, and PARP1, little research has been done in the context of the fallopian tube[76,78–80]. It is currently unknown how much overlap exists in PAX8 function between different organ systems, making it hard to infer what PAX8 may be regulating in the fallopian tube.

Research from Project Achilles identifying PAX8 as a differentially expressed lineage marker necessary for cellular survival supported the idea that PAX8 could make a good drug target in HGSOC[73]. However, two characteristics of PAX8 currently limit its utility as a drug target. First, PAX8, like many nuclear transcription factors, presents an open protein structure unfavorable to traditional drug interactions. Secondly, PAX8 knockdown only results in a decrease in proliferation in a subset of ovarian cancer cell lines, and the molecular mechanisms behind this discrepancy have not been identified. In order to make PAX8 a viable drug target, we needed to understand how PAX8 functions in the fallopian tube. Identifying PAX8 binding partners is particularly important as they may give us insight into why certain cells cannot survive without PAX8, as well as offering alternative drug targets that may impact cell proliferation similar to PAX8 knockdown.

Results

Immunoprecipitation of Endogenous PAX8

Initially, immunoprecipitation (IP) was attempted with endogenous PAX8 from KURAMOCHI cells since they expressed the highest levels of PAX8 in a panel of various ovarian cancer lines (Figure 3.1). However, yield was insufficient and while PAX8 pull down was validated by western blot, silverstains were weak and no band was visible at 48kDA, the MW of PAX8. To increase yield and reduce background noise, a Flag-HA Tandem Affinity Precipitation (TAP)-tag was added to PAX8 and this construct was stably infected into both S3 HeLa and KURAMOCHI cells via a retrovirus. An empty-Flag-HA vector served as a control.

Tandem Affinity Purification with Stably Expressing PAX8 TAP-Tag S3 HeLa Cells

Tandem Affinity Purification (TAP) is a method of immunoprecipitation where the protein of interest is first tagged with two small peptides to create a fusion protein known as a TAP -Tag. The IP can then be conducted by pulling down the protein twice using each small peptide, in this experiment Flag and HA, resulting in a purer sample. Because the Tandem Affinity Purification protocol was optimized in S3 HeLa cells, they are a good system for this protocol and produce the cleanest data and the highest yield. However, they are not ovarian in origin, arising instead from cervical cancer, and do not naturally express PAX8. Thus S3 HeLa cells are the ideal starting point, provided potential binding partners are then validated via Co-IP in more relevant ovarian cancer cell lines.

First, stable expression of the empty and PAX8 TAP-Tag constructs in S3 HeLa were validated by western blot. The empty-TAP-Tag construct has a molecular weight of approximately 35kDA, while the PAX8-TAP-Tag construct has a molecular weight of approximately 55kDA (Figure 7.1).

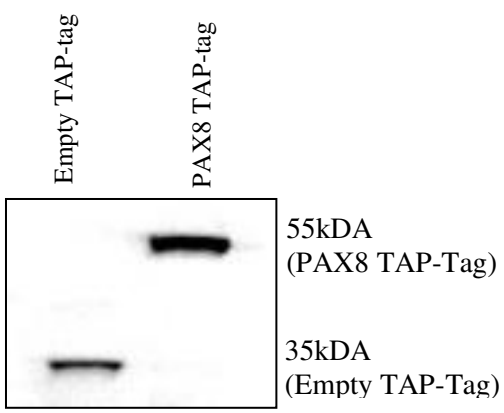

Figure 7.1: Stable Expression of PAX8 and Empty TAP-Tag constructs in S3 HeLa Cells
Western blot was probed with an antibody against HA to validate the expression of PAX8 (55kDA) and Empty (35kDA) TAP-Tag constructs in S3 HeLa cells.

In preparation for immunoprecipitation, seven confluent 15-cm cell culture plates of S3 HeLa PAX8 and Empty TAP-Tag cells were harvested and nuclear fractionation was performed via a series of hypotonic buffer extractions. Cells were first incubated with Flag-agarose beads and bound product eluted with Flag peptide before undergoing a second, identical immunoprecipitation with HA. The final tandem IP product was tested for yield by western blot and for purity by silverstain (Figure 7.2).

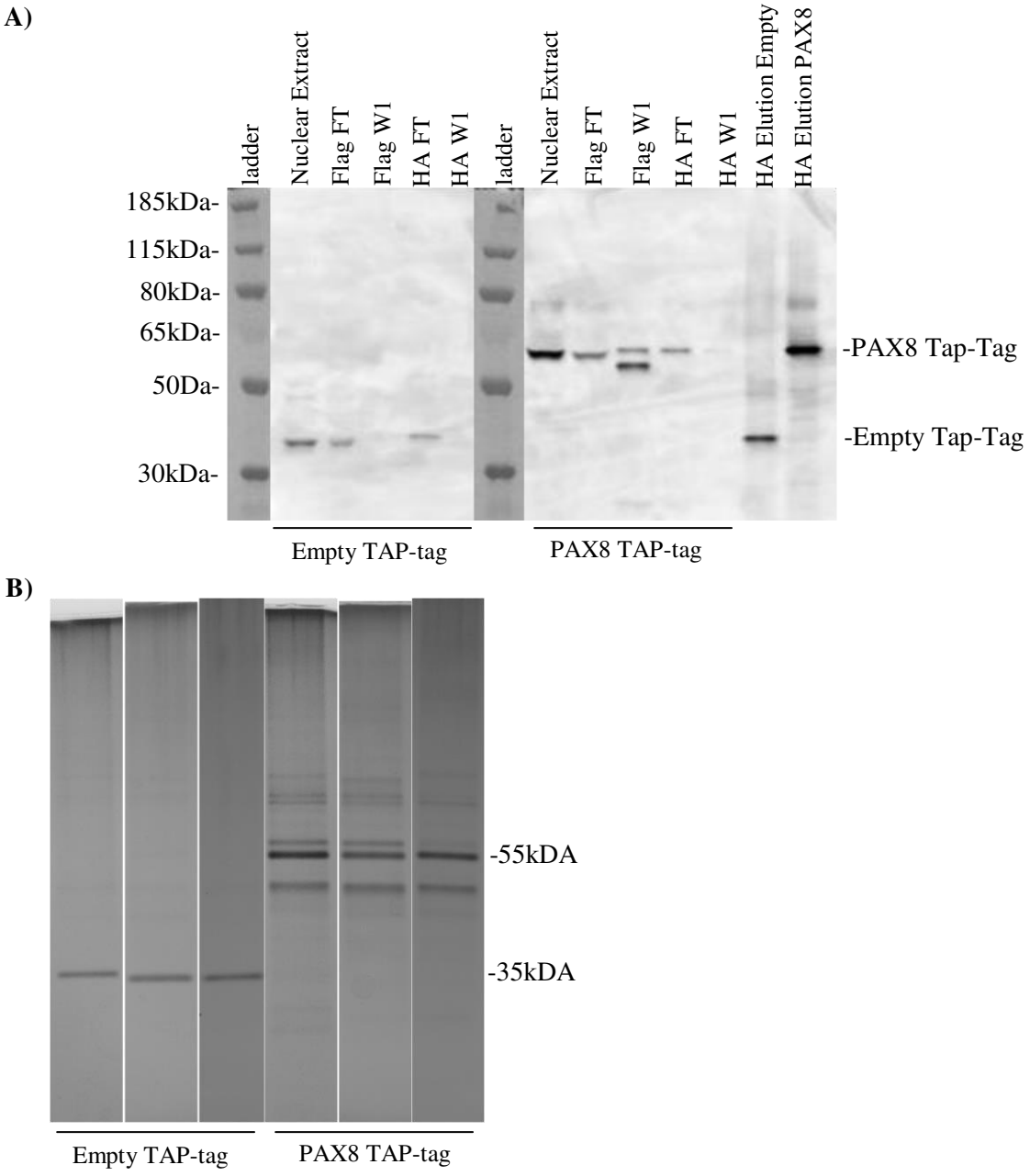

Figure 7.2: Immunoprecipitation of PAX8 and Empty Tap-Tag from S3 HeLa Cells
Nuclear extracts of S3 HeLa cells stably expressing PAX8 or Empty TAP-tag constructs were immunoprecipitated first for Flag and then for HA. A) Western blot of IP samples was probed with anti-HA to identify relative yield of product compared to nuclear extract levels. Flow Through fractions (FT) and the first in a series of 3 washes (W1) were included to identify steps of protein loss. B) Final HA Elutions were also analyzed by silverstain in triplicate. Bands visible at 35 and 55 kDA correspond to Empty and PAX8 TAP-tag constructs, respectively. Other banding visible in PAX8 TAP-tag lanes indicate unidentified potential binding proteins.

Immunoprecipitation was repeated in triplicate and each sample sent off for mass spectrometry analysis. All peptides were required to pass a 1% false discovery rate threshold, resulting in a total of 114 potential interacting proteins. Six of these were unique to the Empty TAP-tag control and 23 were present in both the Empty and PAX8 Tap-tag samples, and were excluded. This left 85 potential PAX8 binding proteins identified that were uniquely pulled down via binding to the PAX8 TAP-tag construct. Sample relevance was further increased by the removal of common lab contaminants measured by tandome detections; the larger the tandome detection the more likely of an identified protein to be a contaminant. Potential interacting proteins were included only if the tandome detection was 0 or 1. Thirty-six potential interacting proteins passed this threshold. Of these, 5 were identified independently in all three replicates, 8 were identified independently in two replicates, and 23 were identified in only one replicate. As the unique peptides identified for these proteins were very low, ranging from 1-5, we chose to include only samples that had been uniquely identified at least twice out of three replicates to increase the likelihood of biological significance.

The 13 potential binding proteins of interest were then categorized by cellular localization as identified by the NCBI gene database (Table 7.1). Six proteins were localized to the mitochondria, three were localized to the cytoplasm, two proteins were involved in protein chaperoning, and four were localized to the nucleus. Since PAX8 is well known to be a nuclear protein, priority was given to nuclear proteins. The four nuclear proteins identified were PAX8, RUVBL2, TIGD2, and BRIP1. We chose to focus our efforts on BRIP1, also known as BACH1 or FANCJ1, as it interacts with BRCA1, one of the main causes of hereditary breast and ovarian cancer[147].

Table 7.1: Potential PAX8 Interacting Proteins Identified in S3 HeLa Cells
Potential PAX8 Binding Partners were identified through Mass Spectrometry on nuclear lysates of S3 HeLa cells stably expressing PAX8 or Empty TAP-Tag constructs immuprecipitated first with Flag and then with HA. A threshold of 1 tandome detection was set, and due to low unique peptides only samples that were identified in 2 or more replicates were included.

Gene	Tandome Detections	Unique Peptides 1st Replicate	Unique Peptides 2nd Replicate	Unique Peptides 3rd Replicate	Total Replicates	Cellular Localization
PAX8	0	4	3	4	3	nucleus
ATAD3A	0	2	3	5	3	mitochondria
TIMM50	0	1	1	1	3	mitochondria
CANX	1	1	4	3	3	chaperone
DNAJA3	1	1	1	2	3	mitochondria, cytoplasm
RUVBL2	0	2	4	0	2	nucleus, cytoplasm
SLC25A19	0	0	2	1	2	mitochondria
BAG2	0	1	1	0	2	chaperone
TIGD2	0	1	1	0	2	nucleus
PYCR1	0	1	2	0	2	mitochondria
BRIP1	0	1	0	1	2	nucleaus
NDUFA4	0	0	2	1	2	mitochondria
BAG3	0	1	1	0	2	cytoplasm

Validation of the putative BACH1-PAX8 interaction was attempted by Co-Immunoprecipitation (Co-IP). Because S3 HeLa cells are cervical in origin, validation was performed in the more relevant ovarian cancer cell line, KURAMOCHI. Immunoprecipitation was performed for PAX8 and the PAX8 bound elution was probed via western blot with BRIP1 (Figure 7.3). Antibodies against IgG served as a negative antibody binding control. No binding was evident as BRIP1 was only observed in the whole cell extract and flow through fractions but not in the PAX8 or IgG bound elutions.

To validate the Co-IP process, the well-established BRIP1-BRCA1 interaction was confirmed. BRIP1 preferentially bound BRCA1 compared to the IgG negative control, although slight binding was observed in the IgG negative control as well (Figure 7.3).

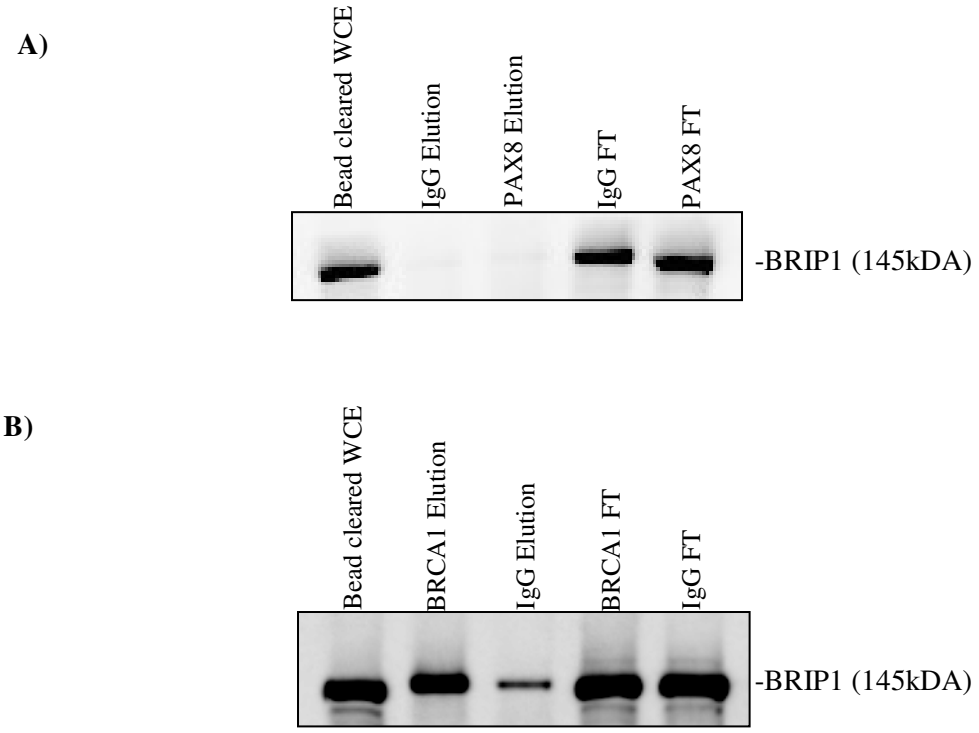

Figure 7.3: Co-Immunoprecipitations Exploring BRCA1-BRIP1-PAX8 Interactions
Co-Immunoprecipitations were performed by first clearing whole cell extracts with beads before incubating sample with A) PAX8 or B) BRCA1 antibodies. IgG antibodies served as a negative control. Bead cleared whole cell extracts (WCE), eluted products, and flow through (FT) fractions were analyzed by western blot for BRIP1. A) BRIP1 does not bind to PAX8 as no BRIP1 was identified in the PAX8 elution. B) BRIP1 binds to BRCA1 as BRIP1 is preferentially bound to BRCA1 as compared to IgG as shown by relative quantities of BRIP1 in the Elution fractions.

Tandem Affinity Purification with Stably Expressing PAX8 Tap-Tag KURAMOCHI Cells

Although Tandem Affinity Purification works best in S3 HeLa cells, they are less relevant than an ovarian cancer cell model that expresses native PAX8. Thus we also tried to perform

immunoprecipitation experiments in KURAMOCHI cells as well. First, stable expression of the empty and PAX8 Flag-HA constructs in KURAMICHI cells were validated by western blot (Figure 7.4). The empty-Flag-HA construct has a molecular weight of approximately 35kDA, while the PAX8-Flag-HA construct has a molecular weight of approximately 55kDA. This is approximately 7 kDA higher than native PAX8, which has a molecular weight of 48kDA. However, it was noted that only one out of four PAX8 antibodies tested would pick up the PAX8-TAP-tag construct, even though all three robustly identified native PAX8.

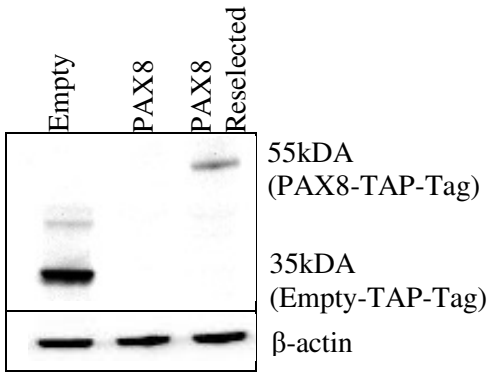

Figure 7.4: Stable Expression of PAX8 and Empty Flag-HA constructs in KURAMOCHI Cells
Western blot was probed with an antibody against HA to validate the expression of PAX8 (55kDA) and Empty (35kDA) Flag-HA constructs in KURAMOCHI cells. Empty Tap-Tag (Empty) expression was significantly higher than PAX8 TAP-Tag (PAX8), even after cells had been re-selected for TAP-Tag expression (PAX8 Reselected).

In preparation for immunoprecipitation, 42-15cm cell culture plates KURAMOCHI PAX8 and Empty TAP-tag cells were harvested. Because attempts to fractionate KURAMOCHI cells with the same hypotonic buffer protocol as S3 HeLa were unsuccessful, alternate fractionation protocols were tested. Ultimately, whole cell extracts were used without fractionation to prevent further loss of protein levels already low due to poor expression levels. Cells were first incubated with Flag-agarose beads and bound product eluted with Flag peptide before undergoing a second, identical immunoprecipitation with HA.

The final tandem IP product was tested for yield by western blot and for purity by silverstain (Figure 7.5). Unfortunately, PAX8 TAP-tag construct yield was still very low, despite increased input and limited protein loss in input samples.

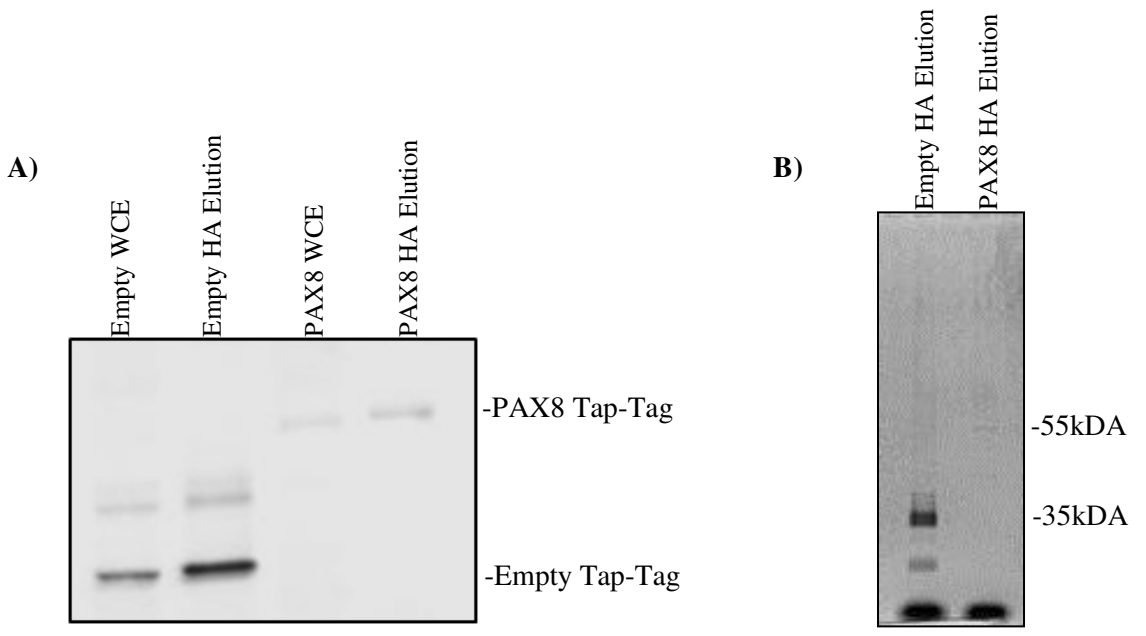

Figure 7.5:Immunoprecipitation of PAX8 and Empty Tap-Tag from KURAMOCHI Cells
Whole cell extracts of KURAMOCHI cells expressing PAX8 or Empty TAP-tag constructs were immunoprecipitated first for Flag and then for HA. A) Western blot of IP samples was probed with anti-HA to identify relative yield of product compared to nuclear extract levels. B) Final HA elutions were also analyzed by silverstain. Bands visible at 35 and 55 kDA correspond to Empty and PAX8 TAP-tag constructs, respectively. PAX8 TAP-tag construct has a much lower yield than Empty TAP-tag construct.

Samples were sent off for mass spectrometry analysis and held to the same standards as the S3 HeLa samples. This resulted in a total of 25 potential interacting proteins. Three of these were unique to the Empty TAP-tag control and 10 were present in both the Empty and PAX8 Tap-tag samples, and were excluded. This left 12 potential PAX8 binding proteins identified that uniquely pulled down via binding to the PAX8 TAP-tag construct (Table 7.2). Common lab contaminants were excluded using a threshold

of 1 tandome detection. Only two proteins passed this threshold, PAX8 and MTCH2. MTCH2 is a mitochondrial protein and thus of questionable significance as PAX8 is a nuclear transcription factor and not known to reside outside the nucleus. Low yield was attributed to extremely low PAX8 TAP-tag expression and no further validation was performed.

Table 7.2: Potential PAX8 Interacting Proteins Identified in KURAMOCHI Cells
Potential PAX8 Binding Partners were identified through Mass Spectrometry on whole cell extracts of KURAMOCHI cells stably expressing PAX8 or Empty TAP-tag constructs immuprecipitated first with Flag and then with HA. Proteins with a Tandome Detection of greater than 1 were considered too likely to be contaminants for analysis.

Gene	Tandome Detections	Unique Peptides
PAX8	0	3
MTCH2	1	1
GTF2I	5	1
VDAC2	6	2
SLC25A3	9	1
SLC25A5	10	1
HNRNPA1	20	1
SPRR2A	21	1
S100A9	22	1
RPS25	23	1
HSPA9	27	1
TUBB	36	3

Tap-Tag Localization in KURAMOCHI and S3 HeLa Cells

Because many potential PAX8 binding proteins identified were localized to extra-nuclear regions, immunofluorescence was performed by co-staining with PAX8 and HA to identify native PAX8 and the TAP-Tag construct, respectively. The only PAX8 antibody that is suitable for immunofluorescence unfortunately does not recognize the TAP-Tag construct; therefore only native PAX8 was identified with this antibody, while HA identified both empty and PAX8 TAP-Tag constructs. Native PAX8 in KURAMOCHI cells was found to localize to the nucleus, as expected, while the PAX8-TAP-Tag

construct also localized to the nucleus in S3 HeLa cells, indicating that the TAP-Tag construct did not affect PAX8 localization (Figure 7.6). Consistent with extremely low expression levels, the PAX8-TAP-Tag construct is not visible in the Kuramochi cells. The Empty-TAP-Tag constructs were preferentially located in the nucleus in both cell lines, with some residual cytoplasmic localization (Figure 7.6). As the empty vector negative control has no function, no particular cellular localization is expected.

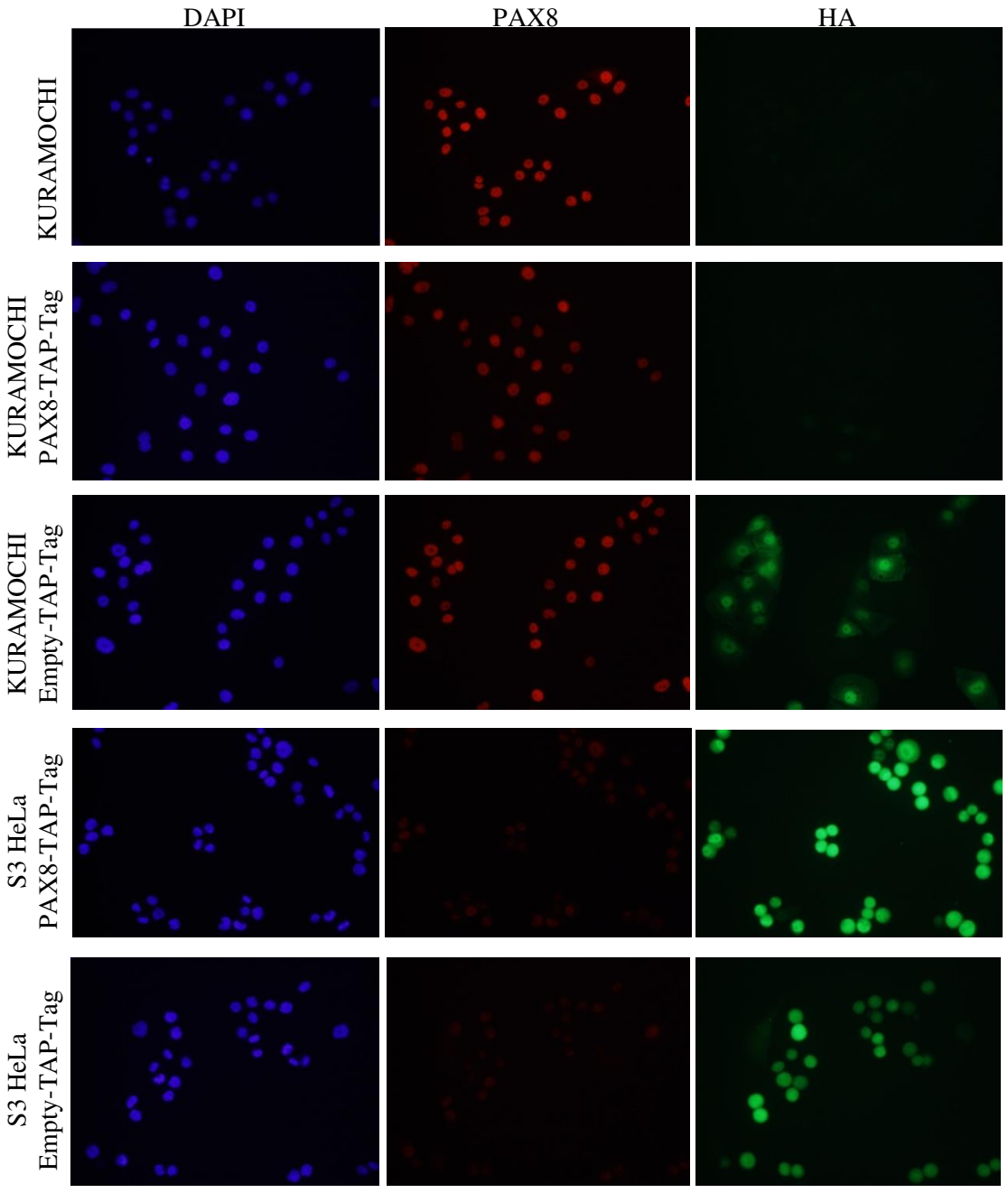

Figure 7.6: Localization of Native PAX8 and PAX8-TAP-Tag Construct
Kuramochi and S3 HeLa cells containing the PAX8 and Empty TAP-Tag constructs were cultured on glass coverslips and stained via immunoflourescence for DAPI, PAX8, or HA to determine the localization of the construct compared to native PAX8.

Discussion

Identification of PAX8 binding proteins by immunoprecipitation was severely limited by low expression levels, low numbers if identified proteins, and unlikely cellular localization of potential binding proteins. In S3 HeLa cells, PAX8-TAP-Tag expression was high and several proteins were successfully pulled down in multiple biological replicates. Of particular interest was BACH1, a nuclear protein known to interact with BRCA1. BRCA1 mutations account for approximately 8.6% of epithelial ovarian cancers, and this hereditary risk factor has profound implications on the lives and medical decisions of affected women[147]. A potential link between PAX8, an essential lineage marker conserved in 99% of HGSOC, and one of the most prominent hereditary risk factors is appealing[67]. However, while we could confirm the BRCA1-BACH1 interaction, co-immunoprecipitation in KURAMOCHI cells failed to support the putative BACH1-PAX8 interaction. Most co-immunoprecipitations can be performed in two directions, first by pulling down with PAX8 and probing for BACH1, and then the reverse. Unfortunately, PAX8 has a MW of 48kDA, which by western blot is indistinguishable from the heavy chain of the antibody used for IP. Thus, we could only pull down with PAX8 and probe with BACH1.

In KURAMOCHI cells, PAX8-TAP-Tag expression was extremely low and cells had to be re-selected which resulted in slightly improved expression levels. Because of this, and the fact that nuclear extraction with hypotonic buffers was incompatible with this cell line, IP yield was unsurprisingly low. This was especially evident in silverstains of the IP product. Unfortunately, Mass Spectrometry yield was low, with only one mitochondrial protein passing threshold. Although S3 HeLa cells are known not to express native PAX8 and therefore may lack relevance, it was nevertheless disappointing to find that there was no overlap between the potential binding proteins identified in S3 HeLa cells compared to the relevant KURAMOCHI cell line. Only one protein was identified in KURAMOCHI cells. This suggests that cellular context may impact PAX8 function, a theory which is supported by the developmental regulatory role played by the PAX proteins, all of which have similar structure but are organ specific[48].

Lastly, some fundamental problems with the TAP-Tag construct may have limited the scope of the experiment. We know the TAP-Tag construct was successfully integrated into cells and transcribed because of the cellular resistance to Puromycin, and also that the localization of the PAX8-TAP-Tag construct was nuclear like the native protein. However, out of four different PAX8 antibodies available in the lab, only one was capable of identifying the PAX8-TAP-Tag construct via western blot. While the addition of a TAP-Tag construct would reasonably cause minor alterations to PAX8 folding, especially to the C terminus where it was attached, western blot analysis is preceded by a denaturing step, which should negate this problem. Supporting the theory that the TAP-Tag constructs interfere with antibody binding is the fact that, although the exact peptides used to develop the antibodies are proprietary, the one PAX8 antibody that successfully identifies the PAX8-TAP-Tag construct was developed against a centrally located peptide while others tended to be developed against the C-terminus. Another strategy commonly employed in immunoprecipitation experiments is to separately tag both ends of the protein. However, as the N terminus of PAX8 is critical to DNA binding, we felt that this would unduly interfere with the protein function and hence its potential protein interactions. In retrospect, the choice to preserve DNA binding over protein binding may have adversely impacted the protein-protein interactions we were trying to identify.

SUPPLEMENTAL CHAPTER 8

The Impact of Ovulation

on the Fallopian Tube Epithelium

Acknowledgements

Susan Fotheringham conducted the initial studies highlighted in the introduction and trained Meg Emori in culturing primary fallopian tubes. Bovine follicular fluid was collected under the direction of Dr. Paul Tsang at the University of New Hampshire, and human follicular fluid was harvested by Dr. Wayne Lin and colleagues at the BWH in vitro fertilization clinic. Fallopian tubes were harvested at BWH and obtained through the tissue bank. Meg Emori was responsible for coordinating pickup from these sources and for sample processing. All other experiments in this chapter were conducted by Meg Emori. The Chowdhury lab generously shared their Comet Assay software.

Introduction

Follicular Fluid Development and Composition

Follicular fluid is initially derived from, and is similar in composition to, thecal capillary serum[129–131]. As the follicle develops, granulosa cells produce large polysaccharides, hormones, and growth factors which cannot pass the 100 kDA follicle-blood barrier, causing an osmotic gradient which further increases FF volume[133,134]. Ultimately, mature follicles in unstimulated women can contain as much as 1,000 fold higher levels of estrogen and progesterone than the serum, whereas other hormones such as follicle stimulating hormone (FSH) are not differentially concentrated[148]. Other potentially harmful factors, such as reactive oxygen species (ROS), have a physiologic window; their presence is required for embryo formation but particularly high levels within the FF are associated with poor embryo formation in IVF patients[135]. FF components include hormones, fatty acids, inflammatory factors, reactive oxygen species, growth factors, and other metabolites[34,35,149]. Mature human follicles reach approximately 23mm in diameter, yielding upwards of 5mL of follicular fluid[150]. During ovulation, FF is released and bathes the surrounding tissue, including the ovarian surface epithelium and the fallopian tube fimbria proximal to the ovary. (Figure 8.1)

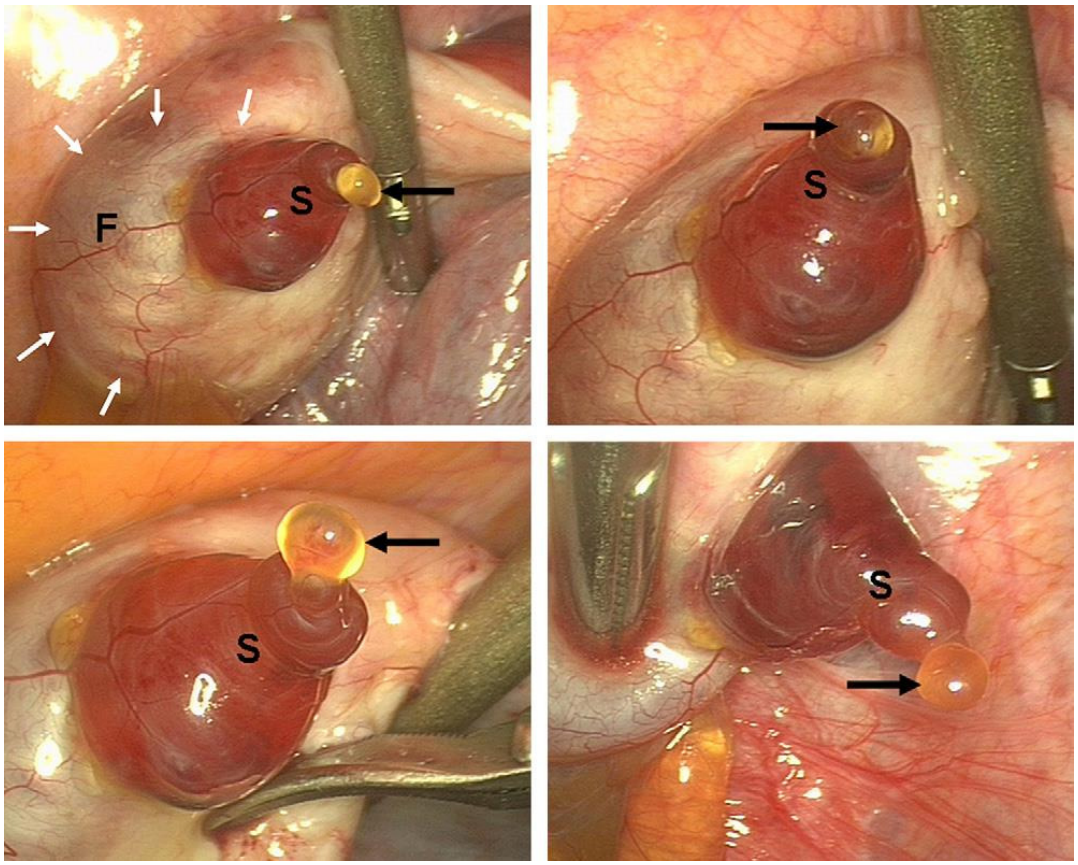

Figure 8.1 Laproscopic Time Course of Human Ovulation.
(From Lousse & Donnez 2008 Laparoscopic Observation of Spontaneous Ovulation) Follicle (F, with white arrows) is shown on the ovarian surface with the rupture point, or stigma (S, a darker red bulge). The expulsion of follicular fluid (black arrows, yellowish liquid), presumably also containing the oocyte, can be seen, bathing the ovarian surface epithelium and surrounding tissue in the process. Note that the fallopian tubes which would be in intimate contact with this surface have been pulled away to better image the ovulatory event.

Models and Sources of Follicular Fluid

Human follicular fluid is derived from women via transvaginal ultrasound-guided aspiration. This procedure is generally conducted in women undergoing IVF who have likely been treated with a series of hormones to force the development of multiple follicles. A typical IVF treatment will use gonadotrophins to stimulate follicle development, FSH to induce ovulation, and may also include LH and GnRH-agonists or GnRH-antagonists depending on the needs of a particular woman and the standard practice of the hospital[151]. Follicular fluid from young, unstimulated egg donors is the gold standard for studying normal

follicular physiology, but is rarely collected due to the invasiveness of the procedure in a largely unobtainable population. Studies comparing unstimulated egg donor samples to IVF FF samples confirm that the composition of the follicular fluid is altered as a result of the IVF hormonal stimulation[119,148].

Human follicular fluid can only be obtained by invasive methods and in small quantities, making follicular fluid derived from other species useful models. As follicular fluid volume corresponds roughly to body size, bovine fluid is attractive for the large quantity that can be obtained as well as the relative ease with which whole bovine ovaries can be obtained from abattoirs. However, previous studies have revealed the levels of major hormones in mature follicles to be several orders of magnitude lower in cows and camels as compared to their human counterparts[152,153]. For the purposes of studying follicular fluid in the context of early ovarian cancer pathogenesis, it is important to note that humans are the only known mammals to develop ovarian cancer. Domestic laying hens, despite being oviparous, also provide a unique model in that they are extremely susceptible to ovarian cancer and reflect several aspects of human disease including age-related onset, metastatic potential, and mutations in TP53 [154].

In Vivo Fallopian Tube Response to Ovulation

In vivo experiments inducing ovulation in mice show no significant induction of oviduct proliferation as a result of ovulation[39]. However, an increase in ɣH2AX foci and inflammatory factors was observed in the oviducts of ovulated mice, suggesting an inflammatory mechanism which may lead to DNA damage[39]. While mouse oviducts are the most accessible and tractable in vivo model for the impact of ovulation on the fallopian tube, is important to note that mice have a bursa which encloses the ovary and distal fallopian tube, and that this prominent tissue structure is not found in humans.

Follicular Fluid and Ex Vivo Cultures

Prior experiments in the Drapkin lab indicate that one fallopian tube grown in multiple ex vivo cultures when treated with different follicular fluids exhibits a range of DNA damage as measured by ɣH2AX foci, whereas multiple fallopian tubes grown in ex vivo culture when treated with the same

follicular fluid exhibit approximately the same level of DNA damage (Fotheringham, unpublished). This indicates that DNA damage is dependent upon the follicular fluid and independent of the fallopian tube. Furthermore, while FF treatment of ex vivo cultured fallopian tube epithelium cells or SKOV3 ovarian cancer cells after 48 hours induced a range of damage from 0-60% of cells exhibiting ɣH2AX foci, the higher DNA damage inducing FF samples produced approximately the percent of cells with ɣH2AX foci as 30uM H_2O_2 control treated cells which averaged approximately 60% (Fotheringham, unpublished) Interestingly, pre-treating either the H_2O_2 controls or the follicular fluid with ROS scavengers N-acetyl-cysteine or butylated hydroxyanisole significantly reduced the levels of DNA damage, whereas heat inactivation at 56°C for 30 minutes had no impact on DNA damage (Fotheringham, unpublished).

In further experiments on ex-vivo cultures of human fallopian tube epithelium treated with human follicular fluid for 24 hours, proliferation was induced as indicated by gene expression profiling and a modest increase in DNA damage as measured by ɣH2AX foci was observed[132].

Ovulation has long been documented epidemiologically to increase a woman's risk of ovarian cancer, and factors which decrease ovulation such as parity and birth control have a protective effect against HGSOC[29,30]. Two current hypotheses for the molecular basis of this phenomenon both implicate the monthly exposure of fallopian tubes to follicular fluid. Follicular fluid is known to contain reactive oxygen species, hormones, and other metabolites that can impact cells by inducing DNA damage, proliferation, or other early oncogenic effects. Initial unpublished studies have suggested that follicular fluid can cause DNA damage and that this can be quenched with reactive oxygen species (ROS) scavengers, suggesting a ROS mediated mechanism (Fotheringham, unpublished). However, the impact of follicular fluid as a whole on fallopian tube cells remains poorly defined. We hypothesized that follicular fluid would induce the types of effects reported by its components, mainly DNA damage and proliferation. To test this, we took follicular fluid and treated models of fallopian tube epithelium.

Due to the transient timing of ovulation and the relatively inaccessible location in which it occurs, it is impractical to measure the direct effect of follicular fluid on fallopian tube epithelium in healthy, fertile women. Thus ex vivo systems and cell lines are a practical and necessary way of modeling the effect of ovulation on fallopian tube epithelium and early cancerous lesions. Three cell lines were used in these experiments: immortalized fallopian tube epithelium cell line FT194 and ovarian cancer cell lines SKOV3 and OVCAR8. Ex vivo cultures of fresh fallopian tube cells, the most representative model for normal fallopian tubes, were used when their growth conditions were compatible with experimental assays.

Previous experiments testing the effects of follicular fluid on fallopian tube epithelium (FTE) relied on frozen follicular fluid samples obtained from the Brigham and Women's IVF facility. Due to the transient nature of many of the potentially damaging components of follicular fluid, we sought out fresh follicular fluid from women undergoing IVF at Brigham and Women's hospital. For comparison and supply purposes, frozen bovine follicular fluid was also obtained in collaboration with Dr. Paul Tsang at the University of New Hampshire and Dr. Marsha Moses at Children's Hospital Boston.

Results

Treatment with Follicular Fluid does not Induce Significant DNA Damage in Fallopian Tube Epithelium as Measured by Comet Assay

To test the hypothesis that follicular fluid induces DNA damage in fallopian tube epithelium, we directly measured the extent of single and double stranded breaks in the DNA via comet assay in immortalized fallopian tube cell lines as well as ovarian cancer cell lines. Comet assays may be performed under two conditions: Neutral, which is most sensitive to double-stranded DNA breaks, and Alkaline, which detects both single and double-stranded DNA breaks as well as DNA adducts. For this experiment the Alkaline assay was chosen as ROS can lead to both single stranded and double stranded DNA breaks, and most commonly causes 8-oxoguanine lesions[155]. Cells were treated with follicular fluid

or diluted hydrogen peroxide as a ROS-inducing control before being immobilized in agarose. Following lysis and denaturing, the isolated DNA is run through electrophoresis which causes the DNA strands to migrate through the agarose; long, undamaged strands running slowly at the comet head, and smaller fragmented DNA strands running faster and causing the comet tail. Stained samples are then quantitatively analyzed with the free comet scoring software Tritek CometScore™Freeware v1.5 to determine the percent of DNA in the comet tail.

The experiment was conducted three times in FT194 cells and once each with SKOV3 and OVCAR8 cells with a total of 3 frozen bovine follicular fluids, 2 frozen human follicular fluids, and 4 fresh human follicular fluids. Both follicular fluids and media controls showed no significant % of DNA in comet tail when measured at 2hr, 6hr, 24hr, or 48hr (Figure 8.2). In FT194 cells, DNA in tail was clearly visible in cells treated with 30uM H2O2 at 2hrs and cells remained damaged through 48hrs. Cells treated with PBS exhibited no damage at 2 hours but sustained increased damage at 24 and 48 hours, likely due to cellular starvation (Figure 8.2). Treatments inducing measurable DNA damage were observed to produce a heterogenous effect upon the cell population (Figure 8.2). One hundred cells were counted per treatment group and 10 cells, 5 with the highest % DNA in tail and 5 with the lowest % DNA in tail were removed from every group as outliers to strengthen overall population trends.

Table 8.1: Comet Assay analysis of follicular fluid treated cell lines.
Percent of DNA in comet tail after various time points measured by Comet Score software ±standard deviation

	day of exp.	Treatment	20min	1hr	2hr	6hr	24hr	48hr
FT194	2-8-2013	Media						2.15±2.68
	2-8-2013	fzn BVFF 324				3.30±5.49		2.88±4.28
	2-8-2013	fzn HFF 3				2.87±4.03		1.03±1.98
	2-8-2013	30uM H2O2						30.35±19.63
	7-8-2013	Media			0.25±0.84		0.93±2.56	0.37±1.24
	7-8-2013	fresh HFF 2			0.44±1.25		0.19±0.66	0.25±0.76
	7-8-2013	Fresh HFF 3			0.75±2.39		0.52±1.68	0.89±2.43
	7-8-2013	30uM H2O2			29.50±22.01		51.06±10.27	49.04±14.03
Ovcar8	2-1-2013	Media				4.28±4.88		
	2-1-2013	fzn BVFF 112		4.21±8.19		5.17±9.50		
	2-1-2013	100uM H2O2	48.89±16.02					
SKOV3	7-1-2014	Media			0.7±1.94	1.25±2.84	0.31±1.12	
	7-1-2014	fresh HFF2			0.60±1.68	0.12±0.46	0.56±1.53	
	7-1-2014	fresh HFF3			0.34±0.93	0.17±0.81	0.35±1.19	
	7-1-2014	30uM H2O2			33.0±24.63	1.01±2.94	2.17±7.07	

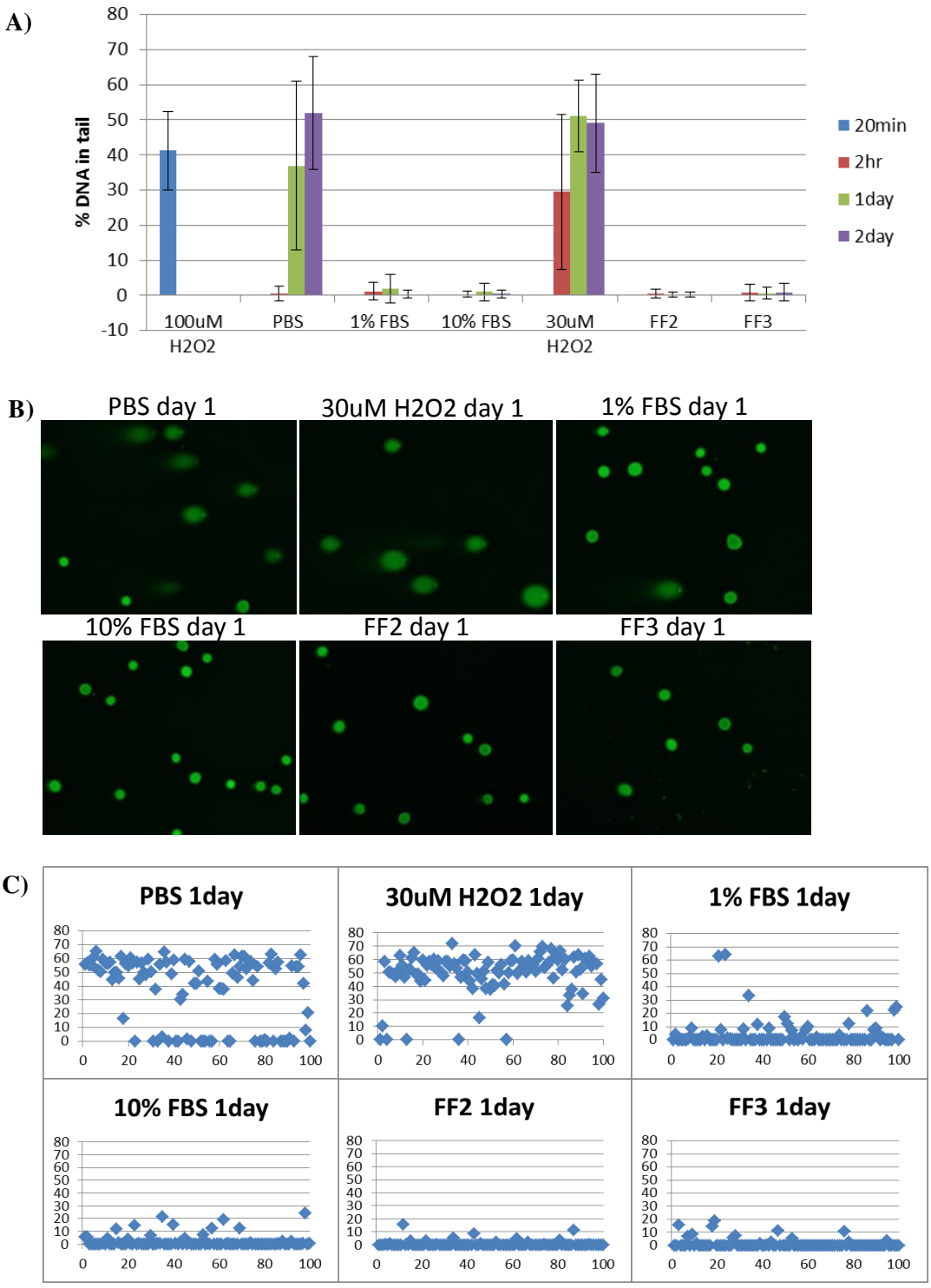

Figure 8.2: Direct DNA Damage in FT194 Cells Treated with Follicular Fluid
Comet assay was performed on FT194 cells treated with fresh human follicular fluid (FF) and controls a) Average % of DNA in tail n=90 cells. Error bars indicate standard deviation. b) Raw comet assay images showing relative fragmented DNA "comets" in various treatment groups c) Scatter plots showing % of DNA in tail of each individual cell for all 100 cells measured per sample group.

Treatment with Follicular Fluid does not Induce Significant DNA Damage Repair Response in Fallopian Tube Epithelium as Measured by H2AX Foci

The DNA damage repair process can be measured by the phosphorylation of histone H2AX. When DNA damage occurs, H2AX is phosphorylated as an initiation step, recruiting DNA repair proteins to the site of damage[156]. Immunofluorescence with ɣ-H2AX specific antibodies can efficiently identify an active DNA repair response. Cells were grown on coverslips or transwell membranes and treated with follicular fluid or diluted hydrogen peroxide as a ROS damage-inducing control before being fixed. Following permeabilization and co-staining with ɣ-H2AX specific antibody and DAPI, cells were imaged at 40x on a fluorescent microscope and quantified as positive or negative for ɣ-H2AX foci.

The experiment was conducted with FT194, SKOV3 and Ovcar8 cells over time periods ranging from 24 to 72 hours and using 5 different bovine follicular fluid samples and 6 frozen human follicular fluid samples. Although minor levels of DNA damage could be observed after treatment with select follicular fluids, no human or bovine follicular fluid was significantly different from media only treated controls (Figure 8.3). Sensitivity to hydrogen peroxide varied significantly by cell line, but significant levels of H2AX foci could largely be observed at doses of 30-100uM. Treatment of cells with 300uM hydrogen peroxide was uniformly lethal to all cell lines. H2AX foci induced by hydrogen peroxide and follicular fluid tend to form a speckling pattern with smaller foci whereas IR tends to induce larger foci (Figure 8.3). Selective samples were co-stained with H2AX and 53Bp1, another protein involved in the cell's response to DNA double stranded breaks, and immunofluorescent signals largely overlapped, supporting the fact that the foci were due to DNA damage repair (Figure 8.3).

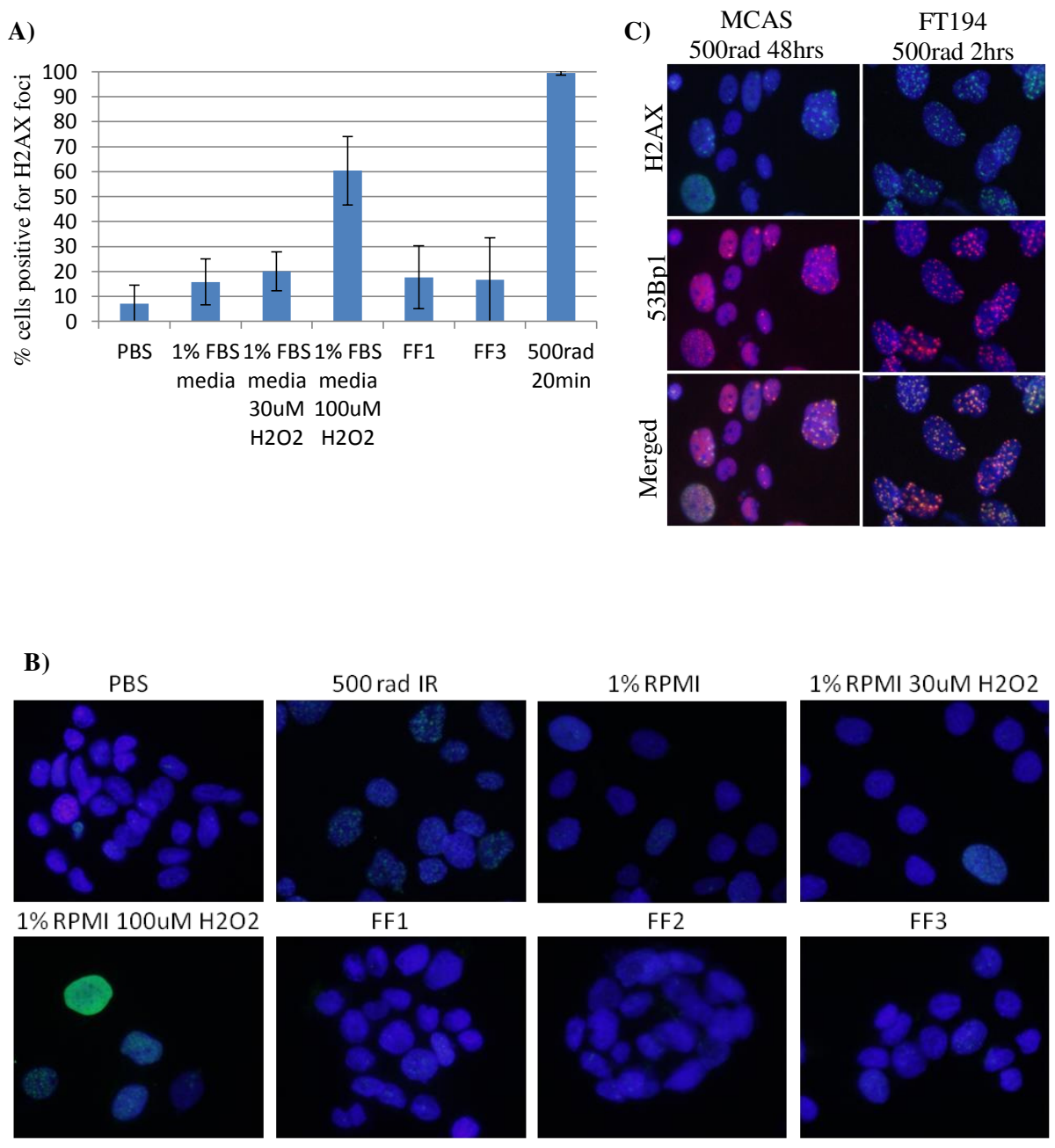

Figure 8.3: DNA Damage Response in Cells Treated with Follicular Fluid
Immunofluorescence for ɣH2AX was performed SKOV3 cells treated with follicular fluid treated for 48hrs. A) Cells positive for H2AX foci were counted and the average of all quantified fields was calculated. Error bars indicate standard deviation. B) Images were taken at 40x with at least 4 fields per treated sample. C) Co-immunofluorescence was performed for ɣH2AX and 53Bp1 in MCAS and FT194 cells to validate DNA damage response.

Treatment with Follicular Fluid Causes Cell Growth Equivalent to 10% Serum-Containing Media

Hormones in follicular fluid, most notably estradiol, have been previously shown to induce proliferation. To test the proliferative effect of follicular fluid on fallopian tube epithelium, Cell Titer Glo and SRB assays were performed. Cell Titer Glo measures ATP activity, which correlates to active cellular metabolism, thus identifying the relative number of live cells in culture at a given time point. SRB assay uses Sulforhodamine B to quantify protein levels, thus estimating the cellular density at a given time point.

FT194 and SKOV3 cells were treated with fresh follicular fluid and harvested at 24, 48, and 72 hours. One follicular fluid sample was flash frozen and thawed before use to discern if freezing inhibited any proliferatory effects. PBS and media with 1% or 10% FBS were used as controls. PBS provides no nutrients for the cells and they will die or remain static over the time course. Media containing 1% FBS provides enough nutrients to maintain cell life but not enough to support proliferation, while media containing 10% FBS is the standard for growing these cells. Fresh follicular fluid treated cells consistently proliferated at higher rates than the static growth observed in 1% FBS containing media or PBS treated cells, and were generally equivalent to the rate of proliferation observed in cells grown in 10% FBS containing media. Subjecting the follicular fluid to a freeze-thaw cycle before treatment did not significantly alter the growth kinetics of the treated cells (Figure 8.4). Results obtained from the Cell Titer Glo and SRB assays were comparable.

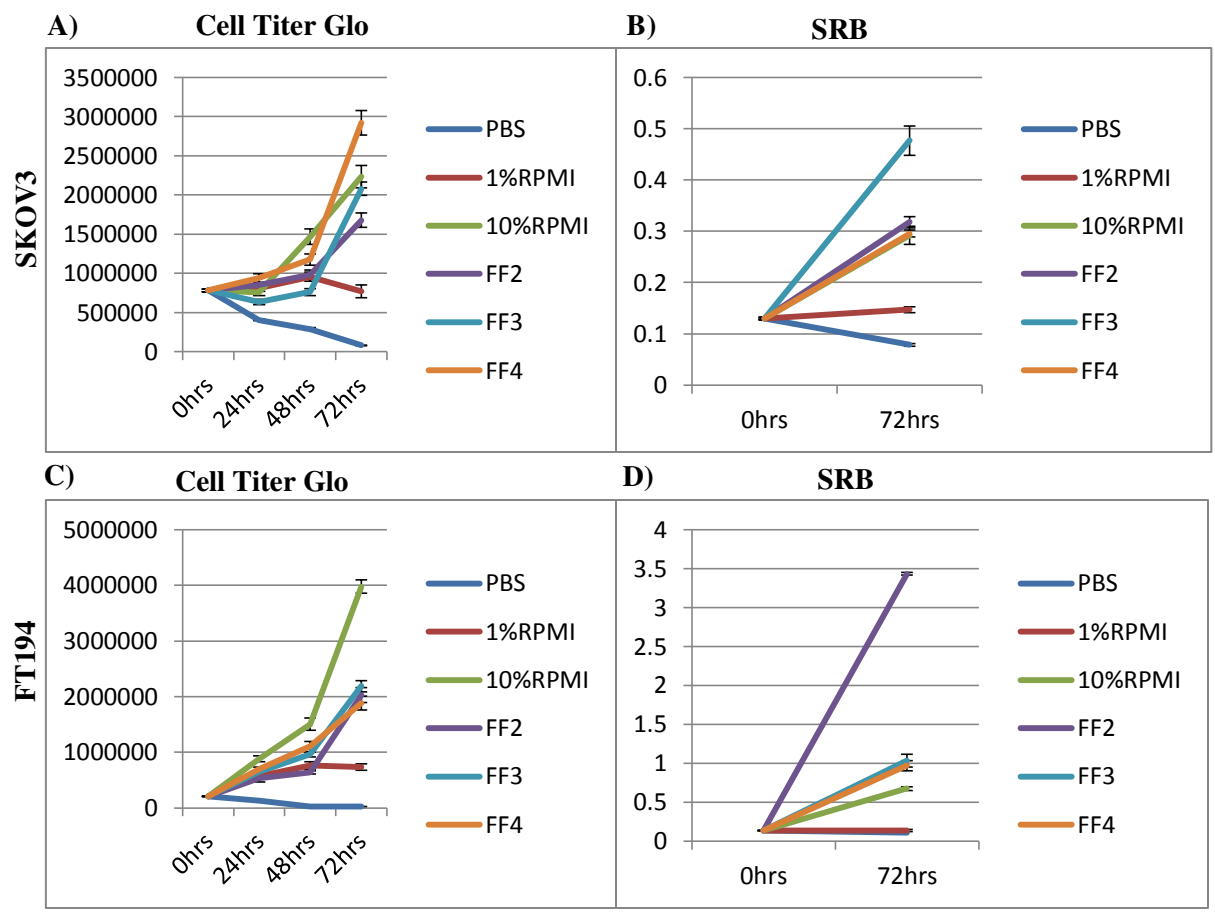

Figure 8.4: Follicular Fluid Induced Proliferation
SKOV3 (a,b) and FT194 (c,d) cells were treated with fresh human follicular fluid (FF) and for 24, 48, or 72 hours. a,c) Cell Titer Glo analysis measuring average relative luminescent signal b,d) SRB assay measuring average optical density. All samples were replicated in 6 wells with identical initial density. Error bars indicate standard deviation.

Treatment of SKOV3 Cells with Follicular Fluid causes a Novel Cluster Phenotype

When grown on glass coverslips, imaging SKOV3 cells with fluorescent microscopy after 48hrs revealed that cells treated with fresh follicular fluid form clusters that are attached to the plate but only semi-adherent whereas cells treated with media alone retained their mono-cellular growth pattern. (Figure 8.5). When cells were fixed for immunofluorescence at 48hrs, semi-adherence of clusters was confirmed with DAPI staining as super-confluent clusters folded up to make quantitative analysis impossible. Interestingly, old follicular fluid that had been stored at -80°C for several years induced a minor

clustering phenotype. Fresh follicular fluid that had been flash frozen in a mixture of ethanol and dry ice before being transferred to -80°C for 15 min and then thawed on ice produced a slightly stronger clumping/ proliferative phenotype, and fresh follicular fluid even when mixed with RPMI exhibited the strongest clumping phenotype and tendency to peel off the coverslip (Figure 8.5).

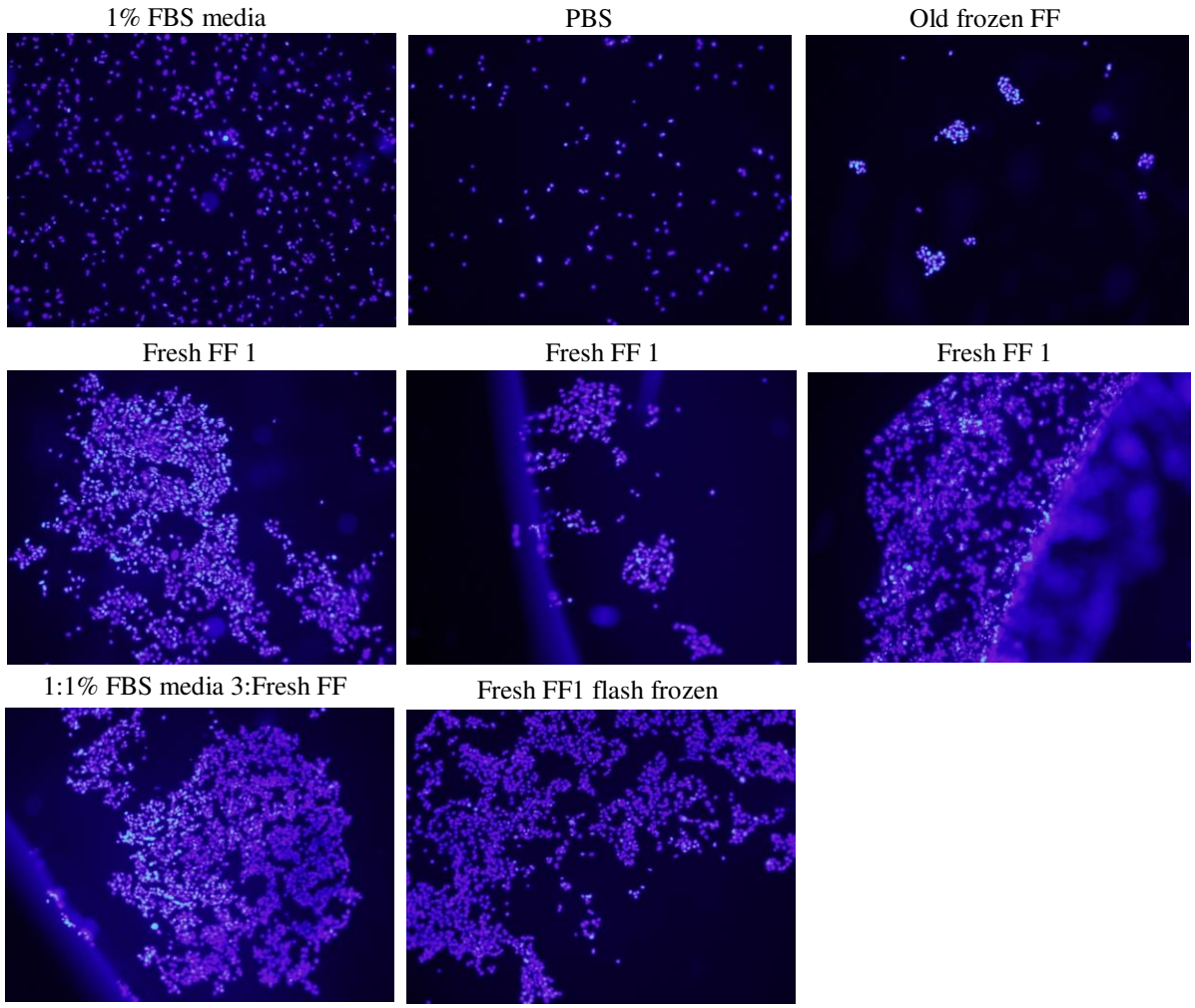

Figure 8.5: Follicular Fluid Induced Growth Morphology
10x Images of DAPI stained SKOV3 cells treated with fresh human follicular fluid (FF) or controls for 48 hours showing clustered and detached sheets of cells. All cells were plated at identical density before treatment.

No Measurable Reactive Oxygen Species were Observed in Follicular Fluid by Luminometer

Follicular fluid reactive oxygen species (ROS) levels must be carefully balanced: too much will result in damage to the oocyte while too little is insufficient for ovulation[157]. Indeed, even in oocyte retrieval during IVF there is a window of optimal ROS levels, and eggs from follicles with ROS levels above or below this are statistically less likely to develop into viable embryos[135]. However, ROS can also cause significant oxidative damage within a cell as it reacts with cellular proteins, lipids, and DNA and repeated exposure can lead to carcinogenesis[158]. ROS levels have previously been successfully measured in follicular fluid[135,159]. While ROS levels can be measured in many ways, luminescence is a widely used technique as it is sufficiently sensitive at low biological concentrations and can be rapidly performed on fresh samples. In luminol based chemiluminescence, luminol is oxidized by an oxidant containing chemical or biological fluid such as hydrogen peroxide, semen, or follicular fluid. The metabolite of luminol, 3-aminophthalate, is generated in an excited state and therefore emits light; the transient photons are magnified via photomultiplier tubes and quantified with the use of a luminometer[149]. Horseradish Peroxidase (HRP) may be used to catalyze the reaction, especially if ROS levels are low[149].

ROS levels in our follicular fluid were measured with a Berthold Sirius Luminometer. This particular instrument was chosen as it has been previously used to measure ROS levels in follicular fluid and semen[135,159–163]. Based on previously published protocols using this machine, we chose to measure luminescence over time using an integration method rather than try to capture photon emission at a fixed point in time[135,159–163]. The integration method is less susceptible to small technical variations including time from sample mixing to readout, and is therefore more reproducible[149]. Samples were prepared as performed previously, with fresh bloody samples spun down to remove iron-containing blood cells which can catalyze the luminol reaction, and frozen samples thawed on ice before being used immediately[159,160,164]. Sample was combined with luminol and counted photons/ min (cpm) was recorded over 15 minutes. A 5 second delay was added to decrease background noise during tube insertion. A full description of the protocol can be found in the methods section.

Ten frozen human follicular fluid samples were measured first alone to obtain background levels and then with luminol added (Figure 8.6). A modest range in counted photons per minute (cpm) was observed across samples, but background levels were the same as luminol containing samples, indicating that measured counts per minute were not generated by luminol oxidation. Negative controls of PBS and water were the lowest readings as expected, and a solution of 1M H2O2 had negligible background readings but a significantly high luminol reading, showing successful luminol oxidation.

To test whether HRP increased signal to background ratio in samples, a 10uL solution of H2O2 was titrated down from 8.8M to 1uM and added to 390uL PBS containing luminol and HRP to establish a standard curve and determine the limit of ROS detection by luminol (Figure 8.6). 8.8M H2O2 overloaded the machine, while 1mM H2O2 produced the first reliable reading. While a clear difference was observed between 30uM H2O2 and 10uM H2O2, 10uM H2O2 was indistinguishable from lower concentrations. Lastly, luminol and HRP were added to frozen human follicular samples to determine if HRP increased signal to background ratio in biological based samples (Figure 8.6). Interestingly, neither the addition of HRP nor luminol increased follicular fluid counted photons per minute. Indeed, all measurements involving follicular fluid fell well below 10uM and 1uM H2O2 measurements which are below the threshold of measurable sensitivity for the luminometer.

While the IRB for fresh follicular fluid had not yet been established, de-identified fresh ascites fluid from Brigham and Women's Hospital was readily available to the lab. As ascites is produced as a result of ovarian cancer and can often be rich with cancer cells known to produce high levels of ROS, this was a good model both for its relevance and availability. Ascites also had the added benefit of coming in liters as compared to the average 500uL of the frozen follicular fluid samples. Fresh ascites was delivered to the lab shortly after it had been removed from the patient, and was still warm at the time of processing. However, as with the follicular fluid samples, no difference was observed between background and luminol treated samples (data not shown).

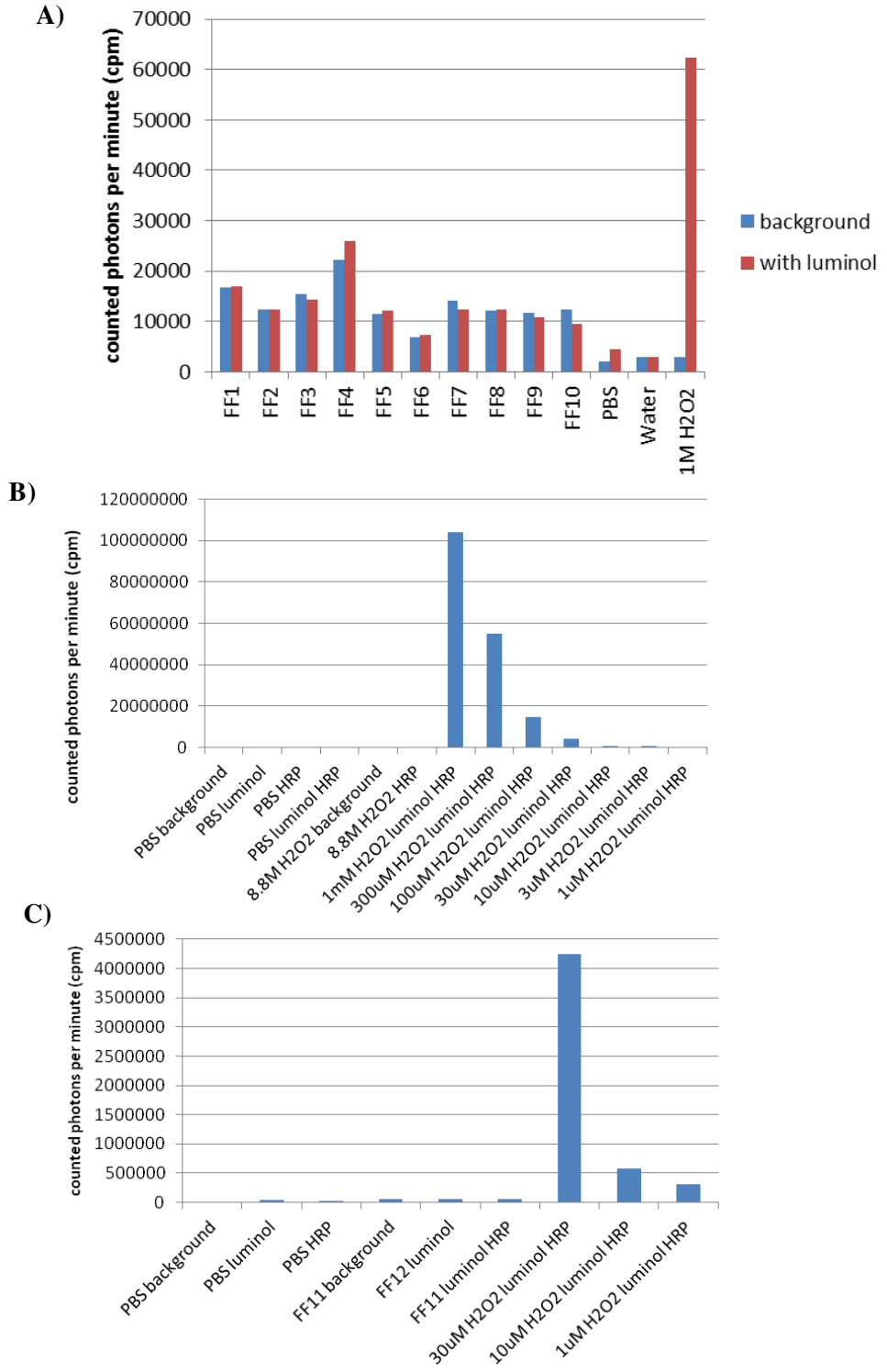

Figure 8.6: Reactive Oxygen Species in Follicular Fluid and Controls
A) 10 follicular fluid samples were measured alone or combined with luminol to determine background levels. B) Titrated hydrogen peroxide was combined with luminol and HRP as a catalyst. C) Follicular fluid was combined with luminol and HRP. All measurements were conducted over an integral of 15 min and measured in counted photons per minute.

We did however observe a striking difference in the shape of the curves generated by biological fluid samples (follicular fluid or ascites) as compared to chemically generated samples (PBS or H2O2) (Figure 8.7). Biological sample curves were less smooth, the initial slope was less steep, and the drop in relative light units per second (RLU/s) in the first minute less drastic. Chemically generated samples were very smooth and had a very steep initial slope and a drop of over 100,000 RLU/s in the first minute.

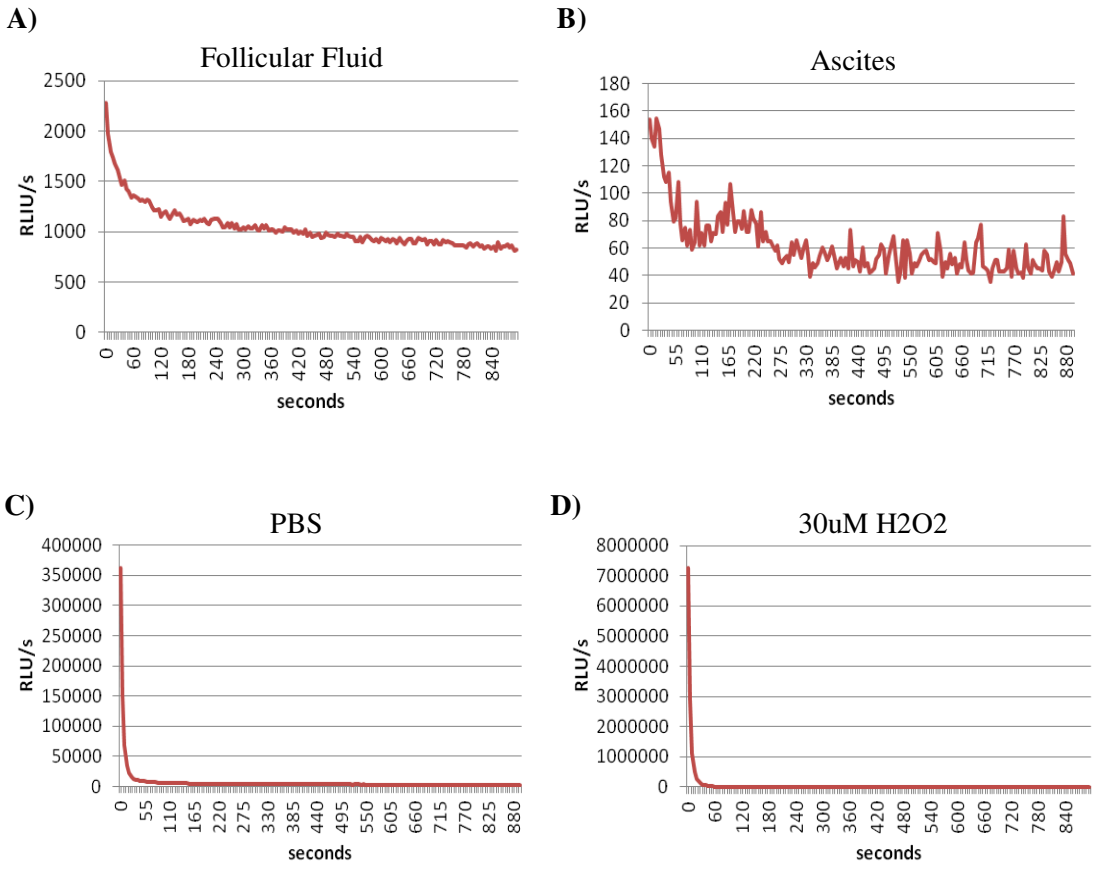

Figure 8.7: Reactive Oxygen Species Curves in Biological and Synthetic Samples
Differences in curve shapes between biological samples A) follicular fluid and B) ascites or non-biological samples C) PBS and D) H2O2. All curves measured in Relative Light Units per second (RLU/s) every 5 seconds over a 15 minute time period.

Discussion

Follicular fluid treatment was sufficient to sustain cells and promote proliferation in a similar manner to serum containing media, but did not present any novel damage or proliferation phenotype. Cells treated with PBS received insufficient nutrients for culture maintenance as evidenced by lack of proliferation and increased DNA damage at 24 and 48 hours. In contrast, cells treated only with follicular fluid and no media proliferated at approximately the same rate as cells treated with 10% serum enriched media and were protected from DNA damage at 24 and 48 hours. This indicates that follicular fluid is sufficient, at least in the short term, to sustain cells in culture. Follicular fluid that had been frozen and thawed retained these effects, indicating that the components responsible for keeping the cells alive are robust to freezing. Heating of the samples to test if active components can be heat inactivated was not attempted as follicular fluid samples can only be heated to 56°C before protein denaturing results in an opaque, gelatinous solid that cannot be used for experiments.

Ultimately, it is not surprising that follicular fluid should closely mimic the properties of serum as follicular fluid is primarily derived from thecal capillary serum and, while hormones and other molecules too large to cross the follicle-blood barrier are highly concentrated in the follicular fluid, the vast majority of smaller components should remain equally distributed between serum and follicular fluid[129,130,133,134,165].

Although in our hands no DNA damage or damage response was consistently observed with bovine or human follicular fluid, it remains unclear why the experiments could not reproduce the increased DNA damage response observed in fallopian tube epithelium treated with follicular fluid previously in the lab (Fotheringham, unpublished). The same experimental design was used, and, although the frozen aliquots used previously were extremely limited in volume, even in the few cases where the same experiments were repeated with the same follicular fluids the same results were not observed. Since the person performing the initial experiments personally trained the person performing the follow up experiments, it seems unlikely that differences in technique would be significant, although the analysis of γH2AX foci is counted blinded, by hand, and can be subjective. Since these results were

collected another group has used similar methods and identified a moderate DNA damage and proliferation response in ex vivo fallopian tube cultures treated with follicular fluid[132].

The one unique phenotype presented by follicular fluid was the tendency of cells to form primary cell-like semi-adherent clusters when treated with follicular fluid. This phenomenon was strongest in cells treated with fresh follicular fluid, diminished in follicular fluid that had previously been frozen, and not observed in cells treated with media or PBS, suggesting that fresh follicular fluid contains components which trigger this change in culture morphology. The clustering phenotype was only observed on cells grown on glass, a surface with less adhesive properties than plastic. Thus it may be that in conventional plastic culture dishes the rate of adhesion is sufficient to overcome any follicular fluid signals enhancing semi-adherent clustering, whereas glass surfaces provide less adhesive resistance.

Although it appeared from DAPI staining that clustering follicular fluid treated cells were also more numerous than their media treated counterparts, this was not strongly supported by the Cell Titer Glo results measuring proliferation. The accuracy of Cell Titer Glo in quantifying semi-adherant cells may be limited as follicular fluid is incompatible with the Cell Titer Glo lysis solution. If the follicular fluid is not removed and the cells rinsed in PBS before lysis occurs, the proteins in the follicular fluid will solidify, obscuring the cells below and preventing accurate luminescence measurements. The necessary rinsing step, while as gentle as possible, may be sufficient to dislodge semi-adherent cells such that they are not included in the final analysis. It is likely that the two blatant outliers in the cell titer glo assay result from inadvertent inclusion of small levels of residual follicular fluid. Alternately, if there is an increase in cell count as measured by follicular fluid, the outliers, which occurred at earlier time points, may have captured the clumping cells in a more adherent state, whereas at later time points the cells may have been more detached and therefore washed away.

While using ovarian cancer lines to model early ovarian cancer events is convenient, women with ovarian cancer are typically menopausal or post-menopausal, such that exposing ovarian cancer to

follicular fluid is not contextually relevant. Even in pre-menopausal woman, ovarian cancer would be expected to interrupt the normal menstruation cycle. Primary fallopian tube cells grown on transwell membranes provide the most relevant ex vivo model, but are limited by sample availability, size, and quality. Further limiting is the fact that many assays such as cell titer glo and SRB are incompatible with ex vivo culture systems.

Immortalized fallopian tube cell lines offer a convenient and easily tractable model of fallopian tube epithelium, and may be similar to the earliest precursor lesions, as P53 signatures and immortalized fallopian tube models have P53 inhibition due to mutations or the use of viral antigens or shRNA, respectively[40]. However, the immortalization process takes the serous cells out of their stromal context and microenvironment, likely decreasing their hormone receptor levels. Therefore hormones in the follicular fluid which would elicit a biological response from primary tissue may not induce a reaction in immortalized models of fallopian tube epithelium.

The follicular fluid obtained for this experiment came from women who had undergoing IVF for oocyte retrieval. Data such as age, which gonadotropins or antagonists/ agonists were injected, reason for infertility and any underlying conditions affecting fertility were blinded and have not been analyzed. All of these factors have been shown to impact follicular fluid composition, and may in turn impact the level of damage caused to the fallopian tube[32]. Since there was no exclusion criteria for the follicular fluid it is unlikely that all of the samples used previously in the lab were distinctly different from the fresh samples collected for the work presented in this thesis, but no data has been analyzed to disprove this.

Reactive oxygen species are extremely transient, the most stable biological examples having an estimated half-life of only 1millisecond[166]. Thus it is likely that the extended frozen time, as well as the thawing process would be sufficient to remove all ROS. It is unclear if additional problems were also responsible for yielding different results on the same machine with the same protocols as previously published. Previous results estimated the range of fresh follicular fluid ROS levels to be between 50 and

130 counted photons per second, whereas our frozen samples fell between 100 and 400 with or without luminol[135].

In addition, the fact that follicular fluid samples treated with luminol and/ or HRP failed to increase even slightly, whereas known ROS negative PBS samples under similar conditions exhibited a slight rise in background noise, suggests that there might be antioxidants present in the follicular fluid which would quench the oxidation process. It is logical that the body would need antioxidants to balance and regulate the presence of potentially dangerous oxygen species, and previous research has indicated that molecules that function as antioxidants, such as melatonin, can be found in the follicle and have an important role in protecting the follicle and ensuring oocyte maturation[167].